Check for updates

ADVANCED ENERGY MATERIALS
www.advenergymat.de

Interfacial Design and Assembly for Flexible Energy Electrodes with Highly Efficient Energy Harvesting, Conversion, and Storage

Yongmin Ko, Seokmin Lee, Cheong Hoon Kwon, Seung Woo Lee, and Jinhan Cho**

Charge transfer between a conductive support and active materials as well as between neighboring active materials is one of the most critical factors in determining the performance of various electrodes in energy harvesting, conversion, and/or storage. Particularly, when preparing energy electrodes using conductive and/or electrochemically active nanoparticles (NPs), the bulky organic materials (i.e., ligand or polymeric binder) covering the NP surface seriously limit the charge transfer within the electrode, thereby restricting the energy storage or conversion efficiency. Furthermore, the flexibility and mechanical stability of the electrode have been considered important evaluation indices for flexible/wearable energy applications. In this regard, considerable research has been directed toward controlling the interfacial structure to enhance the charge transfer efficiency and toward incorporating functional materials into flexible/porous supports. This review describes the central progress in flexible electrodes for energy harvesting, conversion, and storage, along with the challenges in designing high-performance energy electrodes. In particular, layer-by-layer (LbL) assembly is analyzed, which is an ultrathin film fabrication technology that enables fine tuning of the interfacial structure for various electrode materials. It is shown how LbL assembly can be effectively applied to energy electrodes to obtain desired functionalities and improve the charge transfer efficiency of electrodes.

1. Introduction

Since the advent of the ubiquitous networking era of the 1990s, the number of personalized electronic devices has rapidly increased, and this trend has strongly stimulated interest in wireless and portable electronics with higher performance and functionality. At the same time, to realize such high-end flexible or wearable electronic devices, much research has been concentrated on developing an appropriate power supply (i.e., energy harvesting, conversion, and storage) with high energy performance, mechanical flexibility, and operational stability capable of sufficiently driving device functions.[1–10] Although such power system units require different components according to their operation mechanisms and functions, the amount of active materials and the facile charge transfer in their electrodes basically act as key factors determining their output performance. Therefore, one of the main challenges in realizing the power supply of next-generation flexible/wearable electronics is how to effectively integrate a high loading amount of active components into a mechanically deformable substrate (i.e., support).

Numerous approaches have been proposed for assembling flexible energy electrodes that ensure reliable electrical/electrochemical properties under various mechanical deformations. As a result of such efforts, some prototype and commercial products in flexible energy storage applications have been demonstrated (i.e., supercapacitors and lithium-ion batteries).[11] To date, most electrodes for energy storage applications have been fabricated in the form of thin film configurations on nonporous flexible supports (i.e., plastic or metal plates). However, such an electrode configuration has a fundamental limitation on increasing the thickness (or loading amount) of active materials due to the increased charge resistance for thicker electrodes. Accordingly, relatively small amounts of active materials have been deposited onto nonporous electrodes, which has resulted in a limit on significantly enhancing the energy storage performance.[12] That is, given that the loading amounts of active materials strongly depend on the overall surface area of the substrate, the shape and porous structure of flexible substrates are very significant.

Dr. Y. Ko,[+] S. Lee, Dr. C. H. Kwon, Prof. J. Cho
Department of Chemical and Biological Engineering
Korea University
145 Anam-ro, Seongbuk-gu, Seoul 02841, Republic of Korea
E-mail: jinhan71@korea.ac.kr
Prof. S. W. Lee
School of Mechanical Engineering
Georgia Institute of Technology
North Ave NW, Atlanta, GA 30332, USA
E-mail: seung.lee@me.gatech.edu
Prof. J. Cho
KU-KIST Graduate School of Converging Science and Technology
Korea University
145 Anam-ro, Seongbuk-gu, Seoul 02841, Republic of Korea

The ORCID identification number(s) for the author(s) of this article can be found under https://doi.org/10.1002/aenm.202002969.

[+]Present address: Division of Energy Technology, Materials Research Institute, Daegu Gyeongbuk Institute of Science and Technology (DGIST), 333 Techno Jungang-daero, Hyeonpung-eup, Dalseong-gun, Daegu 42988, Republic of Korea

DOI: 10.1002/aenm.202002969

© 2021 Wiley-VCH GmbH

In terms of material conductivity, various redox reaction-based energy materials used for energy storage and conversion applications often have semiconducting or insulating properties. As such, the high mass loading of active materials, such as pseudocapacitive materials for energy storage or enzymes for energy conversion, seriously restricts the charge transfer between adjacent active components within electrodes, resulting in low energy storage and conversion efficiency.[13,14] As an alternative, 3D porous and conductive supports based on textiles or elastomers have received great attention as promising hosts for designing flexible electrodes due to their various unique features, including large surface area, light weight, mechanical stability, and flexible properties.[2,3,15,16] Particularly, considering that they have a biofriendly nature and excellent tolerance to various human body motions (i.e., bending, stretching, compression, and twisting) and shapes, textile- or elastomer-based energy electrodes can be widely applied to functional clothing, patchable diagnostic kits, and implantable artificial skins, as well as to portable communication electronics such as cellular phones, smartwatches, and tablet personal computers.[17]

In the case of energy storage and conversion electrodes composed of active materials and a current collector (or support), the contact resistance occurring at the interface between the active components and current collector has a dominant effect on the total internal resistance of the electrode, which is closely related to the electrical conductivity of the current collector.[18] Therefore, to effectively utilize the notable advantages (i.e., large surface area and flexibility) of textile (or porous elastomer)-based current collectors, insulating textiles should preferentially be converted into conductive textiles with the aid of conductive materials. To this end, a variety of conductive materials, such as carbon materials (mainly carbon nanotubes (CNTs) and/or reduced graphene oxides (rGOs)), metal nanoparticles (NPs), or metal nanowires (NWs), have been incorporated into 3D porous substrates (i.e., textiles, paper, or porous elastomers) through various physical and chemical adsorption processes to provide sufficient electrical conductivity. Since textile or paper materials have a fibrillated bundle network with a number of micro/macropores and such porous structures can act as a notable merit in energy applications, effective preservation of the intrinsic pore structure of textiles in the deposition process for conductive materials is highly desirable to ensure facile ion transfer (or electrolyte wetting) within electrodes.

Furthermore, the surface properties (i.e., interfacial interaction, morphology, and coverage of conductive material) of the insulating substrates and the formed current collectors should be carefully considered and optimized because their outermost layers come into direct contact with conducting materials (for conductor performance) or active materials (for energy performance). That is, favorable interfacial interactions between the current collector and active materials as well as between insulating substrates and conducting materials are key to facilitating charge transfer at the interfaces and to achieving long-term operational stability under various electrochemical and mechanical stimuli (i.e., bending, pressing, or twisting).[19] For example, conventional coating processes based on a highly viscous composite slurry (i.e., a mixture of a polymer binder and active materials, including conductive and/or energy materials) can have much difficulty in simultaneously providing a high degree of mechanical flexibility, electrical conductivity, and/or energy performance due to the poor control of the slurry coating process over the interfacial structure, the relatively high viscosity of the slurry mixture (including active materials), and/or the unfavorable interactions between active materials and substrates. Specifically, these processes can induce aggregation of active components and limit the conformal coating of the entire area (or precise control of the loading amount), ranging from the interior to the exterior of the porous supports. As a result, the nonuniform adsorption of active components onto the current collector inevitably increases the charge transfer resistance at the interfaces, which can lead to poor rate performance under fast current sweep. Therefore, to improve the charge transfer kinetics within slurry-coated electrodes, additional chemical or physical treatments are required after the slurry coating process.[20]

As another example, in the case of preparing electrodes using elastomers, such as poly(dimethyl siloxane) (PDMS), the poor interaction between conductive materials and elastomers causes serious interfacial adhesion failure under repeated mechanical stimuli, which notably increases the electrical resistance of elastomer electrodes. Therefore, elastomer electrodes have been generally prepared in the form of elastomer-encapsulated conductive components. Fan et al. reported a stretchable elastomeric conductor fabricated by transferring a gold (Au) layer encapsulated between polyimide (PI) layers onto a PDMS substrate.[21] In this case, the spin-coated PI layer acts as an adhesion layer to retard strain localization in the Au layer. However, this kind of elastomer electrode has much difficulty in being directly used as a contact electrode, requiring continuous external stimuli such as periodic contact/separation.

Other critical factors determining the charge transfer behavior (or internal resistance) within an energy electrode are the size of the active materials and the presence of bulky ligands bound to the surface of the active materials. Recently, the use of nanosized active materials (particularly energy storage materials such as pseudocapacitive metal oxides) in fabricating energy electrodes has emerged as one of the most effective methodologies that can overcome the limitations of conventional bulk material-based electrodes. That is, reducing the material size has major advantages, such as a fast charge transfer rate, a large active surface area, and tolerance to mechanical deformations, thereby improving the rate performance and energy efficiency. In line with these notable features, nanomaterials with various physical and chemical properties (i.e., dimensionality, conductivity, surface characteristics, and molecular structure) have been synthesized and applied to improve the performance of energy electrodes.

To synthesize nanosized active materials with the above-mentioned properties in aqueous or organic media, the organic ligands bound to the surface of active materials operate as vital elements.[22,23] Although some organic ligands with hydrophilic moieties can also be combined with other functional materials as organic linkers, most organic ligands are electrically and/or electrochemically inactive. Particularly, in the case of bulky organic ligands bound to the surface of active nanomaterials, they can significantly restrict the electron transfer between neighboring active materials. For example, thin films assembled from tetraoctylammonium bromide (TOABr)-stabilized Au NPs (TOA-Au NPs), oleylamine (OAm)-stabilized indium tin oxide NPs (OAm-ITO NPs), or poly(vinyl pyrrolidone)

© 2021 Wiley-VCH GmbH

(PVP)-stabilized Ag NWs (PVP-Ag NWs) do not exhibit electrically conductive properties without effective removal of their bulky organic ligands. Based on these critical effects of organic ligands on the charge transfer kinetics within electrodes, recent research efforts have focused on the interfacial surface chemistry of active nanomaterials. Although a few studies and reviews on the surface chemistry and interfacial engineering of nanomaterials themselves have been reported in the field of lithium-ion batteries and bioelectrochemical applications,[24,25] few on the scalable assembly of active materials with such interface designs have been reported.

Among various solution approaches using interfacial surface chemistry, layer-by-layer (LbL) assembly, which is based on complementary interactions between two or more different components, is potentially the most versatile and powerful approach for preparing organic/organic or organic/inorganic nanocomposites with controlled film thickness, chemical composition, and functionality on various substrates irrespective of their size or shape.[26–30] On the basis of these advantages of LbL assembly, substantial research progress has been made in the development of high-performance energy electrodes that can compensate for the critical drawbacks originating from the abovementioned traditional deposition processes and enhance the charge transfer efficiency within electrodes. For example, electrostatic interaction-induced LbL assembly between cationic components with protonated amine groups ($-NH_3^+$ groups) and anionic components with carboxylate ion groups ($-COO^-$ or SO_3^- groups) in aqueous media could be effectively used for the preparation of nanocomposite films composed of electrostatically charged active components [e.g., cationic or anionic conducting polymers, NH_3^+- or COO^--functionalized CNTs (CNT–NH_3^+ or CNT–COO^-), rGOs with electrostatic charges (r-GO-COO^- or r-GO-NH_3^+), anionic enzymes, anionic pseudocapacitive (PC) NPs, anionic metal NPs, and/or their mixed components] on various substrates.[31–37] Additionally, this LbL approach based on the solution dipping process has enabled active components to be uniformly deposited onto a variety of porous and/or flexible substrates, such as paper, cotton, elastomers, polyester, and nylon, as well as on flat and curved substrates.[38–42] Furthermore, these LbL-assembled multilayer films with desired functionalities could be directly applied to various electrochemical electrodes for rechargeable batteries, supercapacitors, biofuel cells, piezoelectric devices, and electrochromic devices without the use of any insulating polymer binders.[24,43–47]

Despite these notable advantages of LbL assembly, several limitations should be further resolved in designing high-performance flexible energy electrodes. First, electrostatic LbL assembly using charged active components generally induces a low packing density (<30%) due to the long-range electrostatic repulsion between the same charge components.[48,49] A large separation distance between laterally adjacent active components acts as a contact resistance that interrupts the charge transfer within the electrodes. Therefore, to successfully prepare energy electrodes using LbL assembly, the packing density of LbL-assembled active components should be preferentially increased using other complementary interactions such as hydrogen bonding or covalent bonding in organic media without electrostatic repulsion. Second, the use of bulky polymer linkers for LbL assembly significantly restricts the charge transfer between vertically adjacent active components. For example, LbL-assembled (anionic Au NP/cationic polyelectrolyte (PE))$_n$ multilayer films normally exhibit extremely low electrical conductivity close to the insulating property due to the presence of bulky PE layers sandwiched between adjacent Au NPs. As mentioned earlier, Au NPs stabilized by bulky organic ligands, such as TOABr or oleic acid (OA), have insulating properties due to the bulky organic ligands between neighboring Au NPs. In the case of PC NPs (i.e., Fe_3O_4 NPs, MnO_x NPs, SnO_2 NPs, etc.) with high energy storage capacity but poor conductivity, the bulky organic ligands (e.g., OA, palmitic acid (PA), or OAm) adsorbed on the surface of the PC NPs also seriously limit the charge transfer between neighboring PC NPs, resulting in poor charge storage capacity. Therefore, minimizing the amounts of unnecessary organics (particularly organic ligands and/or linkers bound to the surface of active materials) in the electrode is also critical for designing various high-performance energy electrodes, including energy harvesting, conversion and storage electrodes.

In this review, we summarize the interfacial design approaches and recent progress in 3D porous textile-, paper-, and elastomer-based energy electrodes that can be used for energy harvesting, conversion, and storage (**Figure 1**). The main focus of this review is to discuss significant challenges in the area of porous and flexible energy electrodes and potential strategies to address critical obstacles to the development of high-performance energy electrodes. First, we introduce textile-, paper-, and elastomer-based electrical conductors prepared by various approaches. Then, the recent progress in flexible energy harvesting, conversion, and storage electrodes using a variety of interface-controlled assembly approaches is introduced in this review article. Herein, we discuss how interfacial control of active materials can effectively achieve improved charge transfer kinetics within the electrodes. Finally, we present a brief perspective on the direction of interfacial engineering for the realization of high-performance energy electrodes.

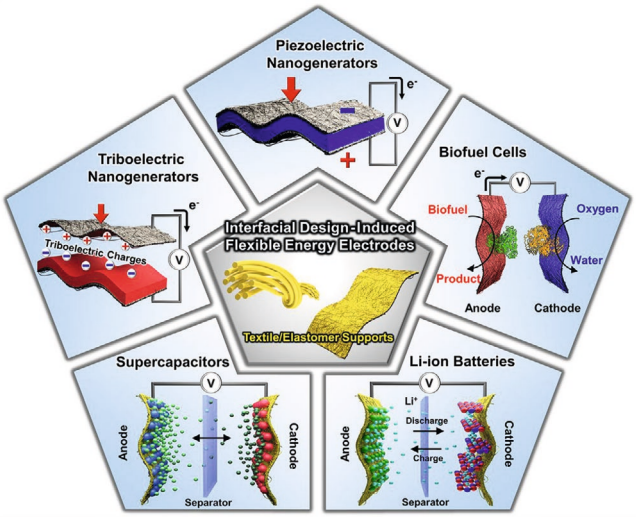

Figure 1. Schematic illustration of the potential applications of various flexible energy devices based on interfacial design.

© 2021 Wiley-VCH GmbH

2. Flexible Conductors Based on Textile Materials and Elastomers

Conventional rigid or poorly deformable substrates, such as metal or plastic plates, have significant limitations in fully addressing the various mechanical stresses encountered in daily human activities. Most commercially available flexible/wearable electronics today only show nondeformable "curved" shapes. Although recent great achievements, such as foldable cellular phones with reliable mechanical performance, have surprised and motivated the global electronics markets,[50] the degree of deformation is still limited to a repetitive bending motion concentrated on a specific area. All functions (especially mechanical properties) of the flexile/wearable electronics under development are focused on human lifestyles, so ultimately, the devices will be used in a form more closely fitting the human body (i.e., carried around by hand, worn like clothing, patched on the skin, and implanted under the skin). In this regard, the substrate must preferentially cover various topological features of the human body. Particularly, considering that in terms of mechanical properties, textile materials and elastomers have unrivaled superiority, such as excellent tolerance to mechanical stresses, low Young's modulus, high mechanical resilience, and toughness,[51] they can have a comparative advantage over other material substrates for flexible/wearable electronics.

As some of the oldest and most familiar materials in human civilization, textile, or paper materials have been actively applied to a myriad of fields, such as clothing, decoration, architecture, and printing, due to their human (eco)friendly nature and easy processability. Particularly, various natural or synthetic textiles, including cotton, wool, silk, polyamide, polyester, and polyacrylonitrile, have a highly porous structure,[52] allowing a high loading of other functional materials; thus, they can act as a functional reservoir in addition to a mechanically flexible substrate. Furthermore, textiles and cellulose paper generally have numerous hydrophilic surface functional groups, such as hydroxyl, carboxyl, and amino groups, which can offer an opportunity for effective combination with other functional nanomaterials through various dry and wet coating techniques. In particular, the presence of hydrophilic moieties on their surface allows good solution wettability that enables uniform and dense deposition of conducting materials in all accessible surface areas of textiles or paper.

Elastomers are another promising substrate material for realizing wearable electronics. Unlike conventional textiles without stretchability, elastomers exhibit excellent restoration behavior under repetitive and severe stretching deformation (i.e., a low Young's modulus and a high failure strain value), which makes them promising support materials for application to various integrated patchable/wearable electronics, such as body motion sensors, portable medical devices, and energy units.[53–56] Elastomers with rubber-like elastic properties are basically synthetic polymers composed of repeating subunits such as urethane, acrylate, ester, and siloxane. These elastomers can generally be classified into thermoplastic and thermosetting polymers according to the formation mechanism of the subunits. In general, thermoplastics are composed of linear polymer chain networks with weak van der Waals interactions between each subunit, while thermosetting polymers with crosslinked structures are based on covalent bonds and are relatively heat resistant (but irreversible). PDMS, the most widely applied elastomer for stretchable conductors, exhibits a very low Young's modulus of <3.6 MPa at 100% strain, showing exceptional mechanical properties. However, as mentioned earlier, most of the synthetic elastomers exhibit low surface energy (i.e., hydrophobicity). Therefore, additional surface modification processes for introducing hydrophilic functional groups onto hydrophobic elastomers or encapsulation processes have been conducted for efficient deposition of other functional materials.

In addition to these efforts exploiting substrates with desired physical and mechanical properties, a number of studies have been performed to convert insulting textiles or elastomers to conductive ones through effective deposition of conducting materials on their surfaces.[57] In general, the electrical conductivity of a composite electrode strongly depends on the structural characteristics of the formed conducting network as well as the intrinsic conductivity of the conductive materials. For example, even if conducting NPs with the same size and shape are homogeneously coated onto substrates, a reduction in the interparticle distance between neighboring NPs (i.e., an increase in the NP packing density) leads to the percolative behavior of electrons being more easily induced.[58,59] However, preservation of the porous structure and mechanical properties of textiles and elastomers in the dense coating process for more facile electron transfer (or high electrical conductivity) is highly desirable. Effectively preserving the porous structure of such flexible materials not only facilitates ion transport of electrolyte-based energy conversion/storage electrodes but also provides breathability and wearability of skin contact-type energy harvesters (more details will be discussed in a later section).

This section reviews the progress in textile-, paper-, or elastomer-based electrical conductors prepared by introducing various types of conductive materials (carbon and metal nanomaterials). Herein, we focus on a variety of methodologies for introducing such conductive materials and further discuss their characteristics and advantages/weaknesses, especially in terms of applicability to energy electrodes.

2.1. Dry Coating Methods

2.1.1. Vapor Phase Deposition

The vapor phase deposition technique is a representative bottom-up-coating (or growth) method that has been steadily applied to various semiconductor or ceramic applications.[60–62] Such approaches can be categorized into two different types, chemical vapor deposition (CVD) and physical vapor deposition (PVD), depending on how the target (source) material is vaporized. In general, CVD is performed under high temperature and high vacuum conditions to produce high-purity precursor vapor, thus limiting the application of this vapor deposition type to thermally sensitive substrates such as soft textile materials. Although the process temperature may be lowered by applying other energy sources, such as electrons (plasma-enhanced CVD, PECVD) or photons (photoinitiated CVD, PICVD), the temperature is still not suitable (≈600 °C[63,64]) for typical textile materials or elastomers, and in addition, short-wavelength

© 2021 Wiley-VCH GmbH

ultraviolet (UV) light can attack the chemical chains of textile materials, which seriously damages their mechanical stability. Therefore, the conventional CVD process has limited choices for target materials.[65,66]

Additionally, magnetron sputtering, a representative PVD technique along with electron (e)-beam evaporation, can form high-quality thin films on various substrates based on various metallic species (e.g., copper (Cu), silver (Ag), Au, and aluminum (Al)) at room temperature.[67–70] In the sputtering process, the electric field between the target materials and the substrate induced by the applied external discharge current generates a number of free electrons, positively charged inert gas atoms (e.g., argon, nitrogen, or a mixture thereof), neutrons, etc. The generated energetic gas ions are then accelerated to the target materials and collide with their surfaces. As a result, the atoms ejected from the target surfaces are deposited on the substrate, coating it at a specific rate.[71] Using this coating process, the sputtering method has been applied to the fabrication of textile-, paper-, or elastomer-based flexible conductors.[67,72–74] Siegel et al. reported commercially available paper-based electronic circuits with metal-like electrical properties as well as mechanical stability through sputtering (or evaporation) deposition (**Figure 2**a–c).[74] These paper-based conductors can be effectively applied to various types of transient or deformable electronics for military and homeland security and biodegradable devices. The formed paper-based electronic circuits can also be easily cut into a variety of desired shapes and be easily burned (Figure 2a,b). However, the formed paper-based electronic circuits exhibit relatively unstable electrical conductivity during curvature degree-dependent folding tests (i.e., severe conductivity deterioration after 10 repetitive folding tests) (Figure 2c). These damages are mainly due to poor adhesion between neighboring metallic components as well as between metallic components and the paper substrate.[75,76]

To date, various types of metallic patterns or thin films have been deposited on soft materials through metal sputtering or e-beam evaporation (another representative PVD approach) techniques at room temperature to create flexible electronic circuits.[73,77–79] Although the flexibility and the outermost surface morphology of the substrates can be preserved by modifying the deposition process conditions (i.e., controlling the deposition time or using textiles with larger pore sizes), the conductive layer is mostly concentrated on the outermost region rather than throughout the entire area of the electrode ranging from the exterior to the interior.

In the typical sputtering process, continuously deposited metal atoms on the surface of the substrate simultaneously form nanoclusters through the nucleation and growth mechanism.[80–82] Such enlarged or aggregated metal nanoclusters can create well-connected conducting networks that act as electron pathways. However, at the same time, this growth mechanism of metal clusters can block the pores of the substrate, thereby significantly decreasing the ion penetration kinetics into the inner region of the porous material-based electrodes.[82,83] Importantly, such a phenomenon can make efficient utilization of the large surface area of textiles or paper difficult, which also has a detrimental effect on applications such as energy storage electrodes that require a high loading (or coverage) of active materials for higher capacity. Furthermore, an excessive increase in the film thickness due to the continuous growth of metal clusters can cause mechanical breakage accompanied by a short circuit of electron flow under various external deformations.[74,84,85] These phenomena are more critical for elastomer-based conductors with stretching deformation. Recently, without fully utilizing the elastic property of metal-coated elastomers, a limited electrode design similar to a helical structure has been proposed.[67]

Thus, to fabricate textile-, paper-, or elastomer-based conductors with highly porous structures and metal-like electrical conductivities as well as good mechanical properties using sputtering or e-beam evaporation deposition methods, the various process parameters (i.e., types of target material, discharge current, deposition time, substrate-to-target distance, pore structure of textile substrates, and interaction between each component) should be minutely controlled.

2.2. Solution-Processable Coating Methods

Solution-based coating methods have attracted much attention because they can effectively realize a large-area product with a relatively simple process without the need for expensive deposition equipment. As mentioned earlier, a number of hydrophilic groups on substrates allow good solution wettability, which is highly effective in solution-processable coating for various hydrophilic conducting materials. Additionally, such functional groups can tightly immobilize incoming conductive materials through strong chemical and/or physical bonding, thereby providing excellent mechanical stability. In this case, the preparation of conductive materials with a high dispersion stability in a deposition solution is an essential prerequisite for solution-coating approaches.[86,87] This section discusses the various solution-based coating methods for realizing textile-, paper-, and elastomer-based conductors.

2.2.1. Electroless Plating/Electroplating

Solution-based metal plating can be classified into electroless plating and electroplating approaches.[88,89] First, electroless plating can deposit a variety of metal, metal oxide, and alloy films onto metallic or nonmetallic substrates through chemical reduction of metal ions without an external current and/or potential.[90–92] To effectively form a metal layer on porous substrates at room temperature, catalysts capable of efficiently reducing metal ions with a reducing agent must be stably and uniformly introduce into the substrate.[93–95] In particular, the use of a proper catalyst can control the electron transfer kinetics and activation barrier in the overall reactions, which affects the reduction behavior of metal ions and the resulting film quality.[96] Liu et al. reported that a metallic cotton yarn conductor could be prepared by scalable electroless deposition of Ni, and additionally, it could be applied to a current collector for a flexible energy storage electrode (Figure 2d–g).[97] In this process, a copolymer (poly(METAC-*co*-MPTS)[98]) was covalently grafted onto the surface of the cotton yarn to immobilize $PdCl_4^{2-}$ (from a $(NH_4)_2PdCl_4$ solution) as a catalyst for efficiently accelerating Ni deposition.[99] The effectively

© 2021 Wiley-VCH GmbH

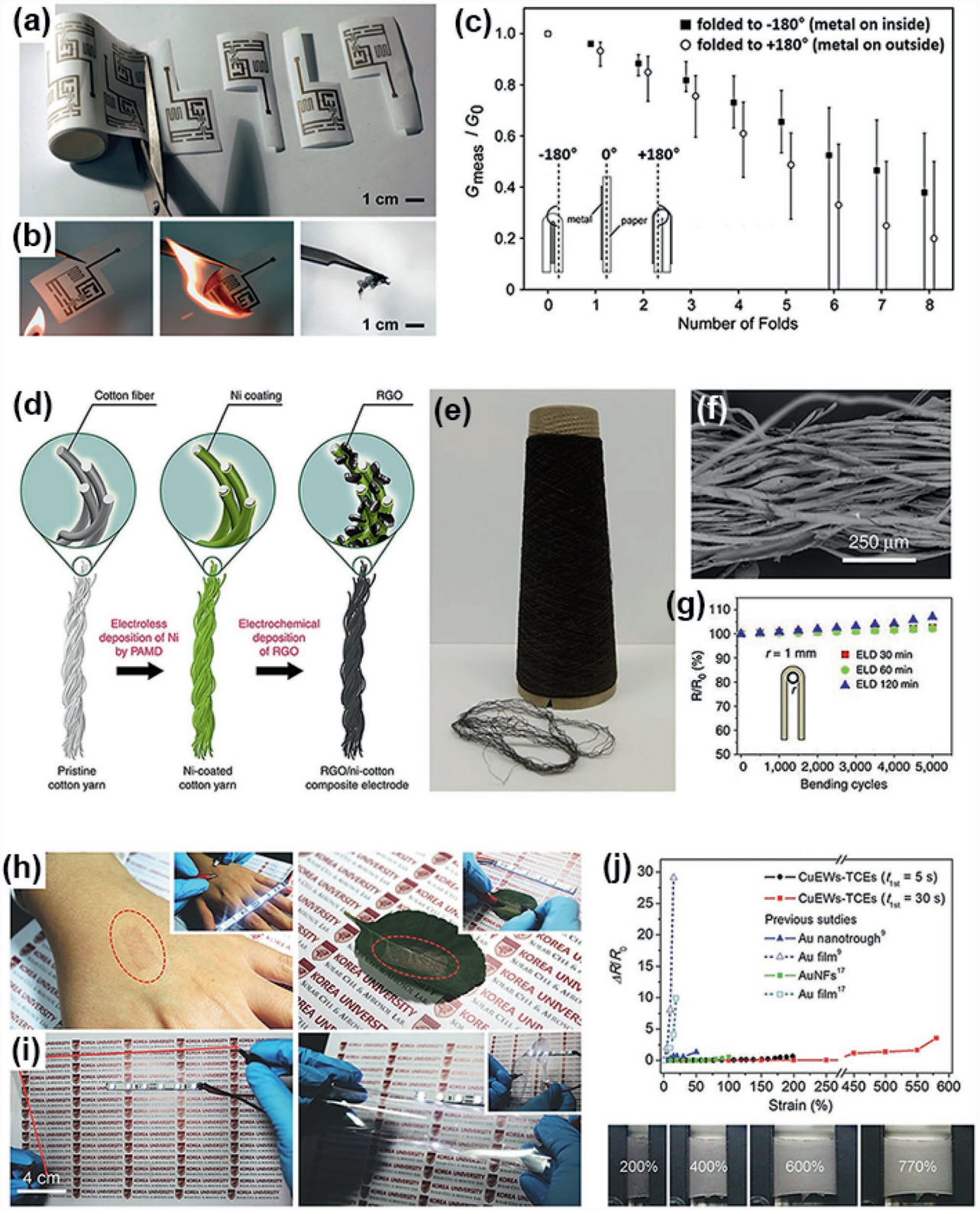

Figure 2. Preparation of flexible conductors. Photographs of a) cutting and b) burning tests of commercial cellulose paper-based electronic circuits prepared by PVD (i.e., sputtering or evaporation). c) Variation in the conductivity ratio (G_{meas}/G_0) of paper-based electronic circuits as a function of mechanical folding number. G_{meas} and G_0 indicate the conductivities in the bent and initial states of the paper-based electronic circuits, respectively. The inset illustrates the folding tests with ±180°. a–c) Adapted with permission.[74] Copyright 2010, Wiley-VCH. d) Schematic illustration of the preparation of a cotton yarn-based conductor and a supercapacitor electrode based on it. PAMD and RGO are abbreviations for "polymer-assisted metal

© 2021 Wiley-VCH GmbH

deposited copolymer layer enables uniform coating of a Ni layer onto the cotton yarn, providing a well-ordered conductive fibril structure (Figure 2f). The electrical resistance of the formed metallic cotton yarn gradually increased from 2.2 to 1.3 Ω cm^{-1} with increasing electroless deposition (ELD) time from 30 to 120 min, which was almost maintained even after 5000 repeated bending deformations (Figure 2g). Although the deposition of a thicker metal layer (≈340 μm) on the cotton surface could improve the mechanical toughness as well as the electrical conductivity, an increase in the mechanical stiffness of the yarn conductor (or brittleness of the metal layer) was unavoidable. In contrast, to maintain the mechanical properties of the flexible substrate, the deposition of a thin metal layer (thickness < 100 nm) led to insufficient coverage of metal clusters, which significantly reduced the electrical conductivity.[92] Particularly, this electroless plating approach requires minute control of various parameters, such as the concentration of active species (i.e., metal ion, reductant, and catalyst), temperature, and pH of the solution, closely related to the reaction kinetics, which have critical effects on the coating qualities of materials deposited onto porous textiles.

This electroless metallization has also been conducted on elastomers.[100,101] In this case, surface functionalization (e.g., silanization) is first performed to form hydrophilic functional sites that can anchor incoming metal particles.[102] However, the quite different tensile characteristics between the elastomer and the deposited metal layer can cause structural fractures upon stretching, interfering with the flow of electrons. To solve this issue, electroless deposition was performed on a prestrained elastomer substrate.[101,103] Wang et al. reported that stretching the PDMS substrates before depositing the Cu layer led to a buckled surface morphology after releasing the substrates, which showed a highly stable metallic conductivity of ≈1.5×10^5 S cm^{-1} at 300% linear strain.[101] This unique structure could provide good adhesion stability between the elastic substrate and the active materials[104,105] and thus could be effectively applied to various wearable energy devices.[106,107]

Since electroplating, which effectively activates metal deposition, can only be performed on conductive substrates, conductive materials such as metal particles, carbon materials, or conducting polymers should be preferentially introduced through various approaches, including wet (i.e., electroless plating) or dry (i.e., sputtering, e-beam evaporation, or carbonization) processes.[54,108,109] In the electroplating process, because the metal ions are first adsorbed and then electrically reduced on the substrate (i.e., cathode side) with conducting sites, the surface coverage of conducting seeds on the substrate is very important for uniform deposition of the metal layer. An et al. reported that electrodeposition of a Cu layer onto electrospun polyacrylonitrile (PAN)-based elastomeric nanofibers could produce a transparent flexible conductor (Figure 2h–j).[110] For this, the initial electrical property of the electrospun PAN-based nanofibers was first provided by platinum seeding. After the electroplating process, the fiber junctions were interconnected through the electroplated Cu, significantly lowering the contact resistance at all junctions. Additionally, the electroplated nanofibers should be dried in an inert atmosphere to avoid oxidation of the deposited Cu layer. These conducting nanofibers showed excellent electrical stability, demonstrating that they could be applied to multifunctional patchable or large-area electronics (Figure 2h,i). In particular, the formed elastomer electrodes showed high functionalities, such as high transparency (T = 97%), a good electrical property (0.42 Ω sq^{-1}), and an excellent elastic property. More interestingly, the Cu-electroplated conducting fiber mats showed superior electrical conductivity retention even at 770% strain, outperforming the previously reported metallic elastomers (Figure 2j).[111–115]

2.2.2. Printing

Screen or inkjet printing with conducting inks (i.e., based on conducting polymers, carbon materials, and metal NPs/NWs) is one of the fastest and simplest ways to create a flexible conductor with desired patterns.[116–121] In particular, the highly porous structure as well as the hydrophilic properties of textiles and paper facilitates the penetration and subsequent adhesion of hydrophilic conducting inks or fillers by capillary forces. Additionally, such deposition behavior can be further adjusted by controlling the fluid dynamics of the conducting inks and the surface properties of the substrates.[122–125] Particularly, a certain level of viscosity is highly required for better printing resolution of conducting ink, which can be controlled by adjusting the amount of metallic filler in specific solvents or by introducing additives (e.g., a binder, a surfactant, and/or a rheology modifier).[126,127] At the same time, although highly viscous conducting inks are suitable for fabricating conductive patterns with high process resolution, these inks allow the formation of a conducting film on only the upper side rather than throughout the entire region of textiles due to their poor penetration behavior, significantly limiting the efficient utilization of the internal area of porous substrates.[128,129]

Carbon materials (i.e., CNTs, graphene, and activated carbon) have been actively used as conducting fillers to form stable conducting networks due to their high electrical conductivity and flexibility.[121,130–132] However, because of their intrinsic property of forming bundle composites (with themselves or other materials) via van der Waals interactions,[133] organic surfactants are essential to maintain dispersion stability for high-quality coating (i.e., smooth and uniform deposition) in the printing

deposition" and "reduced graphene oxide," respectively. e) Photograph of 500 m long mass-produced Ni-coated cotton yarn conductors. f) Scanning electron microscopy (SEM) image of the yarn conductor with Ni deposition for 60 min. g) Bending cycle number-dependent electrical resistance (R/R_0, %) of yarn conductors with different electroless deposition (ELD) times (30, 60, and 120 min). The inset shows an illustration of the bending test. d–g) Adapted under the terms of the CC-BY Creative Commons Attribution 4.0 International License.[97] Copyright 2015, The Authors, published by Springer Nature. h) Photographs of Cu-electroplated transparent elastomer conductors applied to skin and a leaf. i) Large-scale application of the elastomer conductor to poly(ethylene terephthalate) (PET). The insets in Figure h,i show LED operation using the elastic conductors. j) Change in electrical resistance ($\Delta R/R_0$) with strain (%) of various elastic conductors (top), and photographs of stretching tests (bottom). h–j) Adapted with permission.[110] Copyright 2016, Wiley-VCH.

© 2021 Wiley-VCH GmbH

process. However, polymeric surfactants existing between neighboring CNT fibers seriously obstruct facile electron percolation in CNT bundle networks. As an alternative, surface functionalization processes (e.g., acidic solution treatment or photonic irradiation) of CNTs have been conducted to improve their dispersion stability and provide their physical adsorption sites on the substrate.[134,135] However, these harsh surface treatments resulted in the formation of many defects, with decreased electrical conductivity.[136]

Metallic NP (or NW)-based conducting inks can provide higher electrical conductivity than carbon material-based inks. However, in the case of these inks, a postsintering process at high temperature is required to eliminate the polymeric surfactants (or stabilizers) and form a well-connected metal network, which is not suitable for heat-sensitive common soft flexible substrates.[137] To resolve these drawbacks, electrical treatment, a particle-free reactive metal ink-based approach, or a chemical sintering approach at a soft sintering temperature below 100 °C have been proposed.[86,128,138,139] For example, the polycation poly(diallyldimethylammonium chloride) (PDAC) can act as a coagulant for an as-printed Ag NP composite, forming a highly conducting metal layer (sheet resistance of $\approx 5 \times 10^{-2}$ Ω sq^{-1}) on paper substrates without a heating process at a specific composition ratio (PDAC/Ag ≈ 0.2) (**Figure 3**a,b).[86] In this case, the cationic PDAC aggregated with the anionic polyacrylic acid (PAA)-capped Ag NPs (PAA-Ag NPs) deposited on the substrate through a charge neutralization mechanism, simultaneously causing room temperature sintering (Figure 3b). This phenomenon can be explained by the metallic fusion behavior induced by a reduction in the interparticle distance.[140] Similarly, self-sintering of PAA-Ag NPs at room temperature could occur via ligand replacement of bulky PAA with the Cl^- ions of dissolved NaCl during the drying of water-based ink (Figure 3c).[139] This ligand exchange reaction occurred because the Ag NPs have a higher affinity for halides (especially the halogen atom), such as NaCl, HCl, and KCl, than for the native PAA ligand (i.e., the carboxylate ion).[141] As a result, the unstable surface state of Ag NPs led to spontaneous agglomeration and coalescence of neighboring Ag NPs, forming an interconnected metal network with high electrical conductivity (≈40% that of bulk Ag).

Park et al. reported that a highly conductive elastomeric fiber could be prepared by chemical reduction of inkjet-printed Ag precursors ($AgCF_3COO$ (15 wt%) in ethanol) on electrospun rubber fibers (i.e., poly(styrene-*block*-butadiene-*block*-styrene) (SBS)).[116] The rubber fibers were swollen by adsorbing the precursor solvent (i.e., ethanol), and at the same time, the Ag precursor ions in the solvent penetrated into the fibers. After drying at room temperature, when hydrazine as a reducing agent was dropped onto the shrunk rubber fibers, chemically reduced Ag NPs were formed on both the inside and outer shell of the fibers. The formed conductive elastomer showed an excellent electrical conductivity of ≈2200 S cm^{-1} at 100% strain. That is, although partial mechanical damage to the Ag NP shell occurred after the stretching deformation, the electron percolation could be maintained by the well-connected Ag NPs on the rubber fibers. Such highly stretchable conductors have also been developed using a functional conducting ink consisting of a mixture of Ag flakes, a water-based fluorine surfactant, and a fluorine copolymer dispersed in an organic solvent.[142] In this case, the surfactant used provides good affinity between the Ag flakes and copolymer, thus promoting the formation of Ag networks. The formed conductor exhibited a high electrical conductivity of 738 S cm^{-1}, and 182 S cm^{-1} was recorded at 215% strain.

2.2.3. Dip Coating

Dip coating is based on physical or chemical interactions between the substrate and adsorbing materials. Therefore, the complementary interfacial interactions between both components are closely related to the stability, uniformity, and surface coverage of the coated films.[143,144] Hu et al. reported that fabric-based conductors with excellent electrical properties (sheet resistance ≈1 Ω sq^{-1}) and high mechanical flexibility could be prepared through simple dip coating of single-walled CNT (SWNT) inks and subsequent mechanical/chemical treatments (i.e., mechanical pressing and chemical doping) (Figure 3d–g).[38] In this case, the deposited SWNTs could form a conformal coating on the cotton fiber (Figure 3d–f) or polyester fabric substrates (Figure 3g) with highly disordered bundle networks. Furthermore, the authors reported that the highly porous structure of the substrates was well preserved after dip coating of SWNTs (Figure 3f,g), which could be advantageous for improving the electrolyte wettability and ion conductivity. Similarly, Steven et al. reported that a flexible spider silk (SS)-based conductor could be prepared by mechanical mixing and/or dip coating of amine-functionalized multiwalled CNTs (i.e., MWNTs) under mechanical pressing and shearing for easier electron percolation.[145] In this case, the amine groups on the MWNTs were electrostatically bound to the carboxylic acid groups of the SS fibers. Additionally, the formed conductors exhibited a typical 3D variable-range-hopping (VRH) conduction behavior with an electrical conductivity of ≈15 S cm^{-1} (at room temperature) and good mechanical flexibility. Furthermore, based on these carbon material (e.g., CNT, activated carbon, and graphene)-based dipping and dry coating processes, a number of studies on textile- or paper-based flexible current collectors (or supports) for various types of energy conversion and storage devices have been reported.[38,120,146–149]

However, because the surface functionalization through covalent attachment of the active components involves the formation of defect sites in the carbon materials, the electronic (or mechanical) properties are decreased in proportion to the oxidation process, consequently affecting the electrochemical performance.[136] Nian and Teng investigated the influence of oxygen-containing functional groups on the surface of a carbon material on the impedance behavior.[150] As the oxidation content on the surface increased, the diameter of the semicircle in the high-frequency region, which is mainly associated with the contact resistance between the electrode and the current collector,[151,152] notably increased. Surface modification through noncovalent interactions (i.e., van der Waals and π–π interactions), such as wrapping or adsorption by polymeric species, hydrophilic organic compounds, surfactants, and biomolecules, does not affect the intrinsic properties of carbon materials, including the high electrical conductivity and mechanical stability.[153–157] However, the addition of such bulky insulating

© 2021 Wiley-VCH GmbH

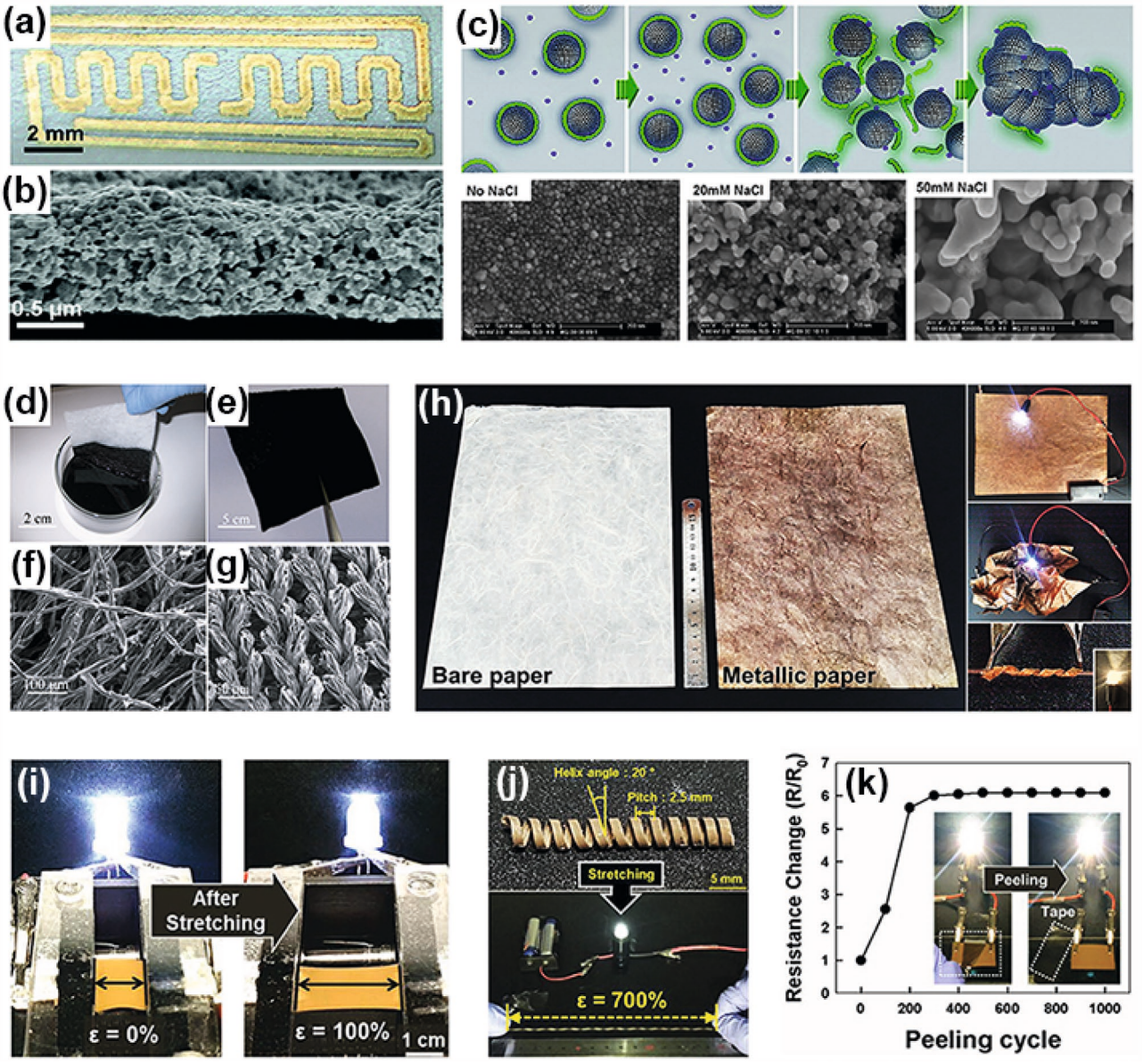

Figure 3. Preparation of flexible conductors by a solution-based approach. a) Photograph of conductive pattern (Ag)-printed cellulose photo paper. b) Cross-sectional high-resolution (HR)-SEM image of a patterned Ag composite. a,b) Adapted with permission.[86] Copyright 2010, American Chemical Society. c) Schematic illustration of the in situ sintering process for Ag NPs through ligand detachment (top), and corresponding morphological details monitored by SEM images for different NaCl concentrations. Adapted with permission.[139] Copyright 2011, American Chemical Society. d) Photographs of dip coating of a cotton fabric sheet into an SWNT dispersion and e) its large-area application (10 cm × 10 cm). Planar SEM images of SWNT-coated f) cotton sheet and g) polyester fabric. d–g) Adapted with permission.[38] Copyright 2010, American Chemical Society. Photographs of metallic h) cellulose paper prepared by ligand exchange reaction-induced LbL assembly. Adapted with permission.[160] Copyright 2017, Springer Nature. i) Photographs of a Au NP-coated PDMS conductor connected to LEDs before and after stretching deformations. j) Electrical stability test of a helical-structured elastomer conductor under stretching. k) Change in resistance (R/R_0) under repetitive peeling using commercial scotch tape. i–k) Adapted with permission.[162] Copyright 2020, Wiley-VCH.

materials to the conductive materials causes a significant increase in the internal resistance of the conductor.

Unlike CNT materials that can self-entangle to form bundle composites with fibril-based textiles, the metal NPs used in slurry processes generally require polymeric binders to form a stable metal NP-based conductive film. However, as mentioned earlier, since the insulating polymeric binders within the formed metal NP composite film can increase the internal resistance, additional posttreatments (i.e., sintering or welding for metallic connection) are essentially required to achieve the desired electrical properties.[158] Furthermore, the bulky organic ligands bound to the metal NP surface, which can provide good dispersion stability and desired physical characteristics, also seriously restrict the electron transfer within the NP-based composite electrodes, resulting in poor electrical conductivity.[159] Therefore, these polymeric binders and bulky organic ligands

© 2021 Wiley-VCH GmbH

should be removed under mild process conditions to effectively realize highly conductive textile conductors.

Recently, metal NP-based films with high mass density have been reported to be formed on various types of flexible materials (cellulose paper, polyesters, and nylon fabrics) via ligand-controlled LbL assembly (Figure 3h).[47,160,161] This approach highlighted that metal NPs covered with hydrophobic ligands could be directly deposited onto substrate materials using the ligand exchange reaction between bulky organic ligands and small molecule linkers during simple dip coating. The formed metal NP film-coated textile or paper substrate exhibited metallic electrical conductivity without any additional posttreatment. Additionally, these metallic textiles perfectly preserved the inherent mechanical properties and porous structure of the raw materials, which is greatly advantageous for use as a current collector for energy electrodes. Specifically, upon alternating LbL deposition of TOA-Au NPs and amine-functionalized small molecule linkers (i.e., tris(2-aminoethyl) amine, TREN), the hydrophobic TOA ligands bound to the surface of the Au NP are completely replaced by TREN due to the higher affinity of the Au NP with the amine (-NH_2) moieties of TREN than with the native ligands.[160] In this case, the separation distance between neighboring Au NPs without electrostatic repulsion is significantly reduced to almost 1 nm due to the use of small molecule linkers (i.e., $M_w \approx 146$ g mol^{-1}), which leads to partial metallic fusion of Au NPs. In particular, these fused Au NPs create a well-connected porous network, inducing bulk metallic conduction behavior.[140]

Basically, the electron percolation is closely related to the amount (or density) of conducting fillers within the composite film. In particular, spherical metal NPs need a higher loading amount (i.e., higher packing density) than metal NW-based conductors to allow efficient percolation networks. However, such densely coated metal NP films can be susceptible to a high degree of stretching deformation due to the different strain moduli. Although loosely packed metal NPs within the elastomeric polymer can preserve the electrical conductivity under stretching due to strain-induced reorganization of metal NPs,[34] numerous metal NP layers (≈1500 layers) and additional posttreatments (i.e., heating and mechanical pressing) are required to overcome the percolation threshold.

Recently, Lee et al. reported a wrinkled structure metallic elastomer electrode prepared by ligand-controlled LbL assembly (or ligand exchange reaction-induced LbL assembly) between hydrophobic Au NPs and NH_2-functionalized organic linkers ($M_w \approx 146$ g mol^{-1}) in organic media (Figure 3i–k).[162] The Au NPs are covalently bonded to the thiol (SH) group-functionalized elastic substrate (PDMS) and/or the NH_2-functionalized linkers, forming densely packed Au NP multilayer networks. In this case, the solvent-induced buckled structure of PDMS exhibited an exceptional electrical conductivity of 170 000 S cm^{-1} in the initial state and 11 000 S cm^{-1} at 100% strain with metallic conduction behavior (Figure 3i). In addition, the helical-structured conductive elastomer showed notable electrical property retention at 700% strain (Figure 3j). In general, the hydrophobic nature of PDMS limits the stable deposition of functional NPs on the surface, causing poor mechanical stability of the formed NP layer. However, in this work, all the Au NPs within the film were covalently bonded with PDMS and/or neighboring Au NPs, maintaining a high electrical conductivity under repetitive peeling tests using commercial scotch tape (Figure 3k). Furthermore, the excellent mechanical and electrical stabilities of the abovementioned elastic conductor were more evidently demonstrated through additional application to the contact electrode of triboelectric nanogenerators (TENGs).

3. Flexible/Wearable Energy Applications

The realization of flexible/wearable energy devices that are fully compatible with various mechanical deformations remains challenging because the respective functional components (i.e., active materials, substrate (support), separator, and/or electrolyte) of energy devices have different mechanical properties and interfacial interactions. That is, the different mechanical characteristics between the flexible substrate and the relatively stiff active layer cause mechanical slipping or delamination under repeated mechanical deformations, resulting in severe failure in the power output.[19,163] In this regard, the use of nanomaterials can provide not only an extremely large surface area that allows high loading of active materials but also a better tolerance to mechanical deformations than bulk materials.[164,165] Particularly, to ensure the mechanical stability of nanomaterial-based flexible electrodes, favorable interfacial interactions between the electrically or electrochemically active materials and substrate should be obtained.

The interparticle distance between adjacent active NPs is closely related to the facile charge transport among all components of the electrode, influencing the energy efficiency (for energy harvesting, conversion, and storage) and output performance. As mentioned earlier, the presence of unnecessary insulating organics (i.e., polymer binders and/or bulky organic ligands) increases the interparticle distance, restricting charge transfer between neighboring active NPs. Therefore, the interface design, including interfacial interactions and interparticle distance, is very significant for developing flexible energy devices with reliable output performance. Although an ideal interface design cannot be realized, the design can be optimized when all the components in the electrode are uniformly distributed without agglomeration or segregation. That is, recent studies have demonstrated that a well-developed interface design in the fabrication of nanocomposite electrodes can satisfy both requirements of structural stability and facile charge transfer within the electrodes. These reports also suggest that various approaches for appropriate interface design can be effectively applied to 3D flexible energy electrodes requiring high mechanical stability, facile charge transfer, and a high loading amount of active materials within the electrode.

The following sections review the recent progress in textile-, paper-, or elastomer-based flexible energy electrodes for energy harvesting (piezoelectric/triboelectric nanogenerators), conversion (mainly biofuel cells), and storage (rechargeable batteries and supercapacitors). Particularly, in addition to the fabrication details for the respective energy electrodes, we also discuss how the interface design affects the charge transfer kinetics and mechanical stability of such flexible energy electrodes.

© 2021 Wiley-VCH GmbH

3.1. Energy Harvesting: Piezoelectric and Triboelectric Nanogenerators

3.1.1. Brief Overview and Challenges

Piezoelectric Nanogenerators (PENGs): Piezoelectricity is the ability of a material to generate electrical charge under mechanical stress or strain. Specifically, when an external mechanical force is applied to piezoelectric materials, the deformation of the crystal structure results in a relative displacement of the charged atoms and generates an electric potential, which can induce a current through an external circuit.[166–169] Based on the piezoelectric properties of materials, PENGs harvest ambient mechanical energy and convert it into useful electricity.[5,170–174] Since Wang et al. demonstrated PENGs using ZnO nanowires, various piezoelectric nanomaterials and device designs have been reported. Recently, many researchers have demonstrated flexible or wearable substrate-based PENGs for harvesting biomechanical energy from body movement, which is one of the most abundant mechanical energy sources in everyday life.[1,175–178]

In PENGs, a piezoelectric layer is assembled between conducting layers that transport charges, which must be mechanically stable under repetitive external stimuli. Otherwise, not only does the active layer lose the piezoactivity, but also, the conducting layers cannot circulate charges efficiently due to the generation of electrical short circuits. Accordingly, considerable research effort has been devoted to achieving a high mechanical stability of PENGs based on flexible and conductive supports. As mentioned earlier, nanosized piezoelectric materials have higher mechanical flexibility and sensitivity to small forces than bulk-sized piezoelectric materials.[179–181] Therefore, fabricating nanomaterial-based piezoelectric layers with adequate interfacial engineering is crucial for the realization of optimized flexible PENGs.

Triboelectric Nanogenerators (TENGs): Triboelectrification is based on charge generation and transfer by periodic contact/separation between two materials with different triboelectric polarities.[182–184] Thus, in the case of nanogenerators using the triboelectrification effect (i.e., triboelectric nanogenerators, TENGs), maximizing the density of the transferred charge is crucial to improve their electrical output performance.[185–187] To this end, numerous studies have been conducted on material design (e.g., triboelectric material selection, chemical modification and/or functionalization) for facile charge transfer (by increasing the difference between triboelectric polarities) and on the structural architecture (e.g., micro/nanopatterns and hierarchical surface structures) to enhance the triboelectrically charged surface area.

Specifically, in view of material design, the selection of two different triboelectric materials is one of the most crucial factors because the quantity of transferred charges directly depends on their triboelectric polarities. For example, fluorine-rich molecules or polymers have been widely used as electronegative materials because of their strong tendency to withdraw charges under physical contact.[188–190] In the case of the structural architecture, the surface of triboelectric materials serves as a reservoir for triboelectrically transferred charges, which induces an electric potential that can pump electrons through external circuits. According to a recent report, triboelectric charges can be further induced and accumulated not only at the direct contact surface area but also at the adjacent surface without direct contact.[191–194] Furthermore, considering that triboelectrification arises from physical contact/separation between two different surfaces, the contacting surface should be mechanically stable under repeated friction and various deformations. In this section, we review various strategies to improve the electrical outputs and mechanical durability of flexible TENGs through interfacial engineering from the aspects of material design and the structural architecture.

3.1.2. Interfacial Design for Flexible PENGs

One of the most widely used methods for the preparation of nanomaterial-based flexible piezoelectric layers is to blend piezoelectric nanomaterials with polymer binders such as polydimethylsiloxane (PDMS) (the used polymer binders do not have piezoelectric properties). However, when piezoelectric nanomaterials aggregate in the polymer matrix, the external mechanical stress is not evenly transmitted to the active materials, resulting in a low conversion efficiency of mechanical to electrical energy. Therefore, the interface design for a high loading amount and a uniform dispersion of the active materials has a decisive effect on the performance of PENGs. The Lee group reported that the blended mixture of CNTs and piezoelectric materials within a PDMS matrix could exhibit a higher dispersibility of piezoelectric materials than the nanocomposites without CNTs.[195–197] Moreover, they described that the added CNTs could reinforce the mechanical properties of the PDMS matrix, and at the same time, an externally applied stress could be more efficiently transferred to the piezoelectric materials (**Figure 4**a). Based on these results, they prepared piezoelectric and elastic nanocomposite films composed of lead-magnesium niobate-lead titanate (PMN-PT) particles and CNTs (Figure 4b). Then, stretchable electrodes with percolated Ag NW networks were transferred onto the surface of the abovementioned nanocomposite films, which generated electricity under various mechanical deformations, such as stretching, twisting, folding, and crumpling.

Instead of using additional dispersant materials in the nanocomposite, Zhang et al. reported piezoelectric paper using a hydrogen bonding interaction between barium titanate NPs (BTO NPs) and a polymeric support (specifically bacterial cellulose).[198] The as-prepared piezoelectric paper exhibited a high mass loading (≈80%) and a uniform dispersion of BTO NPs through hydrogen bonding between BTO NPs and bacterial cellulose, which maintained their piezoelectric property under repeated bending (Figure 4c).

Although polymeric binders, such as PDMS and cellulose, have an extremely low piezoelectric or nonpiezoelectric property, PVDF and/or its copolymers possess a relatively high piezoelectric activity based on the strong electric dipole moment, which originates from the electronegativity of fluorine atoms. Additionally, PVDF exhibits the highest piezoelectric activity in the β-phase with the all-trans (TTTT) conformation. This β-phase can be obtained via mechanical stretching and/or electrical poling under an electric field of PVDF. Particularly,

© 2021 Wiley-VCH GmbH

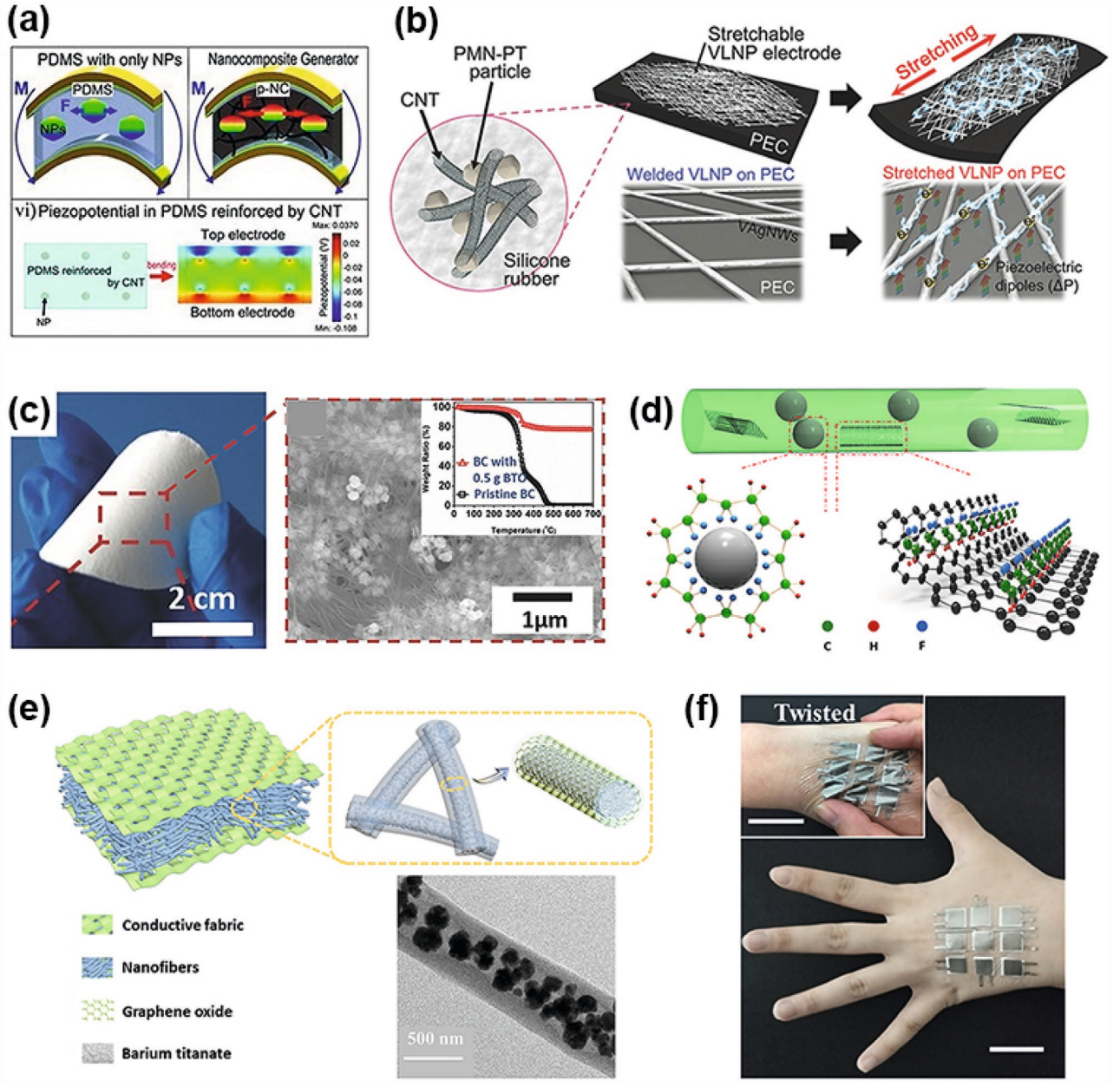

Figure 4. Incorporation of piezoelectric nanomaterials into a polymer matrix based on interfacial design approaches. a) Schematic illustration showing the roles of CNTs as dispersant and stress reinforcing agents. Adapted with permission.[195] Copyright 2012, Wiley-VCH. b) Schematic illustration of stretchable PENGs based on the elastic composite of PMN-PT particles and CNTs. Adapted with permission.[197] Copyright 2015, Wiley-VCH. c) Photograph and SEM image of BTO/BC piezoelectric paper. Adapted with permission.[198] Copyright 2015, Wiley-VCH. d) Schematic illustration showing the mechanism of β-phase formation in the PVDF-based nanocomposite. Adapted with permission.[201] Copyright 2018, Elsevier. e) Schematic illustration showing the structural design of piezoelectric skin. f) Photograph showing a demonstration of piezoelectric skin attached on a hand. e,f) Adapted with permission.[202] Copyright 2020, Elsevier.

given that the electrospinning process can induce mechanical stretching and electrical poling of PVDF at the same time, this approach is very effective in preparing PVDF with the β-phase.[199] In addition, piezoelectric mats made of electrospun nanofibers displayed high mechanical flexibility and durability, making them suitable for wearable PENG devices. However, as mentioned above, the piezoelectric properties of polymers are inferior to those of inorganic materials. Therefore, to further improve the piezoelectric performance, inorganic materials with high piezoelectric properties must be incorporated into polymer matrices.

Additionally, the piezoelectric performance of a PVDF-based nanocomposite can be improved by employing favorable interfacial interactions between neighboring components.[200] For example, Shi et al. reported that the $-CH_2/-CF_2$ dipole of PVDF could form hydrogen bonds with the hydroxyl groups

© 2021 Wiley-VCH GmbH

of the BTO surface as well as electrostatic bonds with the sp^2-hybridized carbon atom on the graphene surface, which had a synergistic effect that could induce the β-phase arrangement (Figure 4d).[201] They also reported that BTO NPs and graphene nanosheets could act as nucleating agents, inducing β-phase formation during the crystalline phase formation of PVDF. Based on these favorable interactions, a flexible PENG device composed of graphene nanosheets, BTO NPs and electrospun PVDF nanofibers was fabricated, which generated an output voltage in response to small-scale mechanical energy such as wrist movement. More recently, Zhu et al. prepared core–shell structured piezoelectric nanofibers to enhance the sensitivity and mechanical properties so that they were suitable for electronic skin (Figure 4e).[202] They also reported that when excessive inorganic nanofillers were introduced, crystallinity degradation of PVDF fibers occurred, and the diameters of electrospun fibers were difficult to control, resulting in a decrease in the piezoelectricity and deterioration of the mechanical properties of the device. To overcome this hurdle, a coaxial piezoelectric fiber (BTO NP-PVDF nanofiber encapsulated by GO-doped PVDF) was prepared, which could exhibit synergistic effects, such as the generation of a β-phase structure in PVDF, as well as enhanced mechanical properties suitable for electronic skin. The prepared coaxial piezoelectric nanofiber was further assembled with a conductive fabric electrode to realize highly shape-adaptive electronic skin (Figure 4f).

As mentioned previously, the incorporation of piezoelectric nanomaterials into polymer matrices has the limitation that overfilling with an inorganic nanofiller inevitably causes degradation of the mechanical properties. Alternatively, various research groups have reported approaches to deposit piezoelectric inorganic particles on the surface of nanofibers rather than inside the polymer matrix. Guan et al. reported that a hierarchically structured piezoelectric layer could be prepared through the deposition of poly(dopamine)-functionalized BTO NPs (Pdop-BT) onto the surface of P(VDF-TrFE) nanofibers (**Figure 5**a).[203] In this case, the poly(dopamine) with hydroxyl and primary amine groups was used as an organic linker between the P(VDF-TrFE) and BTO NPs through hydrogen bonding interactions. Fourier-transform infrared (FT-IR) spectroscopy was used to analyze the interfacial interactions of these nanocomposite films (i.e., Pdop-BT/P(VDF-TrFE)). After adsorption of Pdop-BT, the transmittance peak was slightly shifted to a longer wavenumber, which was caused by the hydrogen bond formed between the $-NH_2$ group of polydopamine and the C—F group of P(VDF-TrFE). In addition, thermogravimetric analysis (TGA) showed that the mass ratio of the deposited Pdop-BT within nanocomposites was approximately 20.4% (Figure 5b). To further demonstrate the superiority of a hierarchically structured piezoelectric nanofiber, they prepared a PENG device based on a Cu–Ni-plated conducting fabric/piezoelectric layer/Cu–Ni-plated conducting fabric structure (Figure 5a). In this case, their output voltage exhibited an enhancement of approximately 68% compared to that of the simple blended nanocomposites (i.e., BTO NP-incorporated P(VDF-TrFE) nanocomposites) without poly(dopamine). They also explained that the higher specific surface area and higher dielectric constant of the hierarchically structured nanofiber than those of the poly(dopamine)-free nanocomposite films could generate a larger amount of piezoelectric charges and effectively induce localized field concentration without any unfavorable interfacial interactions.

Another promising approach for uniformly coating a piezoelectric layer on 3D flexible substrates is the LbL assembly process using the complementary interactions between two different components in deposition solutions. This LbL assembly has the notable advantage of maximizing the active surface area through conformal deposition of the desired functional materials regardless of the structural geometries and size of the substrates. Mahadeva et al. reported that a piezoelectric layer composed of poly(diallyldimethylammonium chloride) (PDDA), poly(sodium 4-styrenesulfonate) (PSS), and BTO NPs on wood cellulose fibers was prepared using electrostatic LbL assembly, which could effectively utilize the large surface area and high mechanical stability of cellulose fiber (Figure 5c).[204] Specifically, a cellulose fiber has abundant carboxyl groups and hydroxyl groups, possibly allowing hydrogen bonding and/or electrostatic bonding. Accordingly, cationic PDDA with ammonium groups and anionic PSS with sulfonic acid groups could be alternatively deposited onto wood cellulose fibers. After the LbL assembly of PDDA/PSS multilayers, anionic BTO NPs were additionally deposited onto the outermost cationic PDDA layer coated on the fibers. They also reported that the loading mass ratio of BTO NPs within the formed piezoelectric fibers could be increased up to 48%.

However, despite these unique features, electrostatic LbL assembly performed in aqueous media is not suitable for achieving a high packing density of active nanomaterials (particularly active NPs) due to the electrostatic repulsion between the same charge nanomaterials.[49] A few years ago, Kim et al. reported that densely packed BTO NP (specifically OA-stabilized BTO NP or OA-BTO NP) films for PENG devices could be prepared using ligand exchange-induced LbL assembly in organic media.[205] In this study, a high affinity between the surface of BTO NPs and the carboxylic acid (COOH) groups of poly(acrylic acid) (PAA) induced the vertical growth of (OA-BTO NP/PAA)$_n$ multilayers (n = bilayer number), with a significant increase in the adsorbed amount of OA-BTO NPs per layer (Figure 5d). A high affinity occurred between PAA and OA-BTO NPs, and the multilayer (i.e., (PAA/OA-BTO NP)$_n$) formed during LbL assembly was characterized through FT-IR measurement. As the bilayer number (n) increased from 0.5 to 3, the absorption peaks (i.e., CH_2 stretching peak at 2860–2960 cm^{-1} and C=O stretching peak at 1720 cm^{-1} for OA ligands and PAA) originating from both PAA and OA-BTO NPs were intensified. These phenomena implied that the COO^- groups from PAA were covalently bound to the Ti^{4+} ion of BTO NPs without exchanging or stripping the native OA ligands (Figure 5e). Furthermore, to quantitatively measure the adsorbed amount of OA-BTO NPs, the mass change of the adsorbed PAA and OA-BTO NPs per layer was monitored using quartz crystal microgravimetry (QCM) measurements. As a result, the number density of OA-BTO NPs in each layer was calculated to be 1.99×10^{11} cm^{-2}. In addition, cross-sectional FE-SEM images of the (PAA/OA-BTO NP)$_n$ film displayed a linear increase in the thickness from 74 to 223 nm with increasing bilayer number (n) from 5 to 20 (Figure 5f). Particularly, when a compressive force of 5.2 kgf was periodically applied to (PAA/OA-BTO NP)$_{n=100}$

© 2021 Wiley-VCH GmbH

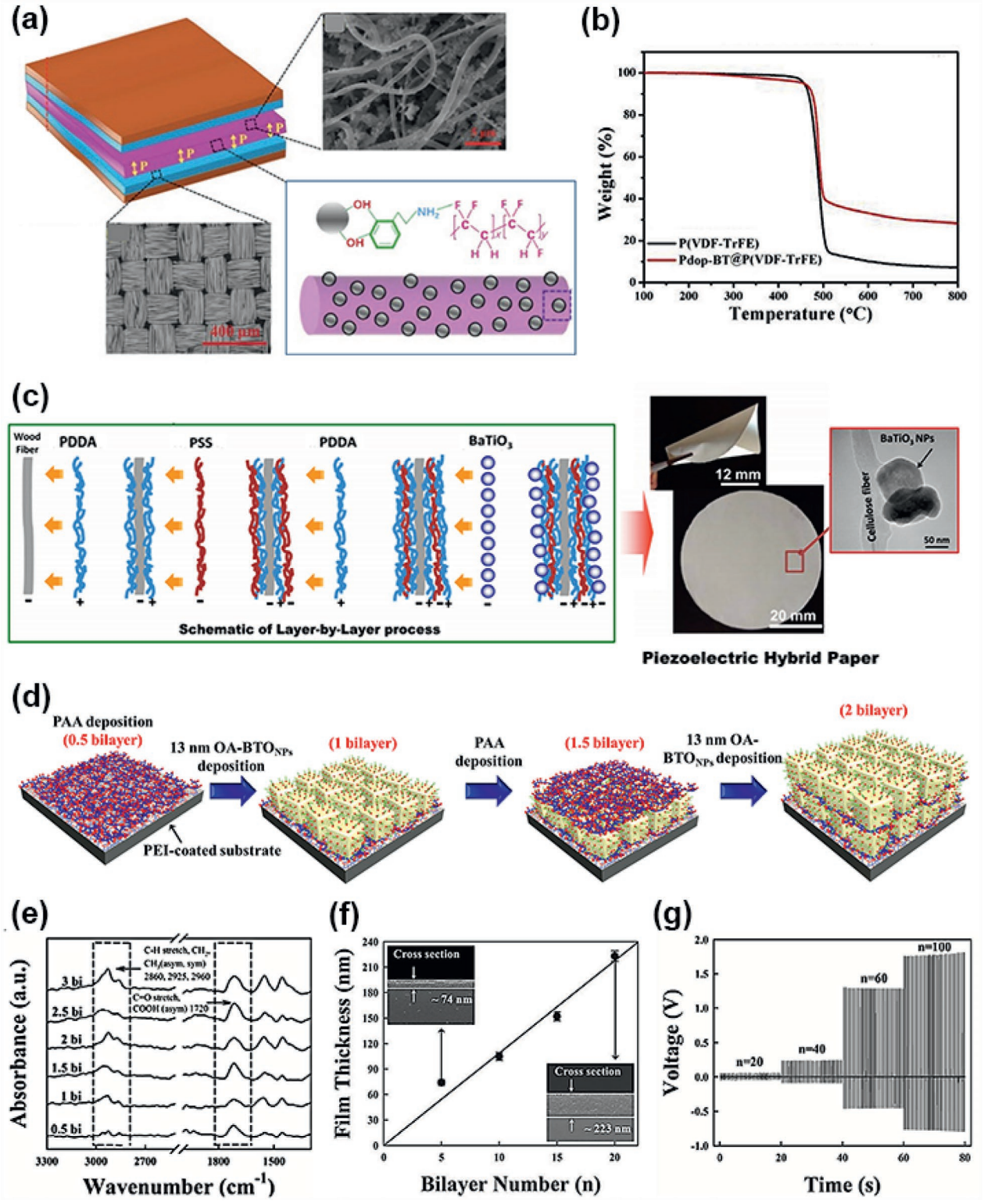

Figure 5. Interfacial design-based approaches to deposit piezoelectric nanomaterials on various supports. a) Schematic illustration showing deposition of Pdop-BT on the surface of an electrospun P(VDF-TrFE) fiber. b) TGA curves of pristine P(VDF-TrFE) and Pdop-BT@P(VDF-TrFE). a,b) Adapted with permission.[203] Copyright 2020, Elsevier. c) Schematic illustration showing the fabrication process of piezoelectric hybrid paper. Adapted with permission.[204] Copyright 2014, American Chemical Society. d) Schematic illustration of the LbL assembly of PAA and OA-BTO NPs. e) FT-IR spectra of $(PAA/OA\text{-}BTO\ NPs)_n$ multilayers. f) Film thickness $(PAA/OA\text{-}BTO\ NPs)_n$ multilayers as a function of the bilayer number (n). The inset shows cross-sectional SEM images of the $(PAA/OA\text{-}BTO\ NPs)_n$ multilayers. g) Output voltage of the multilayer PENGs as a function of the bilayer number (n). d–g) Adapted with permission.[205] Copyright 2014, Wiley-VCH.

© 2021 Wiley-VCH GmbH

multilayers without any electrical poling process, the highest output voltage and current were measured to be 1.8 V and 700 nA, respectively (Figure 5g).

As shown in this section, the interfacial design is one of the most crucial factors in the fabrication of effective piezoelectric layers. However, most reported studies have mainly focused on the interface within the piezoelectric layer (e.g., the interface between inorganic nanoparticles and the polymer matrix), and few studies have investigated the interface between the piezoelectric layer and the conducting layer. Since the conducting layer transports the charges, their interfacial stability strongly affects the performance of the PENGs. Therefore, we believe that interfacial design is crucial for the advancement of flexible/wearable PENGs with high power output and mechanical stability.

3.1.3. Interfacial Design for Flexible TENGs

Fluorine-rich molecules or polymers are the representative materials that have been used for the preparation of tribonegative surfaces due to their excellent charge-withdrawing property. For example, Lee et al. reported that a fluorinated PDMS layer could be coated onto conductive Ni–Cu textile substrates using a reactive-ion etching (RIE) plasma treatment (with Ar and CF_4+O_2 plasma) on PDMS (**Figure 6**a).[206] In the first step, Ar plasma causes cleavage of C—H bonds, resulting in a highly reactive PDMS surface. Then, fluorine-based species, such as F, CF_3, and CF_3^+, are introduced to the PDMS surface through a second plasma treatment with CF_4+O_2. Particularly, these reactive fluorine species induce the formation of fluorocarbon (C—F) bonds with a higher electron affinity. In addition, the RIE treatment can manipulate the structural configuration of the PDMS surface (Figure 6b), which can significantly increase the active surface area of the triboelectric PDMS layer. To clarify the effect of RIE treatment on the triboelectric property, the surface-modified PDMS was assembled on conductive fabric with an Al top electrode to fabricate a textile-type TENG. In this case, the RIE-treated TENG exhibited a four times higher power density than the untreated TENG.

Despite various strategies (e.g., the self-assembled monolayer (SAM) approach,[189] ion injection,[207] and plasma treatment[208]) for introducing tribonegative (withdrawing tribocharges) materials to the triboelectric interface, tribopositive materials have been relatively less studied. Additionally, compared to the various available tribonegative materials, such as PDMS, polyurethane, or polyester, most tribopositive materials do not have mechanical properties suitable for flexible TENGs. Recently, a few research groups have reported effective tribopositive materials with high mechanical flexibility.[209,210] Specifically, Bai et al. reported porous biocomposite (i.e., CP biocomposite) film-based TENGs with high tribopositive property and flexibility that can detect human motion (Figure 6c).[211] To this end, porous cellulose acetate (CA) and polyethyleneimine (PEI) were first employed to prepare the biocomposite (CP biocomposite). The CA can provide a highly flexible/durable property and a large surface area through its porous structure. Moreover, the blending between the amino-functionalized PEI with a high electron-donating property and the CA could realize tribopositive properties of the CP biocomposite. Furthermore, the authors described that the mechanism of enhanced triboelectric charge transfer is based on the increased Fermi level and decreased work function of the composite (due to the large number of electron-donating groups of PEI) (Figure 6d).[212] The biocomposite was then assembled with silicone rubber and conductive fabric to prepare a highly flexible TENG, which could also be used as a self-powered sensor for monitoring human motion.

As previously mentioned, the selection of triboelectric materials plays a central role in triboelectrification. The optimized combination of tribopositive and tribonegative materials with substantially different tribopolarities offers a vast opportunity to effectively enhance the performance of TENGs. However, for the preparation of flexible triboelectric films, not only the triboelectric properties of materials but also the mechanical properties, availability, and processability of materials must be considered for the practical use of TENGs. These factors seriously restrict the choice of triboelectric materials.

To resolve these issues, a few research groups have reported that triboelectric plates with two different electropolarities could be prepared through two different chemical modifications of only the outermost layer.[213,214] Chun et al. reported that electronegative and electropositive plates could be prepared using the same poly(ethylene terephthalate) (PET) coated with ITO nanohelix (NH) structures (i.e., ITO NHs).[215] In detail, when the ITO NHs were coated by amino group-functionalized polymers (i.e., poly-L-lysine), they exhibited a tribopositive property with a hydrophilic surface (a water contact angle of ≈58°). In contrast, when the outermost surface of the ITO NHs was coated by a fluorine-functionalized molecule (4,5-difluoro-2,2-bis(trifluoromethyl)-1,3-dioxole), the surface displayed a tribonegative property with a hydrophobic surface (a water contact angle of ≈151°) (Figure 6e). In this case, the output performance of TENGs based on the two different kinds of surface-modified ITO NH was 340 times that of nonfunctionalized TENGs. Furthermore, the authors demonstrated that the resultant TENG could be effectively operated under the wrist bending motion (Figure 6f).

From the perspective of the structural architecture of the triboelectric interface, employing intrinsically porous and/or durable substrates, such as textiles, paper, and elastomers, is very advantageous for further enhancement of the tribocharge density and practicality. However, fully exploiting the high surface area and mechanical properties of the substrates and further developing an effective triboelectric interface is a daunting task. Therefore, the development of a strategy for conformally introducing triboelectrically favorable morphology and materials to such substrates is essential for the realization of highly effective and flexible TENGs. Recently, Park et al. demonstrated surface-conformal triboelectric nanoporous films (STENFs).[216] These films were prepared based on supramolecular assembly of sulfonic-acid-terminated poly(styrene), poly(2-vinylpyridine) (P2VP), and amine-terminated poly(ethylene oxide) (APEO) (**Figure 7**a). The authors highlighted that the self-assembly of the ternary polymer solution could create nanopores 33 nm in diameter on the surface of substrates without an additional process. Additionally, they explained that the competition between two different supramolecular interactions (that is,

© 2021 Wiley-VCH GmbH

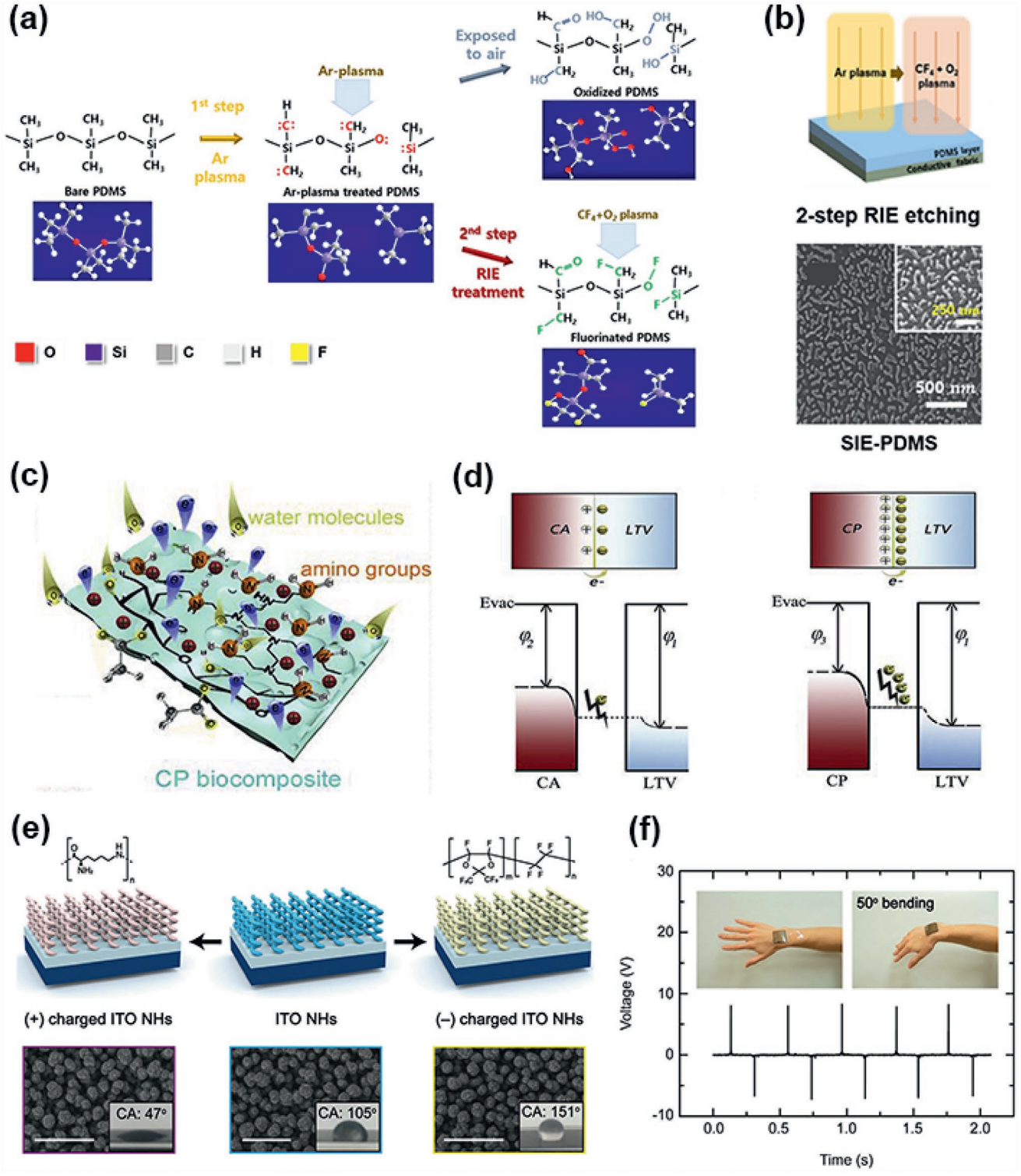

Figure 6. Various approaches to enhance the triboelectric charge transfer and charged surface area on the contacting interface of TENGs. a) Schematic illustration showing the mechanism for RIE plasma treatment of the PDMS surface. b) Schematic illustration and SEM images showing the fabrication process of SIE-PDMS. a,b) Adapted with permission.[206] Copyright 2019, Elsevier. c) Schematic illustration of the porous CP membrane. d) Energy band diagram representing the increased probability of triboelectric charge transfer between CP and low-temperature vulcanized (LTV) silicone rubber. c,d) Adapted with permission.[211] Copyright 2020, Elsevier. e) Schematic illustration showing the chemical functionalization of ITO NHs with opposite tribopolarities. The SEM images show the surface morphologies of the ITO NHs, and the insets show their water droplet contact angles. f) Electrical voltage outputs of ITO NH-based TENGs attached to the back of a hand. e,f) Adapted with permission.[215] Copyright 2019, American Chemical Society.

© 2021 Wiley-VCH GmbH

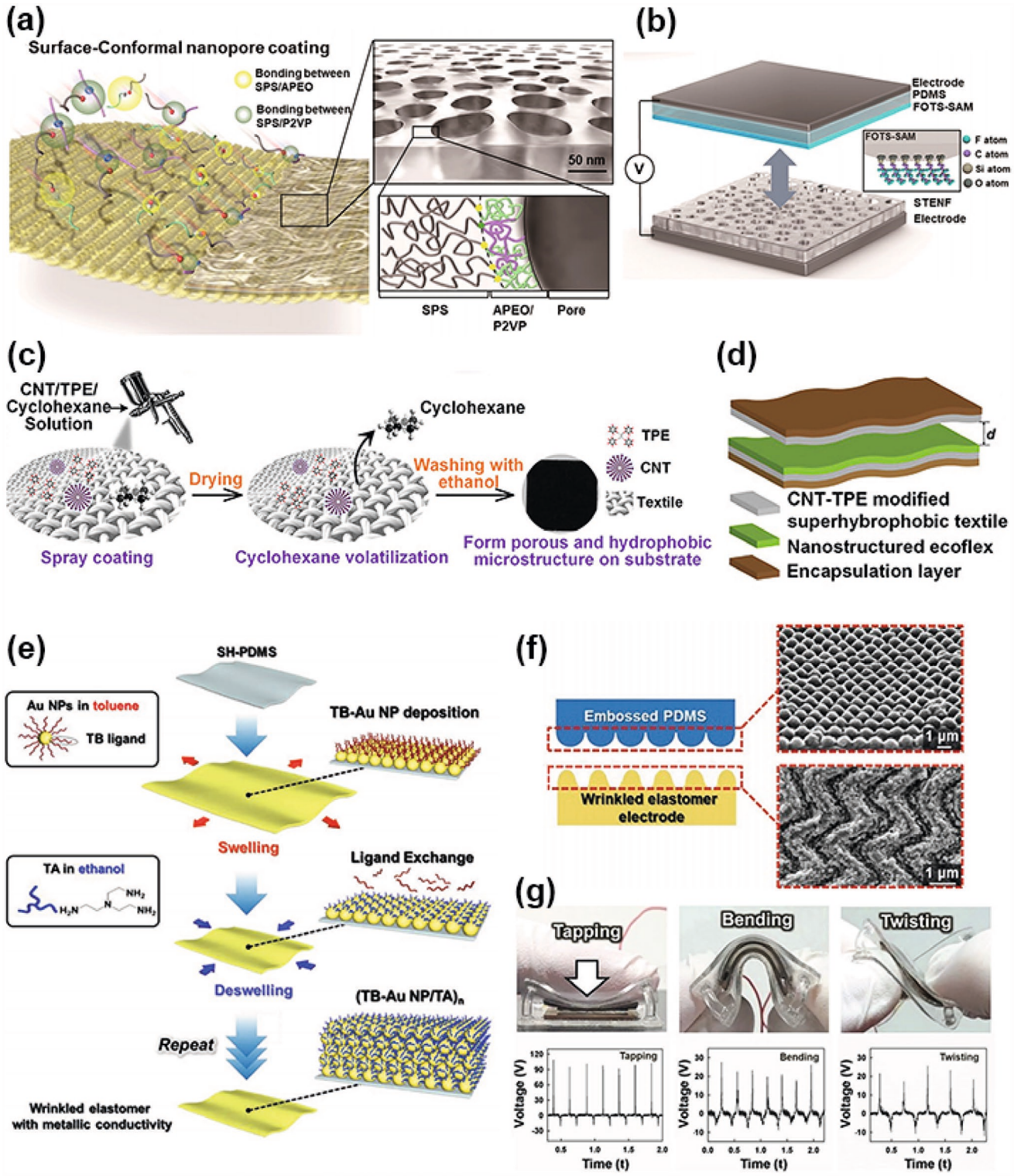

Figure 7. Hierarchically engineered triboelectric interface based on textiles and elastomers. a) Schematic illustration of the surface-conformal nanopore coating with SPS, P2VP, and APEO on a clothes substrate. b) Schematic illustration showing the structural design of TENGs based on STENF. a,b) Adapted with permission.[216] Copyright 2020, American Chemical Society. c) Schematic illustration showing the fabrication process of a superhydrophobic textile. d) Structural design of superhydrophobic textile-based TENGs. c,d) Adapted with permission.[221] Copyright 2020, Wiley-VCH. e) Schematic illustration showing the fabrication process for wrinkled elastomer electrodes using Au NPs and small molecule linkers. f) Schematic illustration and SEM images showing the contacting surfaces of all-elastomer-based TENGs. g) Photographs and voltage outputs of all-elastomer-based TENGs under various deformations. e–g) Adapted with permission.[162] Copyright 2020, Wiley-VCH.

© 2021 Wiley-VCH GmbH

the Lewis acid/base interaction (for the sulfonic acid/ primary amine group) and hydrogen bonding interaction (for the sulfonic acid and secondary amine group)) resulted in open-core nanopores.[217] Moreover, these phenomena could be similarly observed on various substrates, such as buckled PDMS, natural leaves, and fabric. Particularly, when the STENF was used as a bottom contact layer of TENGs (Figure 7b), the output voltage of the device was 1.5 times that of the TENG based on planar films.

One of the critical issues in TENGs is the operational stability under humid environments because the triboelectric surface charges dissipate through water molecules in the air.[218–220] In this regard, a hydrophobic interface that effectively prevents the formation of a water molecule layer (or droplet) can resolve this humidity-related issue of TENGs. Wen et al. reported an approach to transform pristine textiles into triboelectric textiles by endowing them with electrical conductivity and a hydrophobic microstructure through spray coating of CNTs and a thermoplastic elastomer (TPE) (Figure 7c).[221] The polyester textile was spray-coated with a CNT/TPE solution, followed by an ethanol-etching process to form a microstructure on the surface. The formation of a porous and hydrophobic microstructure on the textile substrates generated a superhydrophobic surface with a high contact angle for water droplets of over 160°. Additionally, the CNT/TPE-modified superhydrophobic textile could be used as a tribopositive layer as well as a TENG electrode (Figure 7d). To demonstrate the operational stability under a humid atmosphere, the authors investigated the output voltage of the TENGs under a high relative humidity (RH) of 85%. In this case, the superhydrophobic textile-based TENGs showed better retention of the output voltage (a degree of remaining V_{oc} of ≈22.3% at an RH of 85%), which was in stark contrast to the pristine textile-based TENG (V_{oc} ≈ 0% at an RH of 85%). Furthermore, the authors highlighted that since wearable TENGs are frequently exposed to sweat from daily activities, hydrophobic textiles are advantageous for the practical application of TENGs under various human movements.

Most of the previously reported TENGs based on textile or elastomer conductors require the formation of an additional layer over the conductive layer to introduce a surface morphology or patterns for a larger surface area. In addition, since flexible TENGs are exposed to continuous friction and deformation, they are vulnerable to mechanical failures such as cracks and delamination of the conductive layer. Therefore, polymeric additives that cause contact resistance between conducting materials and/or the encapsulation of the conductive layer with a polymer have been inevitably used to ensure suitable mechanical stability for TENG electrodes. Recently, Lee et al. reported metal-like conductive elastomers with large surface areas and high mechanical stability, without the introduction of additional layers or encapsulation processes, demonstrating all-elastomer-based TENGs.[162] They prepared a highly conductive elastomer through LbL assembly based on the consecutive ligand exchange reaction between TOA ligands of Au NPs and NH_2-functionalized short molecule linkers (TREN). By virtue of this assembly process, the strong covalent interaction between the TREN and Au NPs, as well as between the SH-functionalized PDMS substrate and Au NPs, allowed the formation of a wrinkled hierarchical structure under repetitive swelling and contraction of PDMS in organic solvents (Figure 7e). Specifically, the residual interfacial stress existing between the LbL-assembled film and PDMS generated the wrinkled structure through the buckling instability,[222,223] which provided a larger surface area for triboelectric charges and guaranteed high mechanical stability under continuous contact and separation as well as various deformations of the electrode. Moreover, the wrinkled elastic contact electrodes could be readily deformed under external stimuli, consequently increasing the contact area with the patterned dielectric layer (Figure 7f), which would resultantly enhance the electrical output of TENGs. To ensure the practicality and benefits of elastomer electrodes, the authors prepared all-elastomer-based TENGs. The TENGs exhibited a significant enhancement of the electrical output performance of up to 198 V and 17.2 μA cm^{-2} under a compressive force of 90 N, where TENGs with flat and rigid electrodes exhibited values of 56 V and 3.4 μA cm^{-2}. Furthermore, all-elastomer-based TENGs were demonstrated under finger tapping, bending, and twisting (Figure 7g). These results evidently demonstrate that interfacial control of energy harvesting electrodes, such as PENG and TENG electrodes, has a significant effect on the energy performance, diversity, and scalability of the electrode materials used (**Table 1**).

3.2. Energy Conversion: Biofuel Cells

3.2.1. Brief Overview and Challenges

With the growing interest in sustainable power sources for wireless smart sensors and biomedical electronics, energy conversion devices, which can induce the conversion from chemical reactions to electricity, have been extensively studied. Particularly, among the various energy conversion devices, enzyme-based biofuel cells (BFCs) are one of the representative human body-compliant energy conversion systems, using biofuels (sugars, alcohols or hydrogen at the anode and reduction of oxidants (O_2, H_2O_2) at the cathode) in biocompatible and mild environments.[224–226]

In many cases, these enzyme-based BFCs use carbon material-based host electrodes (mainly CNT yarns or carbon fabrics) with conductive properties, mechanical flexibility, and large surface areas. However, despite the use of these electrodes, the low power output of BFCs, resulting from the poor electron transfer between enzymes and host electrodes and limited mass transfer, has limited their practical applications.[227–230] Particularly, to enhance the electron transfer, various redox mediators between the enzyme and conductive host electrode have been introduced, thereby improving the power performance of BFCs. To the best of our knowledge, the highest power performance of these mediated electron transfer-based BFCs (MET-BFCs) reported to date was measured to be approximately 2.18 mW cm^{-2}.[231] However, they still exhibit relatively low energy performance compared to other energy conversion devices such as commercial fuel cells. Furthermore, the use of redox mediators in BFCs can lead to serious issues, such as toxicity, operational instability, and complicated and expensive synthesis of redox mediators. As an alternative, recent research efforts have been devoted to the development of direct electron transfer-based

© 2021 Wiley-VCH GmbH

Table 1. Performance comparison of PENGs and TENGs based on various interfacial design.

Conductive layer	Active layer	Methods	Current density [μA cm^{-2}]	Power density [μW cm^{-2}]	Stability (working cycles)	Refs.
PENGs						
VLNP[a)]	Silicone-rubber/PMN-PT	Blending	0.05	–	15 000	[197]
Conductive tapes	Cellulose/BTO	Blending	0.19	0.64	3000	[198]
Al foil	PVDF/BTO/GO	Electrospinning	–	0.66	1800	[201]
Conductive textile	PVDF/BTO/GO (Core–shell fiber)	Electrospinning	0.01	0.01	8500	[202]
Cu–Ni plated fabric	P(VDF-TrFE)/BTO	Physical adsorption	0.24	0.88	10 000	[203]
ITO-PEN[b)]	PAA/BTO	LA-LbL[c)]	0.7	–	4500	[205]
TENGs						
Cu–Ni plated textile	PDMS	Reactive-ion etching	2.49	1880	1000	[206]
Cu–Ni plated textile	CA/PEI	Blending	6.3	2210	10 800	[211]
ITO NH	Poly-L-lysine/PTFE AF[d)]	Dip-, spin-coating	85	3400	1000	[215]
P-doped silicon	SPS/P2VP/APEO	Spin-coating	–	77	50 000	[216]
TPE/CNT on textile		Spray-coating	–	18	5000	[221]
Au NP/TA on PDMS		LE-LbL	17.2	1100	18 000	[162]

[a)]VLNP, very long Ag nanowire percolation; [b)]ITO-PEN, indium tin oxide coated polyethylene naphthalate; [c)]LA-LbL, ligand-addition induced layer-by-layer assembly; [d)]PTFE AF, poly(4,5-difluoro-2,2-bis(trifluoromethyl)-1,3-dioxole.

BFCs (DET-BFCs) with power performance without a redox mediator, which are mainly based on the development of 1) host electrodes with a larger surface area and higher flexibility and 2) novel approaches for effectively controlling and enhancing the interfacial interactions (including enzyme immobilization) and charge transfer (or electron communication) between the enzyme and conductive support. However, given that the power output (approximately 10–100 μW cm^{-2}) of DET-BFCs is substantially lower than those (approximately 100 μW cm^{-2}–2.2 mW cm^{-2}) of MET-BFCs, the research goal of high-performance DET-BFCs is considerably challenging and has many difficulties in being easily realized.[231,232]

In this section, we focus on various approaches for improving the power performance of flexible/wearable BFCs as well as the mechanical flexibility. For this, we first review several approaches that have been applied to BFC electrodes for enzyme immobilization on the host electrode, fast electron transfer kinetics, and high power output. Next, we briefly introduce LbL assembly-based BFC electrodes that can allow minute control of the interfacial interactions between the enzymes and host electrode as well as between neighboring enzymes and generate the highest power output among the various BFC electrodes reported to date. Finally, we introduce the recent progress in flexible/wearable BFC devices and then briefly describe other conversion devices (mainly solar cells).

3.2.2. Fabrication of BFC Electrodes Using a Physical Adsorption Approach

Physical adsorption is one of the most widely used approaches for enzyme assembly onto host electrodes.[233–235] For example, when enzymes are adsorbed onto CNT-based host electrodes, the hydrophobic parts of enzymes undergo a hydrophobic interaction with the surface of pristine CNTs (**Figure 8**a).[235–239] This hydrophobic interaction, as a driving force for the direct adsorption of enzymes on CNTs, can effectively maintain the activity of immobilized enzymes compared to that of unbound enzymes.[239] As another example, Campbell et al. reported that a membrane-free/mediator-free BFC could be prepared through enzymes (i.e., glucose oxidase (GOx) for an anode and bilirubin oxidase (BOD) for a cathode) physically absorbed onto a graphene and single-walled carbon nanotube (SWNT) aerogel (i.e., a graphene/SWNT-based BFC electrode).[240] These aerogel electrodes also exhibited a large surface area (≈800 m^2 g^{-1}), allowing high enzyme loading, a large porosity for facile glucose transport, and good electrical conductivity (≈0.2 S cm^{-1}) for efficient electron transfer, resulting in a high power output of ≈190 μW cm^{-2} (Figure 8b). Specifically, the catalytic rate constant (k_{cat}) of immobilized GOx was calculated to be 46 ± 3 s^{-1}, outperforming the native enzymes with a k_{cat} of 316 ± 16 s^{-1} (Figure 8c). In this case, Γ, the surface coverage of electroactive species (i.e., flavin adenine dinucleotide (FAD) sites of GOx) was measured to be 1.44 × 10^{-12} mol cm^{-2}, estimated by the surface area available for adsorption of the electroactive species and the charge integrated from the peak current.[241] In addition, the apparent heterogeneous electron transfer rate (K_s) was estimated using the Laviron method for a surface-controlled electrochemical system.[242] In this case, the K_s of the electrode obtained from the plot of the potential ($E - E_0$) versus scan rate (log ν) was estimated to be 0.23 ± 0.01 s^{-1}, which was slightly lower than other previous results (Figure 8d).[243] The authors described that this low K_s value was caused by sluggish electron transfer due to the excessive increase in the loading amount of enzymes. Furthermore, the enzymes physically adsorbed on the graphene/SWNT host electrode were easily leached out during continuous operation of the BFCs. Therefore, the formation of more robust interfacial interactions between neighboring enzymes as well as between enzymes and host electrodes is highly desirable.

© 2021 Wiley-VCH GmbH

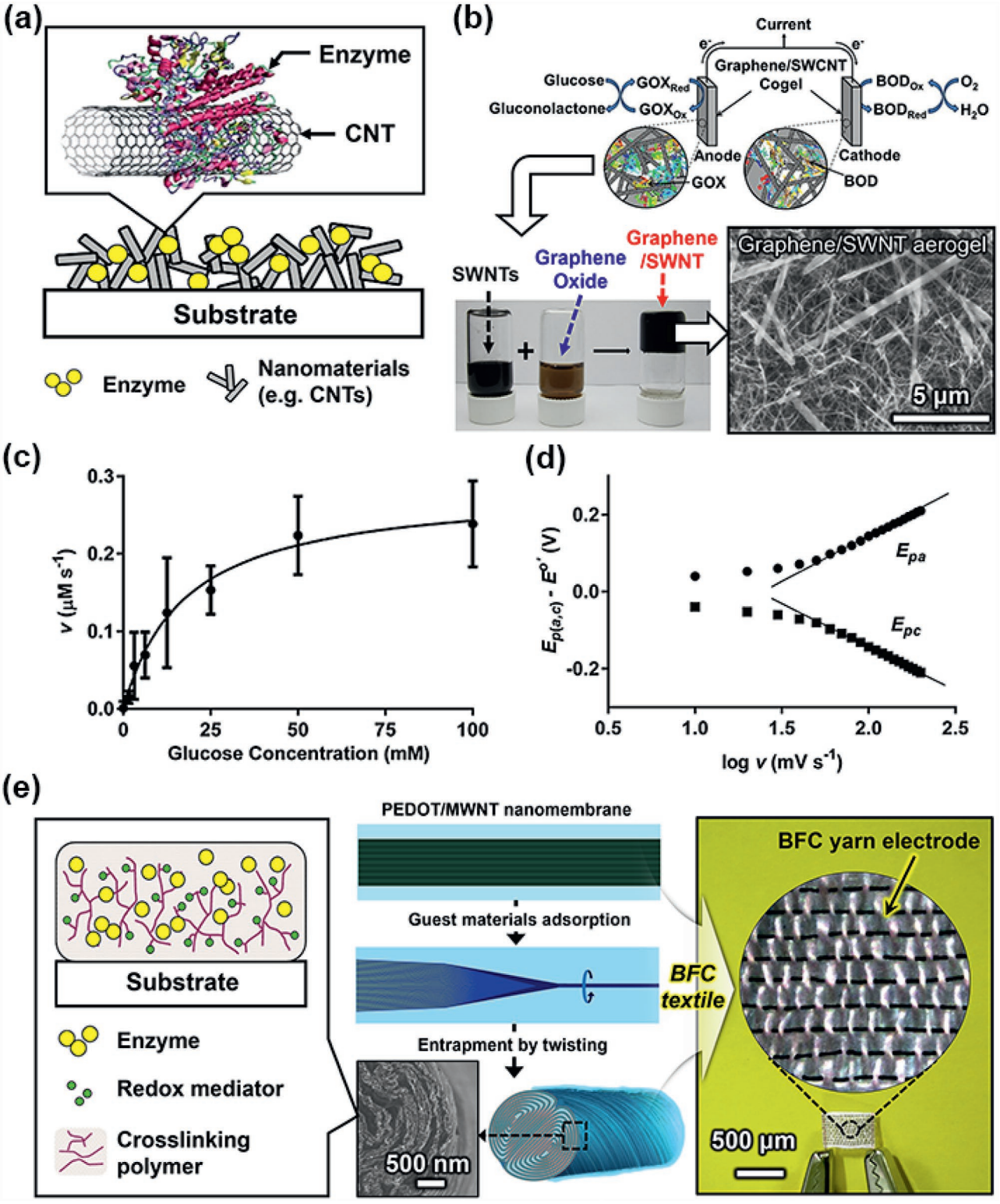

Figure 8. Physical adsorption approach for enzyme immobilization on a host electrode. a) Physical absorption of enzymes around CNTs. Adapted with permission.[235] Copyright 2011, The Royal Society of Chemistry. Adapted by the terms of the CC-BY Creative Commons Attribution 4.0 International license.[236] Copyright 2010, The Authors, published by MDPI. b) Schematic representation of a graphene/SWNT aerogel-based BFC based on the physical adsorption procedure. Glucose oxidase at the anode oxidizes glucose to gluconolactone and transfers electrons to the aerogel electrode. c) Kinetic analysis of physically adsorbed GOx regarding the initial rate of reaction on the graphene/SWNT aerogel. d) Dependence of anodic (circle symbols) and cathodic (square symbols) peak potentials on the logarithm of the scan rate for the GOx-functionalized graphene/SWNT anode at varying scan rates. b–d) Adapted with permission.[240] Copyright 2015, American Chemical Society. e) CNT yarn-constructed BFCs using physical entrapment of

© 2021 Wiley-VCH GmbH

As a complementary approach to the abovementioned physical adsorption, Kim and coauthors reported MWNT yarn-type BFC electrodes that can achieve a higher loading amount and a more stable immobilization of enzymes through additional entrapment processes (i.e., a chemical crosslinking process of guest materials including enzymes, redox mediators, and crosslinking polymers and a physical biscrolling process).[231] They also demonstrated the possibility that this approach could be extended to textile-based BFCs through the weaving process of yarn-type electrodes (Figure 8e).[244] Although these entrapment processes were advantageous for increasing the loading amount of immobilized enzymes in the interior as well as on the exterior of the resultant biscrolled electrodes, the crosslinking of guest materials including enzymes decreased the degrees of freedom of the enzyme and charge transfer efficiency, resulting in a decrease in the power performance of the BFC electrode.[231,245,246]

3.2.3. Fabrication of BFC Electrodes Using LbL Assembly

In LbL assembly using the electrostatic interaction between oppositely charged species in aqueous media, the loading amount, chemical composition, and integrated functionalities of biomaterials per deposited layer can be easily controlled according to the solution pH, ionic strength, and solution concentration. Particularly, in the case of preparing BFC electrodes using LbL assembly, robust enzyme immobilization at the enzyme/enzyme as well as enzyme/host electrode interfaces can be realized through electrostatic interactions, which can also facilitate electron transfer between the enzyme and host electrode. For example, Lesniewski et al. reported that LbL assembly of enzymes onto substrates with 3D porous structures could increase the coverage of redox-active biomolecules (including enzymes) and dramatically increase the current and power output of BFCs.[247,248] Hyun et al. also reported that electrostatic LbL-assembled (GOx/poly(ethylene imine) (PEI))$_n$ multilayers could be deposited onto PEI-wrapped CNTs for the preparation of BFC electrodes, which could exhibit a high power output of 1.34 mW cm^{-2} with a relatively high K_s of 11.3 s^{-1}.[249]

Recently, Kwon et al. reported small molecule linker-based LbL assembly using a cationic TREN molecule linker instead of bulky/insulating polymer linkers.[250] In this case, the use of the small molecule linker (i.e., TREN) could dramatically decrease the separation distance between neighboring GOx, which contributed to an improvement of the charge transfer efficiency of the (GOx/TREN)$_m$-coated electrode. The authors also used a highly conductive Au NP-coated MWNT fiber (i.e., Au–CF) electrode (≈6100 S cm^{-1}) as a BFC cathode as well as a host electrode (**Figure 9**a). Specifically, a BFC anode was prepared through the additional deposition of electrostatically LbL-assembled (GOx/TREN)$_m$ multilayers onto the abovementioned host electrode (i.e., Au–CF electrode) (Figure 9b). On the basis of the LbL-assembled GOx multilayers, the authors first investigated the electron transfer kinetics at the interface between the electrolyte (i.e., glucose solution) and anode by changing the outermost layer of the GOx/TREN multilayers (Figure 9c,d). In this case, glucose with hydroxyl groups had a higher affinity (hydrogen bonding interaction) with NH_2-functionalized TREN than with highly negatively charged GOx at pH 7.4, which induced facile infiltration of glucose into the outermost TREN-deposited multilayers. Therefore, when the outermost layer of the electrode was covered by TREN, the electrode displayed a much lower electron transfer resistance than when the outermost layer was covered by GOx despite a further increase in the layer number (Figure 9d). Therefore, our results strongly suggest that the use of an outermost TREN layer as a small molecule linker for the construction of GOx multilayers has a negligible effect on the electron transport between the GOx and Au–CF electrode. Even though the separation distance of one TREN layer sandwiched between two GOx layers was not investigated, it could be similarly expected to have a short separation distance of just a few Å, considering that the thickness of one TREN layer sandwiched between two TOA–Au NPs was just a few Å (i.e., ≈7 Å), which was simulated by density functional theory.[250] This result implied that the TREN layer between GOx multilayers did not significantly contribute to the decrease in electron transfer between the GOx and Au–CF electrodes.

In this case, Γ was estimated to be 3.73×10^{-8} mol cm^{-2}, which was much higher than those of the electrodes prepared with the conventional physical adsorption method.[240] Furthermore, the K_s of the anode and its power output were measured to be 3.5 ± 0.1 s^{-1} and 1.2 mW cm^{-2}, respectively, showing excellent operational stability (Figure 9e–g). These favorable interfacial interactions between the enzymes and the host electrode as well as between neighboring enzymes can facilitate charge transfer at their interfaces and additionally allow conformal coating of enzymes onto a variety of porous and/or flexible substrates without the aid of any insulating polymer linkers. As a result, this approach can considerably reduce the resistance of the electrode and enhance the overall performance of the BFC, providing long-term operational stability.

3.2.4. Recent Progress in Flexible/Wearable BFC Devices

Despite considerable interest in flexible BFCs, maintaining their energy performance and electrode structure against various and repetitive mechanical deformations remains challenging.[176] To resolve these problems and realize flexible/wearable BFC electrodes, various approaches have been proposed. For example, Kwon et al. reported that ligand exchange reaction-induced LbL assembly between metal NPs (i.e., TOABr–Au NPs) and small molecule linkers (TREN) could be applied to cotton fibers.[47] Based on this unique approach, they prepared highly conductive cotton fibers with bulk metal-like electrical

enzymes, redox mediators, and a crosslinking polymer in a three-dimensional CNT matrix. Schematic illustration of the fabrication of biscrolled yarn electrodes and woven BFC textile. Adapted with permission.[231] Copyright 2014, Springer Nature. Adapted by the terms of the CC-BY Creative Commons Attribution 4.0 International license.[236] Copyright 2010, The Authors, published by MDPI.

© 2021 Wiley-VCH GmbH

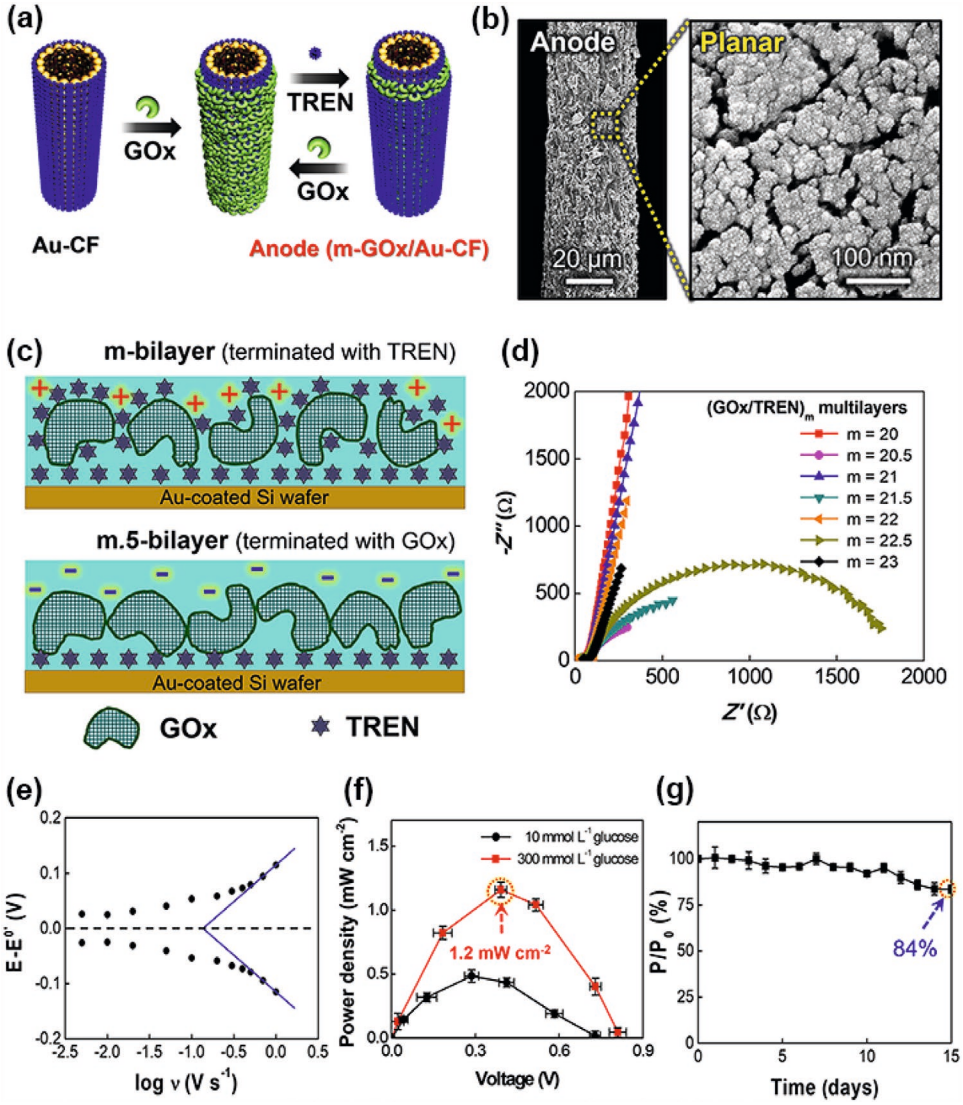

Figure 9. LbL-assembled BFC electrodes. a) Schematic illustration of the enzymatic anode assembly process with GOx and TREN on the (TOABr-Au NP/TREN)$_{20}$/CF structure. Here, *m* is the number of GOx/TREN layers. b) Planar SEM images at low and high magnification of the 20-GOx/Au-CF anode. c) Schematic of the outermost layer-dependent interfacial electron transfer kinetics (tested on a Au-coated Si wafer substrate), which are a function of the outermost layer of the (GOx/TREN)$_m$ multilayers with different surface charges. d) Nyquist plots of (GOx/TREN)$_m$ multilayers as a function of bilayer number (*m*). e) Potential ($E - E^{0'}$) versus log(ν) measured at a scan rate of 100 mV s^{-1} in PBS under ambient conditions. f) Power output of the complete BFC upon applying a fixed external resistance in the range of 1 kΩ to 10 MΩ. g) Relative power retention (P/P_0) of the Au–CF–BFC in 10 mmol L^{-1} glucose for 15 d. a–g) Adapted with permission.[250] Copyright 2019, The Royal Society of Chemistry.

conductivity (i.e., metallic cotton fibers, MCFs) that could be used as the host electrode of BFCs (**Figure 10**a). In particular, the TREN linker used in this study could be directly bridged with TOABr–Au NPs and the GOx layer via covalent bonding and electrostatic interactions, respectively, which could significantly contribute to the mechanical flexibility, robustness, and stable operation of MCF-based BFC electrodes. In this case, the formed BFC electrodes exhibited a remarkable power density of 3.7 mW cm^{-2}, which outperformed the conventional BFCs reported to date (Figure 10b).

Ogawa et al. reported that a host electrode for stretchable BFCs could be prepared through the incorporation of CNTs into a nylon/polyurethane-based textile.[251] After the formation of the host electrode, the textile-based anode and cathode were formed by deposition of D-fructose dehydrogenase and bilirubin oxidase (BOD) onto the host electrode, respectively (Figure 10c). Furthermore, a hydrogel film containing 200 × 10^{-3} M fructose fuel was sandwiched between the anode and cathode to form the complete BFC. The electrical conductance of the resultant stretchable BFC was stable up to 50% stretching for 30 cycles, resulting in a maximum power output of 250 μW cm^{-2} (Figure 10c,d). Considering that the repetitive/continuous movements of the human body can cause long-term mechanical deformation on these wearable devices and that a higher power output is required for practical applications, the mechanical stretchability and power performance of textile BFCs should be further improved.

© 2021 Wiley-VCH GmbH

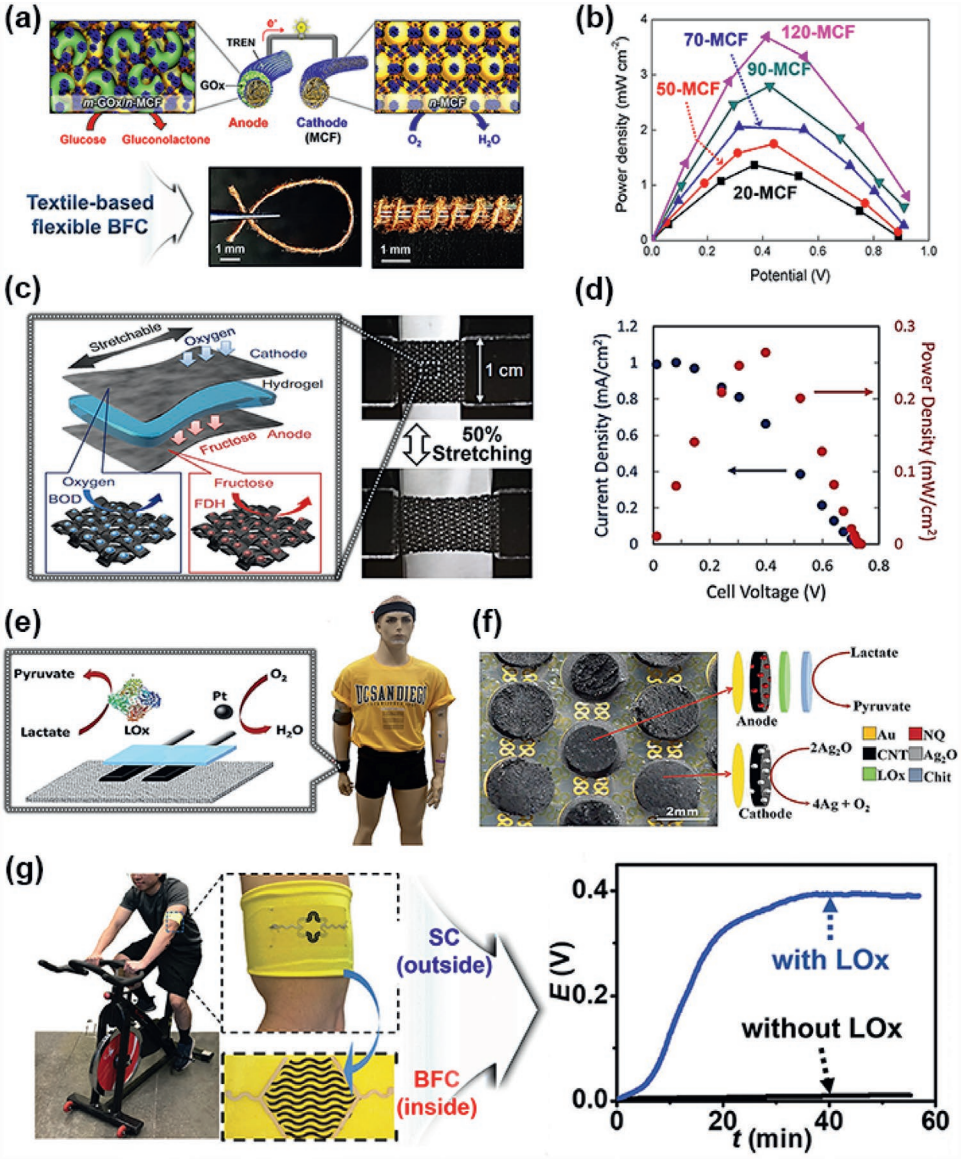

Figure 10. Flexible and stretchable BFCs for efficient energy conversion. a) Schematic of the MCF electrode-based BFC and flexible BFC electrode showing a bent and helically wrapped BFC electrode. b) Power output of MCF-based BFCs (an n-MCF cathode and a 30-bilayer GOx/TREN multilayer-coated 20-bilayer MCF anode) with external resistors (1 kΩ–10 MΩ). a,b) Adapted by the terms of the CC-BY Creative Commons Attributed 4.0 International license.[47] Copyright 2018, The Authors, published by Springer Nature. c) Stretchable fructose/oxygen BFCs with enzyme-modified conductive CNT textiles. d) Current and power density from the cell voltage and the external resistance in the range of 22 Ω–2.2 MΩ. c,d) Adapted with permission.[251] Copyright 2015, Elsevier. e) Textile-based BFC array connected to a DC/DC converter extracting electricity from human sweat. Adapted with permission.[252] Copyright 2014, The Royal Society of Chemistry. f) Island-bridge high power density electronic skin-based lactate/Ag_2O BFCs. Adapted with permission.[253] Copyright 2017, The Royal Society of Chemistry. g) Textile-based hybrid BFC and supercapacitor for converting sweat lactate to bioenergy and storing it in the supercapacitor. Adapted with permission.[255] Copyright 2018, The Royal Society of Chemistry.

The Wang group reported several kinds of flexible and/or stretchable BFCs that could extract electrical energy from human sweat.[39,252–255] For example, for a textile-based stretchable BFC, a lactate oxidase (LOx)-coated anode (for sweat lactate oxidation) and a Pt black-coated cathode (for oxygen reduction) were integrated with various garments, such as headbands or wristbands (Figure 10e).[252] Their research group also designed stretchable BFCs that can generate high power output using pellet-type anodes (composed of CNT–naphthoquinone) and cathodes (composed of CNT–Ag_2O). In this case, the total loading amounts of enzymes and mediators dispersed in the 3D-structured pellet anodes were increased according to the number of pellet electrodes, which resultantly enhanced the power output (Figure 10f).[253] Furthermore, mechanical resiliency of the BFC was realized by connecting the respective pellet electrodes with stretchable serpentine bridges. The resulting BFC displayed a maximum power density of 1.2 mW cm^{-2} with the assistance of a DC/DC converter.

© 2021 Wiley-VCH GmbH

Table 2. BFC performance based on the various flexible/wearable BFC electrodes.

Host electrode	Catalysts[a] anode/cathode	Methods	Power density[b] [μW cm^{-2}]	Stability	Refs.
Carbon fiber	GDH/BOD	Physical adsorption	216	–	[258]
Pantyhose textile	FDH/BOD	Physical adsorption	200	≈80% during 50% stretching cycles	[251]
Gore-Tex textile	LOx + Pt/Lac	Screen printing	70	≈50% after 4 weeks	[254]
Garments (headbands /wristbands)	LOx/Pt-black[c]	Thick-film printing	100	80% after 6 h	[252]
Nylon–spandex textile	Good/BOD	Screen-printing	250	≈100% during 150% stretching cycles	[227]
Ecoflex	LOx/Ag_2O	Lithographically patterning and Screen printing	1200	85% after 2 d	[253]
CNT yarn	GOx/BOD	Physical adsorption	2180	76% after 2 d	[231]
Carbon paper	GOx/Lac	Electrostatic LbL	171	77% after 4 weeks	[259]
CNT fiber	GOx + Au NP/Au NP	Ligand exchange-induced LbL	1200	83% after 15 d	[250]
Cotton	GOx + Au NP/Au NP	Ligand exchange-induced LbL	3700	83% after 20 days	[47]

[a]The abbreviations for different enzymes: glucose dehydrogenase (GDH), fructose dehydrogenase (FDH), lactate oxidase (LOx), glucose oxidase (GOx), bilirubin oxidase (BOD), and laccase (Lac); [b]Maximum power density; [c]Pt-black: platinum-black.

Recent progress in textile-based BFCs includes the development of energy systems combining BFCs and energy storage devices for effectively accumulating the generated electricity. Lv et al. reported a textile-based BFC-supercapacitor system, possibly allowing both energy conversion from human sweat and energy storage.[255] Such a hybrid device system was realized through the preparation of the BFC on the side facing the skin and the supercapacitor device on the other side of the textile (Figure 10g). In this case, a maximum power density of 252 μW cm^{-2} was generated by the BFC device, which was powered to 0.4 V after 37 min by the supercapacitor. This integration of energy conversion and energy storage devices is very attractive in that self-powered systems efficiently store irregular and scavenged biochemical energy in the form of electric energy.[256]

As a result, these textile-based BFCs can effectively convert biochemical energy (from human body fluids) into electricity for powering bioelectronics (**Table 2**). Although active materials, such as enzymes, can be easily deposited onto conductive textiles using simple physical adsorption or printing methods, only a limited surface area of the electrodes can be used for enzyme loading if unfavorable interfacial interactions are formed between the enzymes and textile-type host electrode. These phenomena can also seriously impede the redox reaction kinetics, resulting in a low energy conversion efficiency.[257] Furthermore, given that the energy efficiency of all the BFCs reported to date is not high enough to serve as a practical power source, more considerable research efforts are required to improve the charge transfer efficiency and the resultant power output of BFCs by designing effective interfacial interactions and structures as well as high-performance electrode materials. To expand the applications of and commercialize BFCs, the BFC output performance not only in area power density but also in net power must be increased. The several approaches for improving charge transfer efficiency introduced in this study can greatly contribute to the improvement of a BFC's net output performance by using the expanded size of textile electrodes or connecting them in series.

3.2.5. Other Energy Conversion Devices: Solar Cells

Among various energy conversion devices, photovoltaic cells (PVCs) are considered to be an attractive and promising energy conversion system in the renewable energy market due to their fascinating advantage of using an infinite and clean energy source. Since the first solar cell based on crystalline silicon was developed at Bell Laboratories in 1954,[260] various types of organic/inorganic photovoltaic materials with optimal electrode structures have been intensively applied to achieve a power-conversion efficiency (PCE) comparable to that of silicon.[261] Although some photoactive materials (i.e., absorbers), such as cadmium telluride (CdTe), $CuInGaSe_2$ (CIGS), and amorphous silicon, have been commercialized, crystalline silicon-based PVCs with an outstanding performance balance between PCE and durability remain dominant in the solar cell market (≈92%). However, the complicated and expensive manufacturing processes of crystalline silicon-based PVCs are still a critical challenge. Currently, most of the absorbers and transparent conducting layers (based on indium tin oxide (ITO), aluminum-doped tin oxide (ATO), and fluorine-doped tin oxide (FTO)) are deposited by vacuum evaporation, which accounts for most of the process cost. Thus, cost-effective and simple solution-processed solar cells based on high-quality (in terms of crystallinity, uniform size distribution, and dispersion stability) colloidal nanocrystals have been proposed.[260,262] Solution-based processes, including the sol-gel method, spin-coating, spray coating, roll-to-roll deposition, inkjet/screen printing, and slot-die printing, can be easily applied to various types of flexible substrates (e.g., metal foils, plastics, and textiles) under mild ambient conditions (e.g., low temperature) and are well suited for manufacturing flexible or wearable thin film electrodes with a high power-per-weight through appropriate interfacial design.[262]

Among the promising candidates for high-performance flexible PVCs, perovskite solar cells are receiving considerable attention due to their excellent PCE (24.2% for all-perovskite tandem cells), comparable conventional silicon-based PVCs and

© 2021 Wiley-VCH GmbH

simple and inexpensive solution processes.[263] Recently, the Tan group reported that a highly certified PCE of 24.2% with excellent stability has been achieved for 1 cm^2 area all-perovskite tandem solar cells through effective surface modification by anchoring zwitterionic antioxidants.[263] In particular, when the crystal size decreased to a few nanometers (specifically, up to the exciton Bohr radius) and/or the shape of the material changed, their electrical and optical properties (e.g., quantum confinement effect) changed dramatically, which is highly advantageous for solar cell performance. For example, colloidal quantum dots (CQDs) exhibit a wide light absorption window that extends to the infrared (IR) region, enabling improved output performance.[264] Interestingly, multiple-exciton generation (MEG) of CQDs is considered a key phenomenon that can improve the theoretical conversion limit of silicon (33.7%) by ≈44%.[265]

Efficient charge transfer at the interface of the photoactive layer is a major determinant for the PCE. As mentioned above, the hydrophobic ligands bound to the NP surface provide good dispersion stability in nonpolar solvents without NP aggregation, enabling the manufacture of high-quality (e.g., high film density and uniform coverage with a smooth surface morphology) thin film photovoltaic electrodes on flexible substrates. At the same time, the insulating nature of long aliphatic chains also interferes with facile electron transfer, decreasing the conversion efficiency. However, the ligand elimination process to achieve better charge transfer can create surface defects, causing charge trapping and scattering, ion migration, dot fusion, and structural instability, which can significantly degrade the photovoltaic performance.[266] Therefore, improving the performance of thin film-type solar cells requires appropriate interfacial design to effectively remove polymeric ligands on the surface while introducing a uniform and dense passivation layer using short-chain or atomic ligands.[263]

Theoretically, short organic ligand-based passivation of the CQD surface may be limited because steric hindrance prevents easy penetration into the interior of the electrodes during the ligand exchange process, resulting in insufficient surface coverage of the passivation layer.[262] As an alternative, atomic halide anions (Br^-, Cl^-, and I^-) have been proposed to overcome the drawback of organic ligand-based passivation.[267] The halide anion-based passivation process can be conducted through solid-state ligand exchange based on LbL deposition (mainly spin-coating). Briefly, LbL-assembled densely packed CQD solid-based multilayer thin films are immersed into solutions containing halide precursors. In this case, the halide anions can easily be bound to the cations on the CQD surface by replacing the bulky organic ligands, forming a well-covered passivation layer. To achieve more complete ligand elimination and limit volume contractions of the film, solution-phase ligand exchange has also been performed with the addition of inorganic halide compounds (e.g., lead halide perovskite) during the synthesis procedure.

In general, flexible PVCs show a relatively inferior output performance compared to rigid glass substrate-based PVCs. One of the critical challenges in overcoming this issue is to balance the charge transfer kinetics between the photoactive layer (i.e., the absorber) and the electron transport layer (ETL)/photoactive layer interface.[268] That is, in the case of the heterojunction cell architecture, a relatively slow charge recombination within the photoactive layer compared to that at the ETL/photoactive layer interface limits the facile charge extraction at the interface, causing performance instability with current density (*J*)–voltage (*V*) hysteresis. To solve this problem, the ETL surface (i.e., the ETL/photoactive layer interface) has been modified with inorganic thin films or small molecules, effectively suppressing photogenerated interfacial charge recombination.[269–271] Thus, optimizing the surface chemistry of all solar cell components by appropriate interfacial design is a key route to achieve high PCE and durability. More detailed explanations of the interfacial design and assembly of solar cells are given in other specialized reviews.[261,272]

3.3. Energy Storage: Rechargeable Lithium-Ion Batteries and Supercapacitors

3.3.1. Brief Overview and Challenges

With growing interest in portable/wearable electronics, various efforts have been devoted to realizing flexible energy storage devices (i.e., LIBs and supercapacitors). However, the conventional method of physically coating relatively rigid bulk materials with high energy densities, such as various types of transition metal oxides (TMOs), may limit the efficient integration and coating of highly porous textile or paper materials.[11] In this regard, efficient incorporation of energy materials through favorable interfacial interactions between the substrate and active materials is in strong demand, especially for application to highly deformable substrates. In addition to the mechanical issue, the chemistry at the interfaces of each component, where electrochemical reactions involving continuous multielectron transport occur, is one of the factors influencing the performance of energy electrodes. For example, the polymeric species (i.e., ligand and/or binder) at the interfaces present between neighboring active materials or between the substrate and active materials have a significant effect on the charge transfer behavior within the electrode, which highly depends on the types and hydrocarbon chain lengths of the polymeric species.[46,273,274] In general, the synthesis of high-energy NPs with desired quality (i.e., high crystallinity and size uniformity) in organic media involves numerous organic hydrophobic ligands well covered on the NP surface.[275] These hydrophobic ligands provide excellent dispersion stability suitable for various solution-based deposition processes, but at the same time, the high loading of energy NPs capped with such polymeric ligands increases the internal resistance, resulting in poor energy storage efficiency.[82] Furthermore, a number of hydrophobic ligands exposed at the interface between the electrode and the electrolyte limit facile penetration of the solvated ions in the electrolyte into the electrode, causing an ion concentration gradient and thereby increasing the internal resistance and undesirable side reactions (e.g., metal dendrites in battery applications).[276,277] In addition, drastic changes in the electronic and local structure of the electrode basically occur on the surface within a few nanometers of depth after contact with the electrolyte.[278] Therefore, to efficiently develop flexible energy storage systems based on highly porous soft materials

© 2021 Wiley-VCH GmbH

Table 3. Performance comparison of flexible/wearable LIB and supercapacitor electrodes.

Substrate (current collector)	Active materials	Methods	Performance[a)]	Cycle retention	Refs.
LIB electrode					
Carbon textile	$NiCo_2O_4$ (half-cell)	Hydrothermal reaction	1012 mA h g^{-1} (at 0.5 A g^{-1})	≈84% after 100 cycles (at 0.5 A g^{-1})	[269]
Activated cotton textile	NiS_2-graphene (half-cell)	Thermal treatment	≈1515 mA h g^{-1} (at 0.01 C)	≈1030 mA h g^{-1} after 400 cycles (at 0.1 C) ≈740 mA h g^{-1} after 50 cycles in bent state (at 0.1 C)	[268]
Carbon fabric	$NiCo_2O_4$//V_2O_5 (full-cell)	Hydrothermal reaction	149 mA h g^{-1} (at 100 mA g^{-1}) 364.2 W h $kg^{-1}_{max.}$ 240 W $kg^{-1}_{max.}$	≈86% after 100 bending cycles	[323]
Carbon cloth	MoS_2//$LiCoO_2$ (half-cell, full-cell)	hydrothermal reaction (for MoS_2)	3.5 mA h cm^{-2} (half-cell) 1.41 mA h cm^{-2} (full-cell) (at 0.15 mA cm^{-2})	≈85.7% after 30 cycles (half-cell)	[324]
Carbon fiber(CF)/ECF[b)]	NiO/CD[c)]// LNCMO[d)] (half-cell, full-cell)	Hydrothermal reaction	3.97 mA h cm^{-2} (half-cell) 619.9 W h L^{-1} (full-cell)	98% after 300 cycles (full-cell) (at 5 mA)	[325]
Supercapacitor electrode					
Carbon textile	$NiCo_2O_4$ (half-cell)	Hydrothermal reaction	1283 F g^{-1} (at 1 A g^{-1})	≈100% after 5000 cycles (at 8 A g^{-1})	[269]
Ag-sputtered cotton textile	$FeCoS_4$–$NiCo_2S_4$ (half-cell)	Hydrothermal reaction	1519 F g^{-1} (at 5 mA cm^{-2}) 46 W h $kg^{-1}_{max.}$ (at 1070 W kg^{-1})	92% after 3000 cycles (at 10 mA cm^{-2})	[73]
Carbon textile	GF//NTO[e)] (full-cell)	Hydrothermal reaction	55 W h kg^{-1}_{max} 3000 W kg^{-1}_{max}	≈80.3% after 2500 cycles (at 0.5 A g^{-1})	[326]
Au NP-coated cotton thread	Fe_3O_4//MnO + Au NP (full-cell)	Ligand exchange-induced LbL	179.2 mF cm^{-2} (at 0.3 mA cm^{-2}) 80.7 μW h cm^{-2}_{max} 3.45 mW cm^{-2}_{max}	92.3% after 5000 cycles (at 6 mA cm^{-2}) 97.5% after 1000 bending sycles	[161]
Au NP-coated cellulose paper	Fe_3O_4//MnO + Au NP (full-cell)	Ligand exchange-induced LbL	1.35 F cm^{-2} (at 5 mV s^{-1}) 267.3 μW h cm^{-2}_{max} 15.1 mW cm^{-2}_{max}	≈90% after 5000 cycles	[160]

[a)]Capacity for LIB electrode, capacitance for supercapacitor electrode, and energy/power density; [b)]ECF, exfoliated N-doped carbon fiber; [c)]CD, carbon quantum dot; [d)]LNCMO, $LiNiCoMnO_2$; [e)]GF//NTO, reduced graphene oxide film//$Na_2Ti_3O_7$.

(i.e., textile and paper), the interfacial conditions closely related to the electrical properties of energy materials and the desired tolerance to various mechanical deformations must be carefully considered.

In this regard, the following sections describe the two representative approaches for introducing energy materials onto flexible conductors through direct growth or self-assembly with respect to surface or interfacial engineering of energy materials and electrodes (**Table 3**).

3.3.2. Direct Growth of Active Materials on Flexible Current Collectors

Maintaining mechanical stability with stable output performance is the main purpose of flexible energy applications using flexible substrates. However, in some cases, the resulting flexible electrode does not sufficiently maintain the mechanical properties of the original substrate materials (e.g., textiles or paper), which is mainly due to the bulk loading of a slurry-like active composite through the physical casting and drying process.[78,149,279] Although such high loading of an active material may deliver a high areal energy density because of the good ion transfer kinetics originating from the porous structure of the substrates, it can lead to unreliable mechanical performance. Therefore, the effective incorporation of active materials allowing stable and uniform coating onto a flexible current collector while minimizing the contact resistance is highly required.

In this view, direct growth of energy materials on the surface of the current collector by in situ reduction of precursor ions has been widely applied.[280,281] This approach generally provides conformal deposition of energy materials and direct contact between active materials and the current collector without polymeric binders, allowing facile charge transfer kinetics at the interface as well as good strain tolerance.[282,283] Shen et al. reported mesoporous $NiCo_2O_4$ NW arrays grown on carbon textiles through a surfactant-assisted hydrothermal reaction (**Figure 11**a–c).[282] In this case, despite the dense and conformal coating of $NiCo_2O_4$ NW arrays, the intrinsic flexibility of the carbon textile substrate was well maintained. Interestingly, the as-grown $NiCo_2O_4$ NWs were composed of numerous crystalline NPs with an average diameter of ≈16 nm, providing a mesoporous structure (Figure 11b). This unique structural feature of $NiCo_2O_4$ NWs is highly advantageous in ion transfer kinetics due to the short ion diffusion length, resulting in a high energy storage efficiency even at a fast sweep rate. In addition to the $NiCo_2O_4$ NW array, the highly porous textile also has merits in rate efficiency at the same loading amount, which has been demonstrated by comparison with a nonporous flat metal foil-based electrode. As a result, the carbon textile electrode-based LIB anode showed a high reversible capacity of 1012 mA h g^{-1} at 0.5 A g^{-1} (cycle retention of ≈84% after 100 cycles),

© 2021 Wiley-VCH GmbH

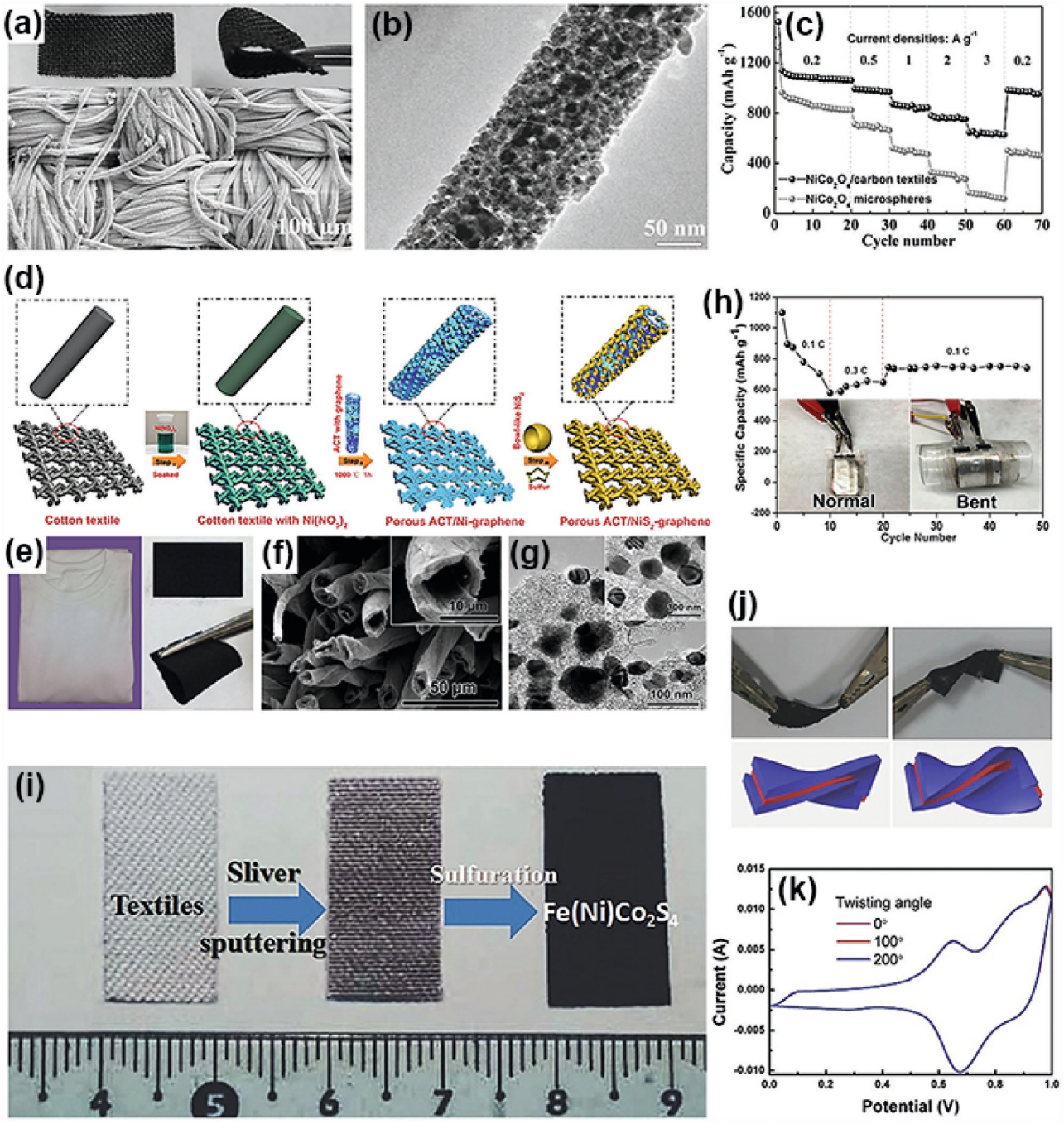

Figure 11. Flexible energy storage electrodes obtained by direct growth of active materials. a) SEM and b) transmission electron microscopy (TEM) images of $NiCo_2O_4$ NW array-deposited carbon textiles. c) Comparison of the capacity retention between a porous carbon textile-based electrode and a nonporous flat substrate-based electrode. a–c) Adapted with permission.[269] Copyright 2014, Wiley-VCH. d) Schematic illustration of the preparation of an ACT/NiS_2–graphene anode electrode on carbon textiles. e) Photographs of a raw cotton T-shirt (left) and ACT/Ni-graphene (right). f) SEM images of a tubular-shaped Ni-graphene composite grown on ACTs. g) TEM image of the NiS_2–graphene composite. h) Cycle retention of ACT/NiS_2–graphene anode electrodes in the normal and bent states. d–h) Adapted with permission.[268] Copyright 2015, American Chemical Society. i) Photographs of the electrode preparation process with color change for pristine cotton textile (left), a Ag-sputtered textile conductor (middle), and a $FeCo_2S_4$–$NiCo_2S_4$ array-coated textile electrode. j) Photographs and illustration of $FeCo_2S_4$–$NiCo_2S_4$ electrodes under twisting, and k) their cyclic voltammograms (CVs) for different twisting angles. i–k) Adapted with permission.[73] Copyright 2017, Wiley-VCH.

whereas the nonporous substrate-based anode exhibited a lower capacity of ≈700 mA h g^{-1} at 0.5 A g^{-1} with poor cycle retention (≈67% of the initial capacity) (Figure 11c). These quite different results are mainly due to the synergistic effect of the unique architecture and the efficient contact of each component (i.e., the current collector and active materials), which significantly

© 2021 Wiley-VCH GmbH

improves the charge transfer kinetics and mechanical stability. In addition, the authors demonstrated the possibility of application to supercapacitor electrodes and achieved a high specific capacitance of 1283 F g^{-1} at 1 A g^{-1} with excellent cycle retention performance.

Another merit of such a direct growth approach is that it can produce various types/shapes of cathodic or anodic transition metal compounds based on oxides,[282,284–286] nitrides,[287] sulfides,[281] phosphides,[288] and selenide[289] on conductive materials. Gao et al. reported a nickel sulfide (NiS_2) nanobowl-coated carbon textile electrode for LIB anodes (Figure 11d–g).[281] The activated cellulose cotton textiles (ACTs) produced by carbonization were used as a current collector for the loading of active materials, which exhibited good electrical conductivity (≈10 Ω sq^{-1}) and flexibility (Figure 11e). Ni NPs were first deposited on the ACT surface during the activation process. In this case, the graphene multilayers resulting from the simultaneous decomposition of carbon species (i.e., methane) uniformly covered the Ni NPs, acting as a bridge between the active materials and electrolyte for efficient ion transport (Figure 11f). Then, NiS_2 was formed by further reaction of the Ni NP/graphene composite-coated ACT with sulfur (Figure 11g). The electrochemical performance of the formed ACT/NiS_2–graphene anode electrode remained stable even with continuous bending deformation (Figure 11h), suggesting that the well-constructed porous and tubular structure of the electrode provides fast charge transport and mechanical stability as well as a large active surface area. Thus, carbonized (or activated) commercial cotton textiles can provide a promising platform for fabricating high-performance flexible energy storage devices due to their unique structure, mechanical properties, and capacitive behavior.[290,291] However, the carbonization process should be carefully controlled to prevent deterioration of the mechanical properties of the fabric materials.[2]

Carbon-based textiles have been actively used as flexible current collectors, mainly in the direct growth of active materials via hydro/solvothermal reactions, but the limited intrinsic electrical conductivity of the carbon composite (<300 S cm^{-1}) can limit fast electron transfer between active materials and the current collector. In this regard, a metallic current collector can be a good candidate that can improve the electrical conductivity. Zhu et al. reported a metallic cotton textile prepared by simple Ag sputtering and applied it to the current collector for a flexible supercapacitor electrode by synthesizing ternary metal sulfide composites ($FeCo_2S_4$–$NiCo_2S_4$) on the surface (Figure 11i).[73] The sputtered Ag film on the textile surface has a controlled thickness of ≈10 nm to effectively maintain the porous structure and mechanical properties of the textiles (see the details in Section 2.1.1.). In this case, the uniformly covered Ag film not only acts as effective active sites for facilitating homogeneous nucleation and growth of tubular sulfide composite active arrays (i.e., $FeCo_2S_4$–$NiCo_2S_4$) but also allows excellent electron transfer kinetics and adhesion at the interfaces of the active material and conducting textile. The benefits of the efficient and robust structural configuration of the formed supercapacitor electrodes were clearly demonstrated by monitoring the electrochemical performance under severe torsional deformations in all-solid-state applications, showing a negligible change in the output performance (Figure 11j,k).

Despite the structural and mechanical advantages of the direct active material growth approach on flexible conductors, the relatively complex procedures still remain major challenges for large-area flexible/wearable energy storage applications. In general, the characteristics of the as-grown active materials, such as the shape, size, crystallinity, composition, and loading amount (or packing density), are highly dependent on various reaction parameters, including the time, temperature, pressure, concentration, and solubility of precursors, which also have a great influence on the electrochemical performance.[292–295] In particular, since the direct growth process is generally performed through one-step synthesis and deposition of active materials on the current collector, the loading amount is controlled by adjusting the reaction parameters described above. However, successive in situ crystal nucleation and growth of active materials lead to mass deposition of active materials with thicker and denser configurations, which can cause poor rate performance and mechanical properties.[296] Therefore, these reaction parameters should be precisely controlled to optimize the structural characteristics to achieve a high energy storage performance.

3.3.3. Interfacial Design-Based Assembly for High-Quality Energy NPs

Another well-known approach to integrating energy materials is to coat the presynthesized energy materials on the current collector based on specific interactions, such as the electrostatic attraction, hydrogen bonding, or covalent bonding. As mentioned earlier (see Section 2), printing (or slurry casting) and dip coating are representative solution-based coating methods for nanomaterials. In terms of the charge transfer and mechanical properties, however, dip coating that can form thin films through self-assembly is more promising than the printing method that forms a relatively bulky active layer. That is, in conventional electrode composite (ink or slurry) preparation methods based on physical blending, polymer binders (or surfactants) have been commonly used to induce entangled networks to confine (or sometimes buffer the external/internal strain of[297,298]) the electrode components (i.e., active materials and conductivity enhancers). However, such polymeric species inevitably increase the internal resistance of the electrode. In other words, although most studies based on the blending method have been conducted with the optimized component ratio (i.e., active material, polymer binder, and conductivity enhancer) to minimize the impact of such polymers on the electron transfer kinetics, increasing the amount of active material to obtain a higher energy will also require the same or a higher proportion of additives (i.e., polymer binder and conductivity enhancer), again causing the internal resistance issue. In addition, the randomly mixed active composite may exhibit poor electrical and mechanical properties compared to the well-aligned structure, especially for a thicker active layer (i.e., high loading).[299] Therefore, the formation of a uniformly distributed energy NP-based active layer with a proper thickness (for easy charge transfer) on a flexible substrate can ensure high energy storage efficiency even under various mechanical deformations.[19]

© 2021 Wiley-VCH GmbH

Well-defined, high-quality nanomaterials are essential for realizing high-performance flexible energy storage electrodes through the dip coating process. With respect to the energy storage performance, various factors of energy NPs, such as the crystallinity, grain size, lattice spacing and size distribution, affect the energy density and rate performance of the formed electrodes. For example, an isooriented nanocrystalline PC material (i.e., α-MoO_3) can deliver high electrochemical performance because of the additional intercalation pseudocapacitance with fast ion transport through the well-aligned crystallographic pathways.[300,301] In addition, reduction of the crystalline domain size of the active material (i.e., α-Fe_2O_3 with a size of <20 nm) more effectively accommodates structural strains caused by Li-ion insertion (in LIBs), allowing a greater amount of Li ions to be inserted without a phase transition than larger size materials (≈0.5 µm). Therefore, this feature of a small-size active material (α-Fe_2O_3) can delay the irreversible phase transition to the rock-salt phase (i.e., from the hexagonal array to cubic close packing), improving the energy storage efficiency and cycle retention.[302] According to a previous report, an energy electrode composed of nanoscale active materials with a narrow size distribution significantly affects the ion diffusion kinetics and structural properties (i.e., pore structure, mass density, and active surface area), thereby influencing the rate performance.[303,304]

In terms of such qualities, hydrophobic NPs dispersed in organic media are more attractive than hydrophilic NPs due to their high crystallinity, narrow size distribution, and excellent long-term dispersion stability.[305] However, at the same time, two factors must be considered to effectively apply these hydrophobic NPs to the dip coating process for energy storage electrodes: 1) the absence of hydrophilic functional groups at the terminal site for specific and strong bonding with adjacent materials and/or the substrate and 2) a number of insulating hydrophobic ligands bound to the NP surface. Although various phase transfer processes have been conducted to introduce hydrophilic ligands (or functional groups) onto the surface of NPs, the yield and quality (size distribution, colloidal stability, and excess polymeric residue) of the resulting products are not suitable for obtaining conformally deposited thin films on a substrate.[306–308] More importantly, electrostatic attraction-based dip coating of hydrophilic NPs can lead to a relatively low packing density within the electrode due to the long-range electrostatic repulsion between the same charge NPs,[49] limiting the high areal or volumetric energy density.[309]

In addition, a number of organic ligands on the surface of NPs act as an insulating shell covering the functional particles, restricting electron transfer between adjacent electrode components. Basically, the loss of energy efficiency (or rate performance) is caused mainly by the internal resistance of the electrochemical system occurring at the interfaces of each electrode component.[310] In this regard, reducing the insulating (or polymeric) species within the electrode is one of the most fundamental and efficient ways to diminish the energy losses. Therefore, an appropriate NP assembly process that can simultaneously modulate the surface chemistry of NPs is strongly needed.

Previous reports have shown that bulky hydrophobic ligands attached to NPs can be effectively eliminated by specific organics.[311,312] In this case, the organics with higher affinity to the NPs can replace the native hydrophobic ligands on the surface of the NPs, resulting in the surface of the NPs being covered with the incoming organics. That is, the surface chemistry of NPs depends on the characteristics (e.g., terminal functional group or chain length) of such newly attached organic linkers. Regarding this, the electron transport behavior between neighboring NPs is reported to be highly dependent on the ligand length (or interparticle distance), which can affect the electrochemical output of the energy devices.[46,313–315] This ligand exchange concept has been expanded to LbL assembly for realizing functional NP-based multilayer films and applied to textile- or paper-based flexible energy storage electrodes.[160,161,316] Shin et al. reported stitchable fiber-type supercapacitor electrodes prepared by ligand exchange-induced LbL assembly of hydrophobic NPs (Fe_3O_4 or MnO and/or Au NPs) and an organic linker (TREN) in organic media (**Figure 12**a).[161] For this, a commercial cotton thread was first converted to a metallic conductor through ligand exchange-induced LbL assembly between hydrophobic Au NPs and the organic linker. As a result, the Au NP-coated cotton threads showed metallic conduction behavior with excellent electrical conductivity (≈2.1×10^4 S cm^{-1}) while maintaining the mechanical nature of cotton. Asymmetric supercapacitor electrodes were fabricated by depositing high-energy TMO NPs (Fe_3O_4 for the negative electrode and MnO for the positive electrode) following the same LbL assembly method onto as-prepared metallic cotton threads, demonstrating high power and energy density of 80.7 µW h cm^{-2} and 3450.1 µW cm^{-2}, respectively. In addition, the authors also investigated the performance stability of the stitched 1D thread-type supercapacitor under various deformations, showing excellent performance retention without notable changes in the galvanostatic charge/discharge (GCD) curves (Figure 12b).

A high areal energy density is a particularly important performance parameter in wearable energy storage applications because of the limited available area of the human body.[317] In this regard, nanomaterial-based LbL assembly, which enables vertical growth of active layers by precisely controlling the loading amount and film uniformity, is an efficient way to fabricate textile-based wearable energy electrodes with high areal performance. In addition, with this LbL assembly process, the intrinsic structural properties (i.e., porosity and flexibility) of the substrate can be mostly preserved even after high loading of active materials.[160] Along with such structural advantages, surface ligand modulation can provide mechanical stability and facilitate charge transfer kinetics within electrodes. Replacing (or eliminating) the bulky insulating ligands bound to the high-energy TMO NPs with hydrophilic small molecule linkers improves the charge transfer kinetics at all the interfaces within the electrode, but the semiconducting nature of TMO NPs can still limit facile electron transfer under high loading conditions (i.e., multilayer deposition). This issue was addressed through alternating LbL deposition of metal NPs and TMO NPs onto metallic cellulose paper as a current collector (Figure 12c).[160] In this case, the periodically inserted metal (Au) NPs act as electron relays between the PC MnO NPs (i.e., an alternating MnO/Au NP electrode), reducing the internal resistance even at a high loading of semiconducting MnO NPs (Figure 12d).

© 2021 Wiley-VCH GmbH

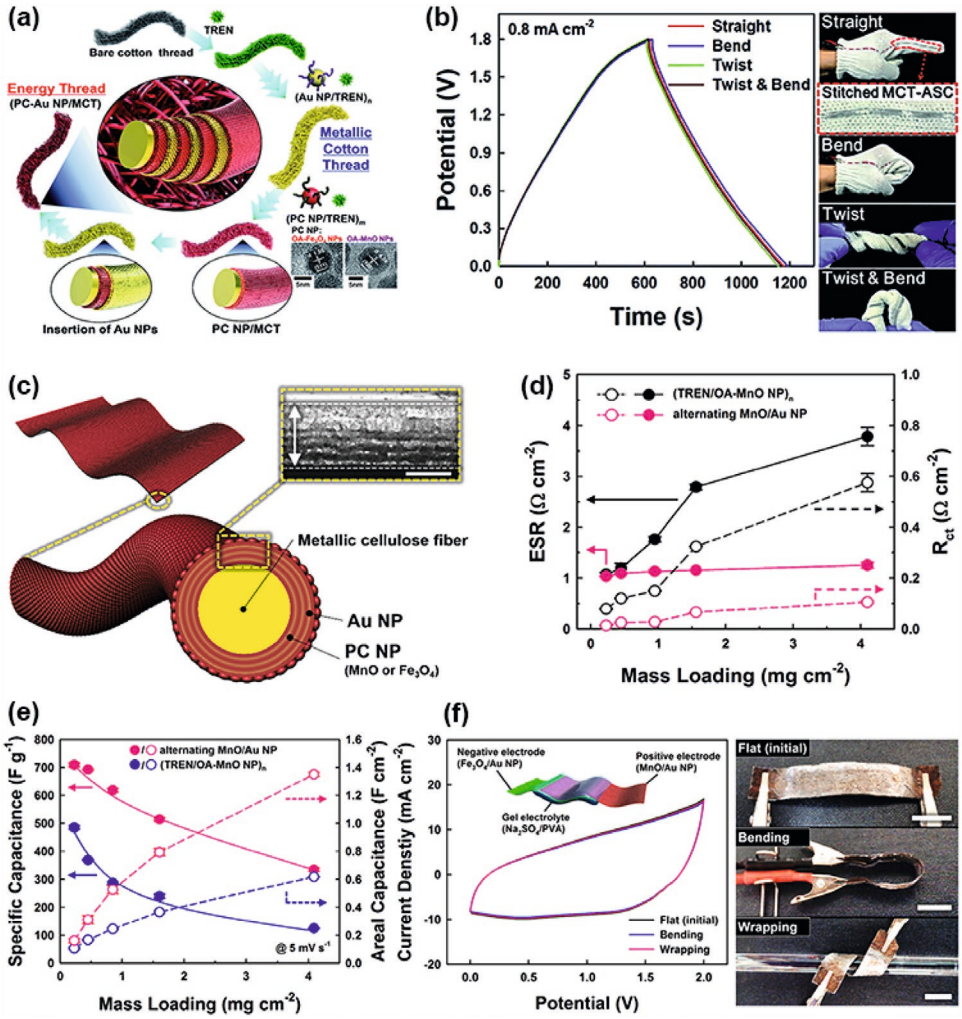

Figure 12. Textile-based supercapacitor electrodes obtained through ligand-controlled LbL assembly. a) Schematic illustration of the preparation of cotton thread-based supercapacitor electrodes based on ligand-controlled LbL assembly between Au NPs and high-energy TMO NPs (i.e., Fe_3O_4 and MnO). b) GCD profiles of cotton thread-based supercapacitor electrodes under different mechanical deformations (photographs on the right side). a,b) Adapted with permission.[161] Copyright 2018, The Royal Society of Chemistry. c) Schematic illustration of alternating deposition of Au NPs and a TMO NP layer using ligand-controlled LbL assembly. The inset presents a cross-sectional SEM image of the alternating TMO NP (i.e., Fe_3O_4 or MnO)/Au NP electrode. d) Change in electrical properties and e) capacitance of the electrodes with insertion of the Au NP layer. f) CVs of all-solid-state asymmetric supercapacitors composed of alternating Fe_3O_4/Au and alternating MnO/Au electrodes obtained under different mechanical stresses (photographs on the right side). c–f) Adapted by the terms of the CC-BY Creative Commons Attribution 4.0 International license.[160] Copyright 2017, The Authors, published by Springer Nature.

As a result, the alternating MnO/Au NP electrode showed two times higher output performance than that without Au NPs. This indicates that reduction of the internal resistance through efficient interface design allows the effective activation of MnO NPs in the electrode (Figure 12e). In particular, since all components within the electrode form a stably integrated NP network with strong covalent bonds, the formed asymmetric supercapacitor showed excellent performance retention upon various mechanical deformations (Figure 12f).

4. Summary and Perspective

Research on the discovery of advanced energy materials is one of the most valuable ongoing works to realize convenient and prosperous human life. However, attaining the theoretical properties of the materials without proper structural design of the electrodes is difficult, and at the core of this issue is the effective design of the interfaces between all electrode components where numerous electrical/electrochemical events occur. Particularly, the use of nanomaterials in energy applications offers many attractive advantages, such as an extremely large active surface area, excellent tolerance to mechanical deformations, and a tunable electrode structure (i.e., porosity and/or surface morphology), resulting in better output performances than bulk materials.[318,319] However, at the same time, this also means increasing the interfaces between each component (i.e., active materials and/or substrate), which can increase the contact resistance (internal resistance) and lead to electrochemical stability issues. In particular, the internal resistance of the

© 2021 Wiley-VCH GmbH

electrode can be more pronounced due to the large number of insulating polymeric species (i.e., polymer binders, surfactants, and organic ligands with long aliphatic chains) adsorbed on the surface of the active nanomaterials. Therefore, to achieve reliable output performance, the separation distance (for lowering the internal resistance) and interfacial interaction between neighboring component materials in the electrode should be carefully tailored through an appropriate interface design including ligand modulation. Furthermore, for realization of high-performance flexible/wearable energy electrodes, the mismatch in mechanical properties between the active layer and conductor (or host electrode) must be resolved.

As described in this review article, the ligand exchange-induced LbL assembly method can produce NP-based nanocomposite thin films for a variety of applications ranging from insulating flexible material (textile, paper, and elastomer)-based electrical conductors to various energy electrodes for energy harvesting, conversion, and storage systems. Uniform and dense coating of functional NPs on flexible substrates can effectively preserve the internal structure as well as the mechanical properties of the substrates, which is very closely related to the output performance of the energy electrodes.[320] In the case of PENG systems, the output power generation efficiency highly depends on the amount of piezoelectric NPs and their uniform distribution on the substrate (or conductor). That is, proper alignment of piezoelectric NPs by controlling the interparticle distance at the optimum value can affect the local electric field under external mechanical strains, thus influencing the piezoelectric performance. In this regard, ligand exchange-induced LbL assembly yields well-aligned multilayers with precisely controlled interparticle distances and mass loadings of the materials. This feature enables the efficient activation of piezoelectric NPs by allowing the external pressure to be evenly applied to each NP in the electrode. In addition, because the power generation of the energy harvesting electrodes (i.e., PENGs and TENGs) occurs essentially as a result of repetitive external mechanical stimuli, structural durability that does not result in delamination of each layer under such mechanical stress is required. Importantly, the surface charge density of the TENG electrodes affects the voltage outputs. In this case, since contact electrification is highly dependent on the chemical potential difference between two electrodes, the charge density can vary depending on the surface chemistry of the electrodes (or materials). For example, surface functionalization of TENGs with amine ($-NH_2$) groups (i.e., for positive electrodes) can significantly improve the output power due to the tribo-positive property of amine groups.[321] In this respect, surface ligand (or chemistry) modulation via LbL assembly can further enhance the output performance of energy-harvesting devices.

On the other hand, for energy conversion/storage electrodes, including active materials with poor electrical properties (e.g., enzymes and TMO NPs), interface engineering may become more important from the perspective of electron/ion transfer kinetics within the electrodes. The trade-off between high loading of active materials and the resulting energy/power output performance is due not only to the poor electrical nature of the active materials but also to the polymeric species (i.e., binders and ligands) within the electrode. In particular, such polymeric species can further increase the internal resistance during dense packing of the energy materials to achieve higher areal or volumetric energy performance. In this regard, electrode design through ligand exchange-induced LbL assembly provides better energy conversion or storage efficiency by minimizing the internal resistance of the electrode.

However, such an LbL approach still has some issues to be solved in terms of mass production and processing time for commercialization. Although various approaches based on rapid automated deposition techniques (e.g., spin coating and spray deposition) have been applied to address these issues, such techniques are not effective in completely washing out detached native hydrophobic ligands due to the volatile nature of organic solvents. In this regard, a large-area coating approach, such as a roll-to-roll process, which can effectively wash out hydrophobic ligands through a controllable immersion time, may be an alternative.[322] More potentially, we envision that the interfacial engineering-based LbL assembly will create new synergies through additional combination with other electrode fabrication approaches such as electrodeposition (see Section 2). That is, the sequential electrodeposition of metal- or metal oxide-based active materials onto LbL-assembled conductive textiles can effectively compensate for the time-consuming issues of LbL assembly methods reported to date in achieving high mass loading of active materials. Therefore, we believe that the assembly process based on favorable interfacial interactions and the resultant energy electrodes can provide important insights for realizing high-performance flexible/wearable electronics with desired functionalities, size and shape.

Acknowledgements

This work was supported by a National Research Foundation (NRF) of Korea funded by the Ministry of Education (2019R1A4A1027627; 2016M3A7B4910619; 2017R1A6A3A04003192). This work was also supported by the DGIST R&D Programs of the Ministry of Science and ICT of Korea (20-ET-08).

Conflict of Interest

The authors declare no conflict of interest.

Author Contributions

Y.K., S.L., and C.H.K. contributed equally to this work. Y.K., S.L., C.H.K., S.W.L., and J.C. wrote and revised the manuscript. All authors discussed the results and comments on the manuscript.

Keywords

energy conversion, energy storage, flexible electrodes, interfacial assembly, interfacial design, ligand control

Received: September 17, 2020
Revised: November 23, 2020
Published online: January 15, 2021

© 2021 Wiley-VCH GmbH

[1] W. Zeng, L. Shu, Q. Li, S. Chen, F. Wang, X.-M. Tao, *Adv. Mater.* **2014**, *26*, 5310.
[2] K. Jost, G. Dion, Y. Gogotsi, *J. Mater. Chem. A* **2014**, *2*, 10776.
[3] Z. Bao, X. Chen, *Adv. Mater.* **2016**, *28*, 4177.
[4] F. R. Fan, W. Tang, Z. L. Wang, *Adv. Mater.* **2016**, *28*, 4283.
[5] Z. L. Wang, J. Song, *Science* **2006**, *312*, 242.
[6] G. Zhu, Z.-H. Lin, Q. Jing, C. P. Bai, C. Pan, Y. Yang, Y. Zhou, Z. L. Wang, *Nano Lett.* **2013**, *13*, 847.
[7] B. Duun, H. Kamath, J.-M. Tarascon, *Science* **2011**, *334*, 928.
[8] J. M. Tarascon, M. Armand, *Nature* **2001**, *414*, 359.
[9] M. Beidaghi, Y. Gogotsi, *Energy Environ. Sci.* **2014**, *7*, 867.
[10] S. K. Cheah, E. Perre, M. Rooth, M. Fondell, A. Hårsta, L. Nyholm, M. Boman, T. Gustafsson, J. Lu, P. Simon, K. Edström, *Nano Lett.* **2009**, *9*, 3230.
[11] U. Gulzar, S. Goriparti, E. Miele, T. Li, G. Maidecchi, A. Toma, F. D. Angelis, C. Capiglia, R. P. Zaccaria, *J. Mater. Chem. A* **2016**, *4*, 16771.
[12] Y. Gogotsi, P. Simon, *Science* **2011**, *334*, 917.
[13] J. Jiang, Y. Li, J. Liu, X. Huang, C. Yuan, X. W. (David) Lou, *Adv. Mater.* **2012**, *24*, 5166.
[14] X.-Y. G. Tian, N. Jiang, B.-L. Su, *Energy Environ. Sci.* **2012**, *5*, 9752.
[15] X. Pu, M. Liu, X. Chen, J. Sun, C. Du, Y. Zhang, J. Zhai, W. Hu, Z. L. Wang, *Sci. Adv.* **2017**, *3*, e1700015.
[16] S. S. Kwak, H. Kim, W. Seung, J. Kim, R. Hinchet, S.-W. Kim, *ACS Nano* **2017**, *11*, 10733.
[17] Y. Xu, B. Sun, Y. Ling, Q. Fei, Z. Chen, X. Li, P. Guo, N. Jeon, S. Goswami, Y. Liao, S. Ding, Q. Yu, J. Lin, G. Huang, Z. Yan, *Proc. Natl. Acad. Sci. USA* **2020**, *117*, 205.
[18] J. P. Zheng, *J. Power Source* **2004**, *137*, 158.
[19] L. Mao, Q. Meng, A. Ahmad, Z. Wei, *Adv. Energy Mater.* **2017**, *7*, 1700535.
[20] C. Lei, F. Markoulidis, Z. Ashitaka, C. Lekakou, *Electrochim. Acta* **2013**, *92*, 183.
[21] J. A. Fan, W.-H. Yeo, Y. Su, Y. Hattori, W. Lee, S.-Y. Jung, Y. Zhang, Z. Liu, H. Cheng, L. Falgout, M. Bajema, T. Coleman, D. Gregorie, R. J. Larsen, Y. Huang, J. A. Rogers, *Nat. Commun.* **2014**, *5*, 3266.
[22] M. Daniel, D. Astruc, *Chem. Rev.* **2004**, *104*, 293.
[23] A. Roucoux, J. Schulz, H. Patin, *Chem. Rev.* **2002**, *102*, 3757.
[24] M. Zhou, S. Dong, *Acc. Chem. Res.* **2011**, *44*, 1232.
[25] K.-X. Wang, X.-H. Li, J.-S. Chen, *Adv. Mater.* **2015**, *27*, 527.
[26] G. Decher, *Science* **1997**, *277*, 1232.
[27] F. Caruso, R. A. Caruso, H. Möhwald, *Science* **1998**, *282*, 1111.
[28] N. I. Kovtyukhova, P. J. Ollivier, B. R. Martin, T. E. Mallouk, S. A. Chizhik, E. V. Buzaneva, A. D. Gorchinsky, *Chem. Mater.* **1999**, *11*, 771.
[29] J. Cho, K. Char, J.-D. Hong, K.-B. Lee, *Adv. Mater.* **2001**, *13*, 1076.
[30] J.-S. Lee, J. Cho, C. Lee, I. Kim, J. Park, Y.-M. Kim, H. Shin, J. Lee, F. Caruso, *Nat. Nanotechnol.* **2007**, *2*, 790.
[31] A. A. Mamedov, N. A. Kotov, M. Prato, D. M. Guldi, J. P. Wicksted, A. Hirsch, *Nat. Mater.* **2002**, *1*, 190.
[32] S. W. Lee, B.-S. Kim, S. Chen, Y. Shao-Horn, P. T. Hammond, *J. Am. Chem. Soc.* **2009**, *131*, 671.
[33] S. Srivastava, N. A. Kotov, *Acc. Chem. Res.* **2008**, *41*, 1831.
[34] Y. Kim, J. Zhu, B. Yeom, M. D. Prima, X. Su, J.-G. Kim, S. J. Yoo, C. Uher, N. A. Kotov, *Nature* **2013**, *500*, 59.
[35] Y.-H. Yang, L. Bolling, M. A. Priolo, J. C. Grunlan, *Adv. Mater.* **2013**, *25*, 503.
[36] Z. Tang, Y. Wang, P. Podsiadlo, N. A. Kotov, *Adv. Mater.* **2006**, *18*, 3203.
[37] S. W. Keller, H.-N. Kim, T. E. Mallouk, *J. Am. Chem. Soc.* **1994**, *116*, 8817.
[38] L. Hu, M. Paster, F. L. M., L. Cui, S. Jeong, H. D. Deshazer, J. W. Choi, S. M. Han, Y. Cui, *Nano Lett.* **2010**, *10*, 708.
[39] Y.-C. Li, S. Mannen, A. B. Morgan, S. Chang, Y.-H. Yang, B. Condon, J. C. Grunlan, *Adv. Mater.* **2011**, *23*, 3926.
[40] Z. Ma, A. Wei, J. Ma, L. Shao, H. Jiang, D. Dong, Z. Ji, Q. Wang, S. Kang, *Nanoscale* **2018**, *10*, 7116.
[41] N. C. Cady, J. L. Behnke, A. D. Strickland, *Adv. Funct. Mater.* **2011**, *21*, 2506.
[42] Y. Wang, A. S. Angelatos, F. Caruso, *Chem. Mater.* **2008**, *20*, 848.
[43] S. W. Lee, J. Kim, S. Chen, P. T. Hammond, Y. Shao-Horn, *ACS Nano* **2010**, *4*, 3889.
[44] S. W. Lee, N. Yabuuchi, B. M. Gallant, S. Chen, B.-S. Kim, P. T. Hammond, Y. Shao-Horn, *Nat. Nanotechnol.* **2010**, *5*, 531.
[45] S. Liu, D. G. Kurth, H. Möhwald, D. Volkmer, *Adv. Mater.* **2002**, *14*, 225.
[46] J. Yun, Y. Song, I. Cho, Y. Ko, C. H. Kwon, J. Cho, *Nanoscale* **2019**, *11*, 17815.
[47] C. H. Kwon, Y. Ko, D. Shin, M. Kwon, J. Park, W. K. Bae, S. W. Lee, J. Cho, *Nat. Commun.* **2018**, *9*, 4479.
[48] K. C. Grabar, K. J. Allison, B. E. Baker, R. M. Bright, K. R. Brown, R. G. Freeman, A. P. Fox, C. D. Keating, M. D. Musick, M. J. Natan, *Langmuir* **1996**, *12*, 2353.
[49] J. Schmitt, G. Decher, W. J. Dressick, S. L. Brandow, R. E. Geer, R. Shashidhar, J. M. Calvert, *Adv. Mater.* **1997**, *9*, 61.
[50] J. Y. Kim, J. Y. Oh, M. L. Lee, K. H. Kim, (Samsung Electronics Co., Ltd.), US Patent 9,684,342, **2017**.
[51] C. Pailler-Mattei, S. Bec, H. Zahouani, *Med. Eng. Phys.* **2008**, *30*, 599.
[52] M. Lewin, *Handbook of Fiber Chemistry*, CRC Press, New York **2006**.
[53] R. Huang, M. Huang, X. Li, F. An, N. Koratkar, Z.-Z. Yu, *Adv. Mater.* **2018**, *30*, 1707025.
[54] G. S. Jeong, D.-H. Baek, H. C. Jung, J. H. Song, J. H. Moon, S. W. Hong, I. Y. Kim, S.-H. Lee, *Nat. Commun.* **2012**, *3*, 977.
[55] T. Q. Trung, S. Ramasundaram, B.-U. Hwang, N.-E. Lee, *Adv. Mater.* **2016**, *28*, 502.
[56] H. Jinno, K. Fukuda, X. Xu, S. Park, Y. Suzuki, M. Koizumi, T. Yokota, I. Osaka, K. Takimiya, T. Someya, *Nat. Energy* **2017**, *2*, 780.
[57] L. M. Castano, A. B. Flatau, *Smart Mater. Struct.* **2014**, *23*, 053001.
[58] K. S. Deepa, M. T. Sebastian, J. James, *Appl. Phys. Lett.* **2007**, *91*, 202904.
[59] J. Li, J.-K. Kim, *Compos. Sci. Technol.* **2007**, *67*, 2114.
[60] K. L. Choy, *Prog. Mater. Sci.* **2003**, *48*, 57.
[61] C. D. Dimitrakopoulos, P. R. L. Malenfant, *Adv. Mater.* **2002**, *14*, 99.
[62] X. Li, W. Cai, J. An, S. Kim, J. Nah, D. Yang, R. Piner, A. Velamakanni, I. Jung, E. Tutuc, S. K. Banerjee, L. Colombo, R. S. Ruoff, *Science* **2009**, *324*, 1312.
[63] J. Wang, M. Zhu, R. A. Outlaw, X. Zhao, D. M. Manos, B. C. Holloway, *Carbon* **2004**, *42*, 2867.
[64] A. Malesevic, R. Vitchev, K. Schouteden, A. Volodin, L. Zhang, G. V. Tendeloo, A. Vanhulsel, C. V. Haesendonck, *Nanotechnology* **2008**, *19*, 305604.
[65] L. Zhang, M. Fairbanks, T. L. Andrew, *Adv. Funct. Mater.* **2017**, *27*, 1700415.
[66] M. Wang, X. Wang, P. Moni, A. Liu, D. H. Kim, W. J. Jo, H. Sojoudi, K. K. Gleason, *Adv. Mater.* **2017**, *29*, 1604606.
[67] A. M. Hussain, F. A. Ghaffar, S. I. Park, J. A. Rogers, A. Shamim, M. M. Hussain, *Adv. Funct. Mater.* **2015**, *25*, 6565.
[68] H. Yabuta, M. Sano, K. Abe, T. Aiba, T. Den, H. Kumomi, *Appl. Phys. Lett.* **2006**, *89*, 112123.
[69] J. F. Pierson, D. Wiederkehr, A. Billard, *Thin Solid Films* **2005**, *478*, 196.
[70] S. X. Jiang, W. F. Qin, R. H. Guo, L. Zhang, *Surf. Coat. Technol.* **2010**, *204*, 3662.
[71] P. J. Kelly, R. D. Arnell, *Vacuum* **2000**, *56*, 159.
[72] D. Tobjörk, R. Österbacka, *Adv. Mater.* **2011**, *23*, 1935.
[73] J. Zhu, S. Tang, J. Wu, X. Shi, B. Zhu, X. Meng, *Adv. Energy Mater.* **2017**, *7*, 1601234.
[74] A. C. Siegel, S. T. Phillips, M. D. Dickey, N. Lu, Z. Suo, G. M. Whitesides, *Adv. Funct. Mater.* **2010**, *20*, 28.

© 2021 Wiley-VCH GmbH

[75] R. Shenhar, T. B. Norsten, V. M. Rotello, *Adv. Mater.* **2005**, *17*, 657.
[76] A. Hajian, Z. Wang, L. A. Berglund, M. M. Hamedi, *Adv. Electron. Mater.* **2019**, *5*, 1800924.
[77] L. Y. Shiroma, M. Santhiago, A. L. Gobbi, L. T. Kubota, *Anal. Chim. Acta* **2012**, *725*, 44.
[78] L. Yuan, X. Xiao, T. Ding, J. Zhong, X. Zhang, Y. Shen, B. Hu, Y. Huang, J. Zhou, Z. L. Wang, *Angew. Chem., Int. Ed.* **2012**, *51*, 4934.
[79] Y.-Z. Zhang, Y. Wang, T. Cheng, W.-Y. Lai, H. Pang, W. Huang, *Chem. Soc. Rev.* **2015**, *44*, 5181.
[80] A. I. Ayesh, N. Qamhieh, H. Ghamlouche, S. Thaker, M. El-Shaer, *J. Appl. Phys.* **2010**, *107*, 034317.
[81] P. Brault, E. C. Neyts, *Catal. Today* **2015**, *256*, 3.
[82] Y. Ko, M. Kwon, Y. Song, S. W. Lee, J. Cho, *Adv. Funct. Mater.* **2018**, *28*, 1804926.
[83] M.-C. Hsieh, C. Kim, M. Nogi, K. Suganuma, *Nanoscale* **2013**, *5*, 9289.
[84] S. Rosset, M. Niklaus, P. Dubois, H. R. Shea, *Adv. Funct. Mater.* **2009**, *19*, 470.
[85] W. Kim, S. Kwon, Y. C. Han, K. C. Choi, S.-H. Kang, B.-C. Park, *Adv. Electron. Mater.* **2016**, *2*, 1600220.
[86] S. Magdassi, M. Grouchko, O. Berezin, A. Kamyshny, *ACS Nano* **2010**, *4*, 1943.
[87] H. Sakai, T. Kanda, H. Shibata, T. Ohkubo, M. Abe, *J. Am. Chem. Soc.* **2006**, *128*, 4944.
[88] G. O. Mallory, J. B. Haidu, William Andrew, *Electroless Plating: Fundamentals and Applications*, American Electroplaters and Surface Finishers Society, Orlando, FL **1991**.
[89] N. Kanani, *Electroplating: Basic Principles, Processes and Practice*, Elsevier Advanced Technology, Oxford, UK **2004**.
[90] T. A. Schaedler, A. J. Jacobsen, A. Torrents, A. E. Sorensen, J. Liam, J. R. Greer, L. Valdevit, W. B. Carter, *Science* **2011**, *334*, 962.
[91] Y. Yu, J. Zeng, C. Chen, Z. Xie, R. Guo, Z. Liu, X. Zhou, Y. Yang, Z. Zheng, *Adv. Mater.* **2014**, *26*, 810.
[92] Y. Shacham-Diamand, A. Inberg, Y. Sverdlov, N. Croitoru, *J. Electrochem. Soc.* **2000**, *147*, 3345.
[93] W. Hao, R. Wu, R. Zhang, Y. Ha, Z. Chen, L. Wang, Y. Yang, X. Ma, D. Sun, F. Fang, Y. Guo, *Adv. Energy Mater.* **2018**, *8*, 1801372.
[94] K. Cheng, M.-H. Yang, W. W. W. Chiu, C.-Y. Huang, J. Chang, T.-F. Ying, Y. Yang, *Macromol. Rapid Commun.* **2005**, *26*, 247.
[95] F. Z. Kong, X. B. Zhang, W. Q. Xiong, F. Liu, W. Z. Huang, Y. L. Sun, J. P. Yu, X. W. Chen, *Surf. Coat. Technol.* **2002**, *155*, 33.
[96] H. M. Lee, S.-Y. Choi, A. Jung, S. H. Ko, *Angew. Chem., Int. Ed.* **2013**, *125*, 7872.
[97] L. Liu, Y. Yu, C. Yan, K. Li, Z. Zheng, *Nat. Commun.* **2015**, *6*, 7260.
[98] C. H. Lee, H. S. Lim, J. Kim, J. H. Cho, *ACS Nano* **2011**, *5*, 7397.
[99] Y. Yu, C. Yan, Z. Zheng, *Adv. Mater.* **2014**, *26*, 5508.
[100] M. S. Miller, G. J. E. Davidson, B. J. Sahli, C. M. Mailloux, T. B. Carmichael, *Adv. Mater.* **2008**, *20*, 59.
[101] X. Wang, H. Hu, Y. Shen, X. Zhou, Z. Zheng, *Adv. Mater.* **2011**, *23*, 3090.
[102] J. L. Valentín, I. Mora-Barrantes, J. Carretero-González, M. A. López-Manchado, P. Sotta, D. R. Long, K. Saalwächter, *Macromolecules* **2010**, *43*, 334.
[103] S. P. Lacour, S. Wagner, Z. Huang, Z. Suo, *Appl. Phys. Lett.* **2003**, *82*, 2404.
[104] Z. F. Liu, S. Fang, F. A. Moura, J. N. Ding, N. Jiang, J. Di, M. Zhang, X. Lepró, D. S. Galvão, C. S. Haines, N. Y. Yuan, S. G. Yin, D. W. Lee, R. Wang, H. Y. Wang, W. Lv, C. Dong, R. C. Zhang, M. J. Chen, Q. Yin, Y. T. Chong, R. Zhang, X. Wang, M. D. Lima, R. Ovalle-Robles, D. Qian, H. Lu, R. H. Baughman, *Science* **2015**, *349*, 400.
[105] Y. Cheng, R. Wang, J. Sun, L. Gao, *ACS Nano* **2015**, *9*, 3887.
[106] X. Hu, Y. Dou, J. Li, Z. Liu, *Small* **2019**, *15*, 1804805.
[107] Y. Cheng, X. Lu, K. H. Chan, R. Wang, Z. Cao, J. Sun, G. W. Ho, *Nano Energy* **2017**, *41*, 511.
[108] Z. Wang, S. Ji, F. Liu, H. Wang, X. Wang, Q. Wang, B. G. Pollet, R. Wang, *ACS Appl. Mater. Interfaces* **2019**, *11*, 29791.
[109] K. Chen, R. Pathak, A. Gurung, K. M. Reza, N. Ghimire, J. Pokharel, A. Baniya, W. He, J. J. Wu, Q. (Quinn) Qiao, Y. Zhou, *J. Mater. Chem. A* **2020**, *8*, 1911.
[110] S. An, H. S. Jo, D.-Y. Kim, H. J. Lee, B.-K. Ju, S. S. Al-Deyab, J.-H. Ahn, Y. Qin, M. T. Swihart, A. L. Yarin, S. S. Yoon, *Adv. Mater.* **2016**, *28*, 7149.
[111] S. Bae, H. Kim, Y. Lee, X. Xu, J.-S. Park, Y. Zheng, J. Balakrishnan, T. Lei, H. R. Kim, Y. I. Song, *Nat. Nanotechnol.* **2010**, *5*, 574.
[112] S. Soltanian, R. Rahmanian, B. Gholamkhass, N. M. Kiasari, F. Ko, P. Servati, *Adv. Energy Mater.* **2013**, *3*, 1332.
[113] H. Wu, D. Kong, Z. Ruan, P.-C. Hsu, S. Wang, Z. Yu, T. J. Carney, L. Hu, S. Fan, Y. Cui, *Nat. Nanotechnol.* **2013**, *8*, 421.
[114] T. Kim, Y. W. Kim, H. S. Lee, H. Kim, W. S. Yang, K. S. Suh, *Adv. Funct. Mater.* **2013**, *23*, 1250.
[115] S. De, P. J. King, P. E. Lyons, U. Khan, J. N. Coleman, *ACS Nano* **2010**, *4*, 7064.
[116] M. Park, J. Im, M. Shin, Y. Min, J. Park, H. Cho, S. Park, M.-B. Shim, S. Jeon, D.-Y. Chung, J. Bae, J. Parkm, U. Jeong, K. Kim, *Nat. Nanotechnol.* **2012**, *7*, 803.
[117] P. Calvert, *Chem. Mater.* **2001**, *13*, 3299.
[118] J. Z. Wang, Z. H. Zheng, H. W. Li, W. T. S. Huck, H. Sirringhaus, *Nat. Mater.* **2004**, *4*, 171.
[119] B. W. An, K. Kim, H. Lee, S.-Y. Kim, Y. Shim, D.-Y. Lee, J. Y. Song, J.-U. Park, *Adv. Mater.* **2015**, *27*, 4322.
[120] K. Jost, C. R. Perez, J. K. Mcdonough, V. Presser, M. Heon, G. Dion, Y. Gogotsi, *Energy Environ. Sci.* **2011**, *4*, 5060.
[121] P. Chen, H. Chen, J. Qui, C. Zhou, *Nano Res.* **2010**, *3*, 594.
[122] M. Kuang, L. Wang, Y. Song, *Adv. Mater.* **2014**, *26*, 6950.
[123] F. Bonaccorso, A. Bartolotta, J. N. Coleman, C. Backes, *Adv. Mater.* **2016**, *28*, 6136.
[124] N. Mastsuhisa, D. Inoune, P. Zalar, H. Jin, Y. Matsuba, A. Itoh, T. Yokota, D. Hashizume, T. Someya, *Nat. Mater.* **2017**, *16*, 834.
[125] A. Kamyshny, S. Magdassi, *Small* **2014**, *10*, 3515.
[126] S. Witomska, T. Leydecker, A. Ciesielski, P. Samori, *Adv. Funct. Mater.* **2019**, *29*, 1901126.
[127] F. Torrisi, T. Hasan, W. Wu, Z. Sun, A. Lombardo, T. S. Kulmala, G.-W. Hsieh, S. Jung, F. Bonaccorso, P. J. Paul, D. Chu, A. G. Ferrari, *ACS Nano* **2012**, *6*, 2992.
[128] S. B. Walker, J. A. Lewis, *J. Am. Chem. Soc.* **2012**, *134*, 1419.
[129] K. Pan, Y. Fan, T. Leng, J. Li, Z. Xin, J. Zhang, L. Hao, J. Gallop, K. S. Novoselov, Z. Hu, *Nat. Commun.* **2018**, *9*, 5197.
[130] M. Singh, H. M. Haverinen, P. Dhagat, G. E. Jabbour, *Adv. Mater.* **2010**, *22*, 673.
[131] K.-H. Choi, J. Yoo, C. K. Lee, S.-Y. Lee, *Energy Environ. Sci.* **2016**, *9*, 2812.
[132] L. Li, E. B. Secor, K.-S. Chen, J. Zhu, X. Liu, T. Z. Gao, J.-W. T. Seo, Y. Zhao, M. C. Hersam, *Adv. Energy Mater.* **2016**, *6*, 1600909.
[133] L. Hu, D. S. Hecht, G. Grüner, *Chem. Rev.* **2010**, *110*, 5790.
[134] K. Kordás, T. Mustonen, G. Tóth, H. Jantunen, M. Lajunen, C. Soldano, S. Talapatra, S. Kar, R. Vajtai, P. M. Ajayan, *Small* **2006**, *2*, 1021.
[135] T. Mustonen, J. Mäklin, K. Kordás, N. Halonen, G. Tóth, S. Saukko, J. Vähäkangas, H. Jantunen, S. Kar, P. M. Ajayan, R. Vajtai, P. Helistö, H. Seppä, H. Hoilanen, *Phys. Rev. B* **2008**, *77*, 125430.
[136] S. W. Lee, B. M. Gallant, Y. Lee, N. Yoshida, D. Y. Kim, Y. Yamada, S. Noda, A. Yamada, Y. Shao-Horn, *Energy Environ. Sci.* **2012**, *5*, 5437.
[137] B. Y. Ahn, E. B. Duoss, M. J. Motala, X. Guo, S.-I. Park, Y. Xiong, J. Yoon, R. G. Nuzzo, J. A. Rogers, J. A. Lewis, *Science* **2009**, *323*, 1590.
[138] H. Shahariar, I. Kim, H. Soewardiman, J. S. Jur, *ACS Appl. Mater. Interfaces* **2019**, *11*, 6208.

© 2021 Wiley-VCH GmbH

[139] M. Grouchko, A. Kamyshny, C. F. Mihailescu, D. F. Anghel, S. Magdassi, *ACS Nano* **2011**, *5*, 3354.
[140] Y. Song, D. Kim, S. Kang, Y. Ko, J. Ko, J. Huh, Y. Ko, S. W. Lee, J. Cho, *Adv. Funct. Mater.* **2019**, *29*, 1806584.
[141] J. D. Padmos, M. L. Personick, Q. Tang, P. N. Duchesne, D. Jiang, C. A. Mirkin, P. Zhang, *Nat. Commun.* **2015**, *6*, 7664.
[142] N. Matsuhisa, M. Kaltenbrunner, T. Yokota, H. Jinno, K. Kuribara, T. Sekitani, T. Someya, *Nat. Commun.* **2015**, *6*, 7461.
[143] D. K. Schwartz, *Annu. Rev. Phys. Chem.* **2001**, *52*, 107.
[144] Y. Xiang, S. Lu, S. P. Jiang, *Chem. Soc. Rev.* **2012**, *41*, 7291.
[145] E. Steven, W. R. Saleh, V. Lebedev, S. F. A. Acquah, V. Laukhin, R. G. Alamo, J. S. Brooks, *Nat. Commun.* **2013**, *4*, 2435.
[146] J. Kim, A. S. Campbell, B. E. F. de Ávila, J. Wang, *Nat. Biotechnol.* **2019**, *37*, 389.
[147] G. Yu, L. Hu, N. Liu, H. Wang, M. Vosgueritchian, Y. Yang, Y. Cui, Z. Bao, *Nano Lett.* **2011**, *11*, 4438.
[148] H. Sun, S. Xie, Y. Li, Y. Jiang, X. Sun, B. Wang, H. Peng, *Adv. Mater.* **2016**, *28*, 8431.
[149] L. Hu, F. L. Mantia, H. Wu, X. Xie, J. McDonough, M. Pasta, Y. Cui, *Adv. Energy Mater.* **2011**, *1*, 1012.
[150] Y.-R. Nian, H. Teng, *J. Electroanal. Chem.* **2003**, *540*, 119.
[151] T. Momma, X. Liu, T. Osaka, Y. Ushio, Y. Sawada, *J. Power Source* **1996**, *60*, 249.
[152] A. Lewandowski, A. Olejniczak, M. Galinski, I. Stepniak, *J. Power Source* **2010**, *195*, 5814.
[153] R. Andrews, D. Jacques, D. Qian, T. Rantell, *Acc. Chem. Res.* **2002**, *35*, 1008.
[154] V. C. Moore, M. S. Strano, E. H. Haroz, R. G. Hauge, R. E. Smalley, *Nano Lett.* **2003**, *3*, 1379.
[155] K. Yurekli, C. A. Mitchell, R. Krishnamoorti, *J. Am. Chem. Soc.* **2004**, *126*, 9902.
[156] R. J. Chen, Y. Zhang, D. Wang, H. Dai, *J. Am. Chem. Soc.* **2001**, *123*, 3838.
[157] E. Katz, I. Willner, *ChemPhysChem* **2004**, *5*, 1084.
[158] S. Gong, W. Schwalb, Y. Wang, Y. Chen, Y. Tang, J. Si, B. Shirinzadeh, W. Cheng, *Nat. Commun.* **2014**, *5*, 3132.
[159] S. C. Warren, L. C. Messina, L. S. Slaughter, M. Kamperman, Q. Zhou, S. M. Gruner, F. J. DiSalvo, U. Wiesner, *Science* **2008**, *320*, 1748.
[160] Y. Ko, M. Kwon, W. K. Bae, B. Lee, S. W. Lee, J. Cho, *Nat. Commun.* **2017**, *8*, 536.
[161] D. Shin, C. H. Kwon, Y. Ko, B. Lee, S. W. Lee, J. Cho, *J. Mater. Chem. A* **2018**, *6*, 20421.
[162] S. Lee, Y. Song, Y. Ko, Y. Ko, J. Ko, C. H. Kwon, J. Huh, S.-W. Kim, B. Yeom, J. Cho, *Adv. Mater.* **2020**, *32*, 1906460.
[163] S.-I. Park, J.-H. Ahn, X. Feng, S. Wang, Y. Huang, J. A. Rogers, *Adv. Funct. Mater.* **2008**, *18*, 2673.
[164] X. Peng, L. Peng, C. Wu, Y. Xie, *Chem. Soc. Rev.* **2014**, *43*, 3303.
[165] S. Choi, H. Lee, R. Ghaffari, T. Hyeon, D.-H. Kim, *Adv. Mater.* **2016**, *28*, 4203.
[166] D. Damjanovic, *Rep. Prog. Phys.* **1998**, *61*, 1267.
[167] H. Fu, R. E. Cohen, *Nature* **2000**, *403*, 281.
[168] C. Ederer, N. A. Spaldin, *Phys. Rev. Lett.* **2005**, *95*, 257601.
[169] J. Zhang, C. Wang, C. Bowen, *Nanoscale* **2014**, *6*, 13314.
[170] Y. Gao, Z. L. Wang, *Nano Lett.* **2007**, *7*, 2499.
[171] X. Wang, J. Song, J. Liu, Z. L. Wang, *Science* **2007**, *316*, 102.
[172] Z. L. Wang, *Adv. Mater.* **2007**, *19*, 889.
[173] S. Xu, Y. Qin, C. Xu, Y. Wei, R. Yang, Z. L. Wang, *Nat. Nanotechnol.* **2010**, *5*, 366.
[174] X. Wang, *Nano Energy* **2012**, *1*, 13.
[175] J.-H. Lee, K. Y. Lee, M. K. Gupta, T. Y. Kim, D.-Y. Lee, J. Oh, C. Ryu, W. J. Yoo, C.-Y. Kang, S.-J. Yoon, J.-B. Yoo, S.-W. Kim, *Adv. Mater.* **2014**, *26*, 765.
[176] G. Chen, Y. Li, M. Bick, J. Chen, *Chem. Rev.* **2020**, *120*, 3668.
[177] K. Dong, X. Peng, Z. L. Wang, *Adv. Mater.* **2020**, *32*, 1902549.
[178] F. Mokhtari, Z. Cheng, R. Raad, J. Xi, J. Foroughi, *J. Mater. Chem. A* **2020**, *8*, 9496.
[179] Y. Qin, X. Wang, Z. L. Wang, *Nature* **2008**, *451*, 809.
[180] V. Bhavanasi, D. Y. Kusuma, P. S. Lee, *Adv. Energy Mater.* **2014**, *4*, 1400723.
[181] C. K. Jeong, C. Baek, A. I. Kingon, K.-I. Park, S.-H. Kim, *Small* **2018**, *14*, 1704022.
[182] L. S. McCarty, G. M. Whitesides, *Angew. Chem., Int. Ed.* **2008**, *47*, 2188.
[183] Z. L. Wang, *ACS Nano* **2013**, *7*, 9533.
[184] Z. L. Wang, *Mater. Today* **2017**, *20*, 74.
[185] F.-R. Fan, Z.-Q. Tian, Z. Lin Wang, *Nano Energy* **2012**, *1*, 328.
[186] S. Wang, L. Lin, Z. L. Wang, *Nano Lett.* **2012**, *12*, 6339.
[187] Z. L. Wang, *Faraday Discuss.* **2014**, *176*, 447.
[188] H. Y. Li, L. Su, S. Y. Kuang, C. F. Pan, G. Zhu, Z. L. Wang, *Adv. Funct. Mater.* **2015**, *25*, 5691.
[189] G. Song, Y. Kim, S. Yu, M.-O. Kim, S.-H. Park, S. M. Cho, D. B. Velusamy, S. H. Cho, K. L. Kim, J. Kim, E. Kim, C. Park, *Chem. Mater.* **2015**, *27*, 4749.
[190] M. P. Kim, Y. Lee, Y. H. Hur, J. Park, J. Kim, Y. Lee, C. W. Ahn, S. W. Song, Y. S. Jung, H. Ko, *Nano Energy* **2018**, *53*, 37.
[191] K. Y. Lee, J. Chun, J.-H. Lee, K. N. Kim, N.-R. Kang, J.-Y. Kim, M. H. Kim, K.-S. Shin, M. K. Gupta, J. M. Baik, S.-W. Kim, *Adv. Mater.* **2014**, *26*, 5037.
[192] J. Chun, J. W. Kim, W.-S. Jung, C.-Y. Kang, S.-W. Kim, Z. L. Wang, J. M. Baik, *Energy Environ. Sci.* **2015**, *8*, 3006.
[193] J. Chen, H. Guo, X. He, G. Liu, Y. Xi, H. Shi, C. Hu, *ACS Appl. Mater. Interfaces* **2016**, *8*, 736.
[194] Q. Zheng, L. Fang, H. Guo, K. Yang, Z. Cai, M. A. B. Meador, S. Gong, *Adv. Funct. Mater.* **2018**, *28*, 1706365.
[195] K.-I. Park, M. Lee, Y. Liu, S. Moon, G.-T. Hwang, G. Zhu, J. E. Kim, S. O. Kim, D. K. Kim, Z. L. Wang, K. J. Lee, *Adv. Mater.* **2012**, *24*, 2999.
[196] K.-I. Park, C. K. Jeong, J. Ryu, G.-T. Hwang, K. J. Lee, *Adv. Energy Mater.* **2013**, *3*, 1539.
[197] C. K. Jeong, J. Lee, S. Han, J. Ryu, G.-T. Hwang, D. Y. Park, J. H. Park, S. S. Lee, M. Byun, S. H. Ko, K. J. Lee, *Adv. Mater.* **2015**, *27*, 2866.
[198] G. Zhang, Q. Liao, Z. Zhang, Q. Liang, Y. Zhao, X. Zheng, Y. Zhang, *Adv. Sci.* **2016**, *3*, 1500257.
[199] P. Martins, A. C. Lopes, S. Lanceros-Mendez, *Prog. Polym. Sci.* **2014**, *39*, 683.
[200] H.-J. Ye, W.-Z. Shao, L. Zhen, *J. Appl. Polym. Sci.* **2013**, *129*, 2940.
[201] K. Shi, B. Sun, X. Huang, P. Jiang, *Nano Energy* **2018**, *52*, 153.
[202] M. Zhu, M. Lou, I. Abdalla, J. Yu, Z. Li, B. Ding, *Nano Energy* **2020**, *69*, 104429.
[203] X. Guan, B. Xu, J. Gong, *Nano Energy* **2020**, *70*, 104516.
[204] S. K. Mahadeva, K. Walus, B. Stoeber, *ACS Appl. Mater. Interfaces* **2014**, *6*, 7547.
[205] Y. Kim, K. Y. Lee, S. K. Hwang, C. Park, S.-W. Kim, J. Cho, *Adv. Funct. Mater.* **2014**, *24*, 6262.
[206] C. Lee, S. Yang, D. Choi, W. Kim, J. Kim, J. Hong, *Nano Energy* **2019**, *57*, 353.
[207] S. Wang, Y. Xie, S. Niu, L. Lin, C. Liu, Y. S. Zhou, Z. L. Wang, *Adv. Mater.* **2014**, *26*, 6720.
[208] X.-S. Zhang, M.-D. Han, R.-X. Wang, B. Meng, F.-Y. Zhu, X.-M. Sun, W. Hu, W. Wang, Z.-H. Li, H.-X. Zhang, *Nano Energy* **2014**, *4*, 123.
[209] S. S. Kwak, S. M. Kim, H. Ryu, J. Kim, U. Khan, H.-J. Yoon, Y. H. Jeong, S.-W. Kim, *Energy Environ. Sci.* **2019**, *12*, 3156.
[210] S. Li, Y. Fan, H. Chen, J. Nie, Y. Liang, X. Tao, J. Zhang, X. Chen, E. Fu, Z. L. Wang, *Energy Environ. Sci.* **2020**, *13*, 896.
[211] Z. Bai, Y. Xu, Z. Zhang, J. Zhu, C. Gao, Y. Zhang, H. Jia, J. Guo, *Nano Energy* **2020**, *75*, 104884.
[212] Y. Zhou, C. Fuentes-Hernandez, J. Shim, J. Meyer, A. J. Giordano, H. Li, P. Winget, T. Papadopoulos, H. Cheun, J. Kim, M. Fenoll,

© 2021 Wiley-VCH GmbH

A. Dindar, W. Haske, E. Najafabadi, T. M. Khan, H. Sojoudi, S. Barlow, S. Graham, J.-L. Brédas, S. R. Marder, A. Kahn, B. Kippelen, *Science* **2012**, *336*, 327.
[213] S. Wang, Y. Zi, Y. S. Zhou, S. Li, F. Fan, L. Lin, Z. L. Wang, *J. Mater. Chem. A* **2016**, *4*, 3728.
[214] S.-H. Shin, Y. E. Bae, H. K. Moon, J. Kim, S.-H. Choi, Y. Kim, H. J. Yoon, M. H. Lee, J. Nah, *ACS Nano* **2017**, *11*, 6131.
[215] S. Chun, I. Y. Choi, W. Son, J. Jung, S. Lee, H. S. Kim, C. Pang, W. Park, J. K. Kim, *ACS Energy Lett.* **2019**, *4*, 1748.
[216] C. Park, M. Koo, G. Song, S. M. Cho, H. S. Kang, T. H. Park, E. H. Kim, C. Park, *ACS Nano* **2020**, *14*, 755.
[217] S. M. Cho, G. Song, S. K. Hwang, R. H. Kim, J. Lee, S. Yu, J. Huh, H. J. Park, C. Park, *Chem. - Eur. J.* **2015**, *21*, 18375.
[218] D. Jang, Y. Kim, T. Y. Kim, K. Koh, U. Jeong, J. Cho, *Nano Energy* **2016**, *20*, 283.
[219] D. Kim, S. Lee, Y. Ko, C. H. Kwon, J. Cho, *Nano Energy* **2018**, *44*, 228.
[220] S. Lee, B. Yeom, Y. Kim, J. Cho, *Nano Energy* **2019**, *56*, 1.
[221] F. Wen, Z. Sun, T. He, Q. Shi, M. Zhu, Z. Zhang, L. Li, T. Zhang, C. Lee, *Adv. Sci.* **2020**, *7*, 2000261.
[222] N. Bowden, S. Brittain, A. G. Evans, J. W. Hutchinson, G. M. Whitesides, *Nature* **1998**, *393*, 146.
[223] S. Yang, K. Khare, P.-C. Lin, *Adv. Funct. Mater.* **2010**, *20*, 2550.
[224] A. T. Yahiro, S. M. Lee, D. O. Kimble, *Biochim. Biophys. Acta.* **1964**, *88*, 375.
[225] X. Xiao, H.-Q. Xia, R. Wu, L. Bai, L. Yan, E. Magner, S. Cosnier, E. Lojou, Z. Zhu, A. Liu, *Chem. Rev.* **2019**, *119*, 9509.
[226] I. Jeerapan, J. R. Sempionatto, J. Wang, *Adv. Funct. Mater.* **2020**, *30*, 1906243.
[227] I. Jeerapan, J. R. Sempionatto, A. Pavinatto, J.-M. You, J. Wang, *J. Mater. Chem. A* **2016**, *4*, 18342.
[228] X. Xiao, T. Siepenkoetter, P. Ó. Conghaile, D. Leech, E. Magner, *ACS Appl. Mater. Interfaces* **2018**, *10*, 7107.
[229] G. Valdés-Ramírez, Y.-C. Li, J. Kim, W. Jia, A. J. Bandodkar, R. Nunez-Flores, P. R. Miller, S.-Y. Wu, R. Narayan, J. R. Windmiller, R. Polsky, J. Wang, *Electrochem. Commun.* **2014**, *47*, 58.
[230] G. Güven, S. Şahin, A. Güven, E. H. Yu, *Front. Energy Res.* **2016**, *4*, 4.
[231] C. H. Kwon, S.-H. Lee, Y.-B. Choi, J. A. Lee, S. H. Kim, H.-H. Kim, G. M. Spinks, G. G. Wallace, M. D. Lima, M. E. Kozlov, R. H. Baughman, S. J. Kim, *Nat. Commun.* **2014**, *5*, 3928.
[232] V. Coman, R. Ludwig, W. Harreither, D. Haltrich, L. Gorton, T. Ruzgas, S. Shleev, *Fuel Cells* **2010**, *10*, 9.
[233] P. Asuri, S. S. Karajanagi, H. Yang, T. J. Yim, R. S. Kane, J. S. Dordick, *Langmuir* **2006**, *22*, 5833.
[234] S. S. Karajanagi, A. A. Vertegel, R. S. Kane, J. S. Dordick, *Langmuir* **2004**, *20*, 11594.
[235] A. Le Goff, M. Holzinger, S. Cosnier, *Analyst* **2011**, *136*, 1279.
[236] I. Ivanov, T. Vidaković-Koch, K. Sundmacher, *Energies* **2010**, *3*, 803.
[237] K. Matsuura, T. Saito, T. Okazaki, S. Ohshima, M. Yumura, S. Iijima, *Chem. Phys. Lett.* **2006**, *429*, 497.
[238] Y. Gao, I. Kyratzis, *Bioconjugate Chem.* **2008**, *19*, 1945.
[239] J. T. Cang-Rong, G. Pastorin, *Nanotechnology* **2009**, *20*, 255102.
[240] A. S. Campbell, Y. J. Jeong, S. M. Geier, R. R. Koepsel, A. J. Russell, M. F. Islam, *ACS Appl. Mater. Interfaces* **2015**, *7*, 4056.
[241] Y. F. Gao, T. Yang, X. L. Yang, Y. S. Zhang, B. L. Xiao, J. Hong, N. Sheibani, H. Ghourchian, T. Hong, A. A. Moosavi-Movahedi, *Biosens. Bioelectron.* **2014**, *60*, 30.
[242] E. Laviron, *J. Electroanal. Chem.* **1979**, *101*, 19.
[243] V. Mani, B. Devadas, S. M. Chen, *Biosens. Bioelectron.* **2013**, *41*, 309.
[244] A. Heller, *Curr. Opin. Chem. Biol.* **2006**, *10*, 664.
[245] C. M. Moore, N. L. Akers, A. D. Hill, Z. C. Johnson, S. D. Minteer, *Biomacromolecules* **2004**, *5*, 1241.
[246] T. L. Klotzbach, M. Watt, Y. Ansari, S. D. Minteer, *J. Membr. Sci.* **2008**, *311*, 81.
[247] A. Lesniewski, M. Paszewski, M. Opallo, *Electrochem. Commun.* **2010**, *12*, 435.
[248] J. Zhang, X. Huang, L. Zhang, Y. Si, S. Guo, H. Su, J. Liu, *Sustainable Energy Fuels* **2020**, *4*, 68.
[249] K. H. Hyun, S. W. Han, W. Koh, Y. Kwon, *J. Power Sources* **2015**, *286*, 197.
[250] C. H. Kwon, Y. Ko, D. Shin, S. W. Lee, J. Cho, *J. Mater. Chem. A* **2019**, *7*, 13495.
[251] Y. Ogawa, Y. Takai, Y. Kato, H. Kai, T. Miyake, M. Nishizawa, *Biosens. Bioelectron.* **2015**, *74*, 947.
[252] W. Jia, X. Wang, S. Imani, A. J. Bandodkar, J. Ramirez, P. P. Mercier, J. Wang, *J. Mater. Chem. A* **2014**, *2*, 18184.
[253] A. J. Bandodkar, J.-M. You, N.-H. Kim, Y. Gu, R. Kumar, A. M. V. Mohan, J. Kurniawan, S. Imani, T. Nakagawa, B. Parish, M. Parthasarathy, P. P. Mercier, S. Xu, J. Wang, *Energy Environ. Sci.* **2017**, *10*, 1581.
[254] W. Jia, G. Valdes-Ramirez, A. J. Bandodkar, J. R. Windmiller, J. Wang, *Angew. Chem., Int. Ed.* **2013**, *52*, 7233.
[255] J. Lv, I. Jeerapan, F. Tehrani, L. Yin, C. A. Silva-Lopez, J.-H. Jang, D. Joshuia, R. Shah, Y. Liang, L. Xie, F. Soto, C. Chen, E. Karshalev, C. Kong, Z. Yang, J. Wang, *Energy Environ. Sci.* **2018**, *11*, 3431.
[256] X. Pu, W. Hu, Z. L. Wang, *Small* **2018**, *14*, 1702817.
[257] I. Shitanda, K. Takamatsu, A. Niiyama, T. Mikawa, Y. Hoshi, M. Itagaki, S. Tsujimura, *J. Power Sources* **2019**, *436*, 226844.
[258] S. J. Yin, Z. W. Jin, T. Miyake, *Biosens. Bioelectron.* **2019**, *141*, 111471.
[259] M. Christwardana, K. J. Kim, Y. Kwon, *Sci. Rep.* **2016**, *6*, 30128.
[260] D. M. Chapin, C. S. Fuller, G. L. Pearson, *J. Appl. Phys.* **1954**, *25*, 676.
[261] Y. Zhang, S.-W. Ng, X. Lu, Z. Zheng, *Chem. Rev.* **2020**, *120*, 2049.
[262] M. Yuan, M. Liu, E. H. Sargent, *Nat. Energy* **2016**, *1*, 16016.
[263] K. Xiao, R. Lin, Q. Han, Y. Hou, Z. Qin, H. T. Nguyen, J. Wen, M. Wei, V. Yeddu, M. I. Saidaminov, Y. Gao, X. Luo, Y. Wang, H. Gao, C. Zhang, J. Xu, J. Zhu, E. H. Sargent, H. Tan, *Nat. Energy* **2020**, *5*, 870.
[264] D. Zhitomirsky, O. Voznyy, L. Levina, S. Hoogland, K. W. Kemp, A. H. Ip, S. M. Thon, E. H. Sargent, *Nat. Commun.* **2014**, *5*, 3803.
[265] R. J. Ellingson, M. C. Beard, J. C. Johnson, P. Yu, O. I. Micic, A. J. Nosik, A. Shabaev, A. L. Efros, *Nano Lett.* **2005**, *5*, 865.
[266] J. M. Ball, A. Petrozza, *Nat. Energy* **2016**, *1*, 16149.
[267] X. Zheng, B. Chen, J. Dai, Y. Fang, Y. Bai, Y. Lin, H. Wei, X. C. Zeng, J. Huang, *Nat. Energy* **2017**, *2*, 17102.
[268] R. Azmi, H. Aqoma, W. T. Hadmojo, J.-M. Yun, S. Yoon, K. Kim, Y. R. Do, S.-H. Oh, S.-Y. Jang, *Adv. Energy Mater.* **2016**, *6*, 1502146.
[269] X. Zhang, P. K. Santra, L. Tian, M. B. Johansson, H. Rensmo, E. M. Johansson, *ACS Nano* **2017**, *11*, 8478.
[270] N. Wang, K. Zhao, T. Ding, W. Liu, A. S. Ahmed, Z. Wang, M. Tian, X. W. Sun, Q. Zhang, *Adv. Energy Mater.* **2017**, *7*, 1700522.
[271] T. Bu, J. Li, F. Zheng, W. Chen, X. Wen, Z. Ku, Y. Peng, J. Zhong, Y.-B. Cheng, F. Huang, *Nat. Commun.* **2018**, *9*, 4609.
[272] M. Craetzel, R. A. J. Janssen, D. B. Mitzi, E. H. Sargent, *Nature* **2012**, *488*, 304.
[273] H. Yang, W. Fan, A. Vaneski, A. S. Susha, W. Y. Teoh, A. L. Rogach, *Adv. Funct. Mater.* **2012**, *22*, 2821.
[274] F. P. Zamborini, L. E. Smart, M. C. Leopold, R. W. Murray, *Anal. Chim. Acta* **2003**, *496*, 3.
[275] S. Sivaramakrishnan, P.-J. Chia, Y.-C. Yeo, L.-L. Chua, P. K.-H. Ho, *Nat. Mater.* **2007**, *6*, 149.
[276] J. L. Schaefer, D. A. Yanga, L. A. Archer, *Chem. Mater.* **2013**, *25*, 834.
[277] X. Geng, Y. Jiao, Y. Han, A. Mukhopadhyay, L. Yang, H. Zhu, *Adv. Funct. Mater.* **2017**, *27*, 1702998.
[278] D. Takamatsu, Y. Koyama, Y. Orikasa, S. Mori, T. Nakatsutsumi, T. Hirano, H. Tanida, H. Arai, Y. Uchimoto, Z. Ogumi, *Angew. Chem., Int. Ed.* **2012**, *124*, 11765.
[279] Y. Zhu, M. Yang, Q. Huang, D. Wang, R. Yu, J. Wang, Z. Zheng, D. Wang, *Adv. Mater.* **2020**, *32*, 1906205.

© 2021 Wiley-VCH GmbH

[280] Y. Luo, J. Luo, J. Jiang, W. Zhou, H. Yang, X. Qi, H. Zhang, H. J. Fan, D. Y. W. Yu, C. M. Li, T. Yu, *Energy Environ. Sci.* **2012**, *5*, 6559.
[281] Z. Gao, N. Song, Y. Zhang, X. Li, *Nano Lett.* **2015**, *15*, 8194.
[282] L. Shen, Q. Che, H. Li, X. Zhang, *Adv. Funct. Mater.* **2014**, *24*, 2630.
[283] J. Liu, Y. Li, X. Huang, R. Ding, Y. Hu, J. Jiang, L. Liao, *J. Mater. Chem.* **2009**, *19*, 1859.
[284] L. Shen, B. Ding, G. Cao, X. Zheng, *Adv. Energy Mater.* **2013**, *3*, 1484.
[285] B. Liu, J. Zhang, X. Wang, G. Chen, D. Chen, C. Zhou, G. Shen, *Nano Lett.* **2012**, *12*, 3005.
[286] X. Min, B. Sun, S. Chen, M. Fang, X. Wu, Y. Liu, A. Abdelkader, Z. Huang, T. Liu, K. Xi, R. V. Kumar, *Energy Storage Mater.* **2019**, *16*, 597.
[287] J. Guo, Q. Zhang, J. Sun, C. Li, J. Zhao, Z. Zhou, B. He, X. Wang, P. Man, Q. Li, J. Zhang, L. Xie, M. Li, Y. Yao, *J. Power Source* **2018**, *382*, 122.
[288] W. Li, L. Gan, K. Guo, L. Ke, Y. Wei, H. Li, G. Shen. T. Zhai, *Nanoscale* **2016**, *8*, 8666.
[289] J. Balamurugan, T. T. Nguyen, V. Aravindan, N. H. Kim, S. H. Lee, J. H. Lee, *Nano Energy* **2019**, *65*, 103999.
[290] L. Bao, X. Li, *Adv. Mater.* **2012**, *24*, 3246.
[291] Q. Huang, D. Wang, Z. Zheng, *Adv. Energy Mater.* **2016**, *6*, 1600783.
[292] Z. Gao, N. Song, X. Li, *J. Mater. Chem. A* **2015**, *3*, 14833.
[293] H. Wang, H. S. Casalongue, Y. Liang, H. Dai, *J. Am. Chem. Soc.* **2010**, *132*, 7472.
[294] H. Zhang, G. Cao, Z. Wang, Y. Yang, Z. Shi, Z. Gu, *Nano Lett.* **2008**, *8*, 2664.
[295] W. Jiang, D. Yu, Q. Zhang, K. Goh, L Wei, Y. Yong, R. Jiang, J. Wei, Y. Chen, *Adv. Funct. Mater.* **2015**, *25*, 1063.
[296] W. Xu, J. Lu, W. Huo, J. Li, X. Wang, C. Zhang, X. Gu, C. Hu, *Nanoscale* **2018**, *10*, 14304.
[297] H. Gao, W. Zhou, J.-H. Jang, J. B. Goodenough, *Adv. Energy Mater.* **2016**, *6*, 1502130.
[298] T. Liu, Q. Chu, C. Yan, S. Zhang, Z. Lin, J. Lu, *Adv. Energy Mater.* **2019**, *9*, 1802645.
[299] S.-H. Park, P. J. King, R. Tian, C. S. Boland, J. Coelho, C. (John) Zhang, P. McBean, N. McEvoy, M. P. Kremer, D. Daly, J. N. Coleman, V. Nicolosi, *Nat. Energy* **2019**, *4*, 560.
[300] T. Brezesinski, J. Wang, S. H. Tolbert, B. Duun, *Nat. Mater.* **2010**, *9*, 146.
[301] K. Brezesinski, J. Wang, J. Haetge, C. Reitz, S. Q. Steinmeueller, S. H. Tolbert, B. M. Smarsly, B. Duun, T. Brezesinski, *J. Am. Chem. Soc.* **2010**, *132*, 6982.
[302] D. Larcher, C. Masquelier, D. Bonnin, Y. Chabre, V. Masson, J.-B. Leriche, J.-M. Tarascon, *J. Electrochem. Soc.* **2002**, *150*, A133.
[303] P. Poizot, S. Laruelle, S. Grugeon, L Dupont, J.-M. Tarascon, *Nature* **2000**, *407*, 496.
[304] M. Wagemaker, F. M. Mulder, *Acc. Chem. Res.* **2013**, *46*, 1206.
[305] R. D. Palma, S. Peeters, M. J. V. Bael, H. V. d. Rul, K. Bonroy, W. Laureyn, J. Mullens, G. Borghs, G. Maes, *Chem. Mater.* **2007**, *19*, 1821.
[306] Y. Wang, J. F. Wong, X. Teng, X. Z. Lin, H. Yang, *Nano Lett.* **2003**, *3*, 1555.
[307] Y. Kim, C. Lee, I. Shim, D. Wang, J. Cho, *Adv. Mater.* **2010**, *22*, 5140.
[308] V. Muhr, S. Wilhelm, T. Hirsch, O. S. Wolfbeis, *Acc. Chem. Res.* **2014**, *47*, 3481.
[309] Y. Ko, D. Shin, B. Koo, S. W. Lee, W.-S. Yoon, J. Cho, *Nano Energy* **2015**, *12*, 612.
[310] Z. Bo, W. Zhu, W. Ma, Z. Wen, X. Shuai, J. Chen, J. Yan, Z. Wang, K. Cen, X. Feng, *Adv. Mater.* **2013**, *25*, 5799.
[311] H. G. Bagaria, E. T. Ada, M. Shamsuzzoha, D. E. Nikles, D. T. Johnson, *Langmuir* **2006**, *22*, 7732.
[312] Z. Liang, K. L. Dzienis, J. Xu, Q. Wang, *Adv. Funct. Mater.* **2006**, *16*, 542.
[313] P. Kanninen, C. Johans, J. Merta, K. Kontturi, *J. Colloid Interface Sci.* **2008**, *318*, 88.
[314] J. Choi, D. Nam, D. Shin, Y. Song, C. H. Kwon, J. Cho, S. W. Lee, J. Cho, *ACS Nano* **2019**, *13*, 12719.
[315] S. Kang, D. Nam, J. Choi, J. Ko, D. Kim, C. H. Kwon, J. Huh, J. Cho, *ACS Appl. Mater. Interfaces* **2019**, *11*, 12032.
[316] Y. Ko, H. Baek, Y. Kim, M. Yoon, J. Cho, *ACS Nano* **2013**, *7*, 143.
[317] K. Jost, D. Stenger, C. R. Perez, J. K. McDonough, K. Lian, Y. Gogotsi, G. Dion, *Energy Environ. Sci.* **2013**, *6*, 2698.
[318] Z. L. Wang, W. Wu, *Angew. Chem., Int. Ed.* **2012**, *51*, 11700.
[319] L. Ji, Z. Lin, M. Alcoutlabi, X. Zhang, *Energy Environ. Sci.* **2011**, *4*, 2682.
[320] M.-L. Seol, J.-H. Woo, D.-I. Lee, H. Im, J. Hur, Y.-K. Choi, *Small* **2014**, *10*, 3887.
[321] C. Wu, A. C. Wang, W. Ding, H. Guo, Z. L. Wang, *Adv. Energy Mater.* **2019**, *9*, 1802906.
[322] J. J. Richardson, J. Cui, M. Björnmalm, J. A. Braunger, H. Ejima, F. Caruso, *Chem. Rev.* **2016**, *116*, 14828.
[323] J.-M. Son, S. Oh, S.-H. Bae, S. Nam, I.-K. Oh, *Adv. Energy Mater.* **2019**, *9*, 1900477.
[324] H. Yu, C. Zhu, K. Zhang, Y. Chen, C. Li, P. Gao, P. Yang, Q. Ouyang, *J. Mater. Chem. A* **2014**, *2*, 4551.
[325] Y. Huang, H. Yang, T. Ziong, D. Adekoya, W. Qiu, Z. Wang, S. Zhang, M.-S. Balogun, *Energy Storage Mater.* **2020**, *25*, 41.
[326] S. Dong, L. Shen, H. Li, G. Pang, H. Dou, X. Zhang, *Adv. Funct. Mater.* **2016**, *26*, 3703.

Yongmin Ko received his Ph.D. degree at the Department of Chemical and Biological Engineering in Korea University in 2016. He was a postdoctoral researcher at Georgia Institute of Technology in Atlanta until 2019. Currently, he is working as a senior researcher at the Division of Energy Technology at the Daegu Gyeongbuk Institute of Science and Technology (DGIST) in Republic of Korea. His research interest is focused on energy conversion and storage devices based on various functional nanomaterials.

© 2021 Wiley-VCH GmbH

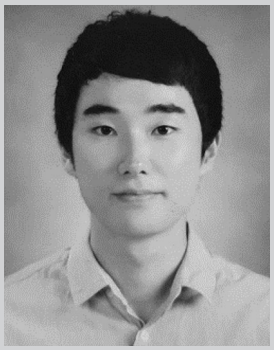

Seokmin Lee is a Ph.D. candidate under Prof. Jinhan Cho at the Department of Chemical and Biological Engineering in Korea University. Currently, his research interest has focused on flexible/stretchable energy electrodes based on the interfacial engineering of functional nanomaterials.

Cheong Hoon Kwon received her Ph.D. degree at the Department of Chemical and Biological Engineering in Korea University in 2008. She is a postdoctoral researcher at Harvard Medical School in Boston (in 2009–2010). In 2010–2015, she was a research professor in Hanyang University. Currently, she is a senior researcher at the Department of Chemical and Biological Engineering in Korea University. She has expertise in the surface modification of metal or metal oxide nanoparticles for electrochemical sensors (or actuators), biofuel cells, and energy storage devices. She has now focused on developing various energy electrodes using metal nanoparticle-based layer-by-layer assembly.

Seung Woo Lee is an associate professor of the Woodruff School of Mechanical Engineering at Georgia Institute of Technology. He has expertise in electrode materials and electrochemical measurement techniques for energy storage and conversion devices, including rechargeable batteries, supercapacitors, fuel-cells, and electrolyzers. He has focused on studying surface chemistry and electronic structure of various electrode materials, such as carbon nanotubes, graphenes, and metal (oxide) nanoparticles, correlating with their electrochemical properties.

Jinhan Cho is a professor at the Department of Chemical & Biological Engineering in Korea University since 2010. His research career started in POSTECH and Seoul National University, where completed M.S. and Ph.D., respectively. Then, he had post-doc courses at Max Planck Institute of Colloids and Interfaces (2001–2002) and University of Melbourne (2003). In 2006–2010, he had an academic career as an assistant professor in Kookmin University. His research interests have been focused on studying the surface chemistry and electrochemical properties of various electrode materials, such as carbon-based materials, metal, and metal oxide nanoparticles onto textile substrates.

© 2021 Wiley-VCH GmbH